Predicting Radiated Emission of Apparatus Configured of Modules by Means of Numerical Methods and Module Level Measurements

Sørensen, Morten

Publication date:
2018

Document Version
Publisher's PDF, also known as Version of record

PREDICTING RADIATED EMISSION OF APPARATUS CONFIGURED OF MODULES BY MEANS OF NUMERICAL METHODS AND MODULE LEVEL MEASUREMENTS

BY
MORTEN SØRENSEN

DISSERTATION SUBMITTED 2018

AALBORG UNIVERSITY
DENMARK

Predicting Radiated Emission of Apparatus Configured of Modules by Means of Numerical Methods and Module Level Measurements

Ph.D. Dissertation

Morten Sørensen

Dissertation submitted October 5, 2018

Dissertation submitted:	October 5, 2018
PhD supervisor:	Prof. Gert Frølund Pedersen Aalborg University
Assistant PhD supervisors:	Assoc. Prof. Hans Ebert Aalborg University
	Assoc. Prof. Ondrej Franek Aalborg University
PhD committee:	Associate Professor Ole Kiel Jensen (chairman) Aalborg University
	Associate Professor Ville Viikari Aalto University
	Project Leader Sven Kühn Schmid & Partner Engineering AG
PhD Series:	Technical Faculty of IT and Design, Aalborg University
Department:	Department of Electronic Systems

ISSN (online): 2446-1628
ISBN (online): 978-87-7210-338-9

Published by:
Aalborg University Press
Langagervej 2
DK – 9220 Aalborg Ø
Phone: +45 99407140
aauf@forlag.aau.dk
forlag.aau.dk

Printed in Denmark by Rosendahls, 2018

Abstract

It's a big problem in the industry when the final apparatus, few weeks before it is released for production, fails the legally mandatory EMC test. It can cause extremely complicated, expensive, and time-consuming modifications of an otherwise completed apparatus and, in worst case, delays. Conversely, the fear of failed legally mandatory EMC test late in a project phase can cause overdesign and, hence, unnecessary and costly improvements. Therefore, there is a need for methods to predict EMC properties early in the project phase.

This thesis addresses different methods to estimate the radiated emission from an apparatus configured of modules early in the project phase and long time before the apparatus is finalized. The methods make use of both module measurements, simulations and a combination of these.

Radiated emission from an apparatus can be divided into radiation due to common mode currents on attached cables (common mode emission) and direct radiation from modules. Regarding the common mode emission, the thesis shows that the "Workbench Faraday Cage" method (IEC standard 61967-5) unfortunately cannot be used as pre-compliance test, because the Faraday cage itself interferes with both the voltage driven and current driven coupling to attached cables. In addition, it is shown that common mode emission from even a simple microstrip board is too complicated to be described by a lumped element model and that the radiation can vary as much as 20 dB depending on the printed circuit board's (PCB) orientation.

By making a free space measurement of the module alone, it can be estimated how much direct radiated emission the module will cause in the final apparatus. However, when the module is mounted in an apparatus, the radiation can change significantly due to enclosure, cables and other obstacles.

Therefore, the thesis will focus on near-field scans as source for simulations. The main idea is to measure the tangential electrical and magnetic fields on a "Huygens' box" (HB) that encloses the sources and use the measured fields as source for simulation (the HB method). The thesis investigates how step size and uncertainty in the measurement of the phase affect the prediction of free space radiated emission. In addition, it is investigated

whether attached cables perturb the HB method, and whether all six sides of the HB are needed. The thesis shows that in many cases, the effect of scattering and reflection from nearby obstacles can be simulated by including the ground plane and substrate of the PCB in the HB. The limitations of the latter method are also investigated and it is shown that the method fails when strong resonances occur or when ground plane resonances are a source of radiation.

Finally, it is discussed how to calibrate and characterize near-field probes at high frequencies and how to reduce the number of measurement points in ”Emission Source Microscopy”, a measurement method that, contrary to near field scans, directly reveals the locations of the sources for emission.

Resumé

I industrien er det et stort problem, når et apparat, få uger før det skal gå i produktion, ikke består EMC-myndighedstesten. Dette kan give anledning til dyre forbedringer af apparatet og i værste fald forsinkelser. Omvendt kan frygten for fejl i EMC-myndighedstesten sent i en projektfase medføre, at der overdesignes, og at unødvendige og fordyrende tiltag indføres. Derfor er der brug for metoder til at forudsige EMC-egenskaber tidligt i projektfasen.

Denne afhandling omhandler forskellige metoder til, tidligt i projektfasen og længe før apparatet står færdigt, at skønne udstrålingen fra et apparat sammensat af moduler. Metoderne gør brug både af modulmålinger, simuleringer og en kombination af disse.

Udstråling fra apparater kan deles op i ledningsbåret udstråling pga. common mode strøm på kabler og direkte udstråling fra moduler. Om den ledningsbårne udstråling viser denne afhandling, at "Workbench Faraday Cage"-metoden (IEC standard 61967-5) desværre ikke kan bruges som pre-compliance test, da selve Faraday kassen forstyrrer både den spændingsdrevne og strømdrevne kobling til vedhæftede kabler. Tillige vises det, at ledningsbåret udstråling fra selv et simpelt microstrip printkort er for kompliceret til at kunne beskrives med kredsløbsteori, og at udstrålingen kan variere op til 20 dB afhængigt af, hvordan printkortet vender.

Ved at lave en fritfelt-måling af modulet alene kan man få et estimat af den direkte udstråling, som modulet forårsager i det færdige apparat. Men når modulet monteres i et apparat, kan udstrålingen ændre sig signifikant pga. kabinet, kabler osv.

Derfor er nærfeltsscanninger som kilde til simuleringer i fokus i denne afhandling. Hovedideen er at måle de elektriske og magnetiske tangentielle felter på en "Huygens' box" (HB), der omslutter kilderne, og bruge de målte felter som kilde til simulering (HB-metoden). Afhandlingen undersøger, hvad stepstørrelse og usikkerhed i målingen af fasen betyder for forudsigelsen af fritfelt-udstrålingen. Derudover undersøges det, om vedhæftede kabler perturberer HB-metoden, og om alle seks sider af HB'en er nødvendige. Afhandlingen viser, at ved at inkludere printkortets ground plane og substrat i HB'en kan man i mange tilfælde simulere effekten af

spredninger og refleksioner. Sidstnævnte metodes begrænsninger undersøges også, og det vises, at metoden fejler, når der opstår stærke resonanser, eller når ground plane resonanser er kilde til udstrålingen.

Endelig behandles også, hvordan man kan kalibrere og karakterisere nærfeltsprober ved høje frekvenser, og hvordan man reducerer antallet af målepunkter i "Emission Source Microscopy" - en målemetode, der modsat nærfeltsscanninger, direkte viser lokationerne af kilderne til udstrålingen fra det testede modul.

Contents

Thesis Details

Thesis Title:	Predicting Radiated Emission of Apparatus Configured of Modules by Means of Numerical Methods and Module Level Measurements
Ph.D Student:	Morten Sørensen
Academic Supervisors:	Prof. Gert F. Pedersen
	Assoc. Prof. Hans Ebert
	Assoc. Prof. Ondrej Franek
Industrial Supervisors	EMC Consultant Knud A. Baltsen
	Technology Specialist Søren Kjærulff Christensen

[A] M. Sørensen, O. Franek, S. Christensen, G. Pedersen, and H. Ebert, "Assessment of the Usability of the Workbench Faraday Cage Method," *Electromagnetic Compatibility (EMC), 2011 IEEE International Symposium on*, Aug 2011, pp. 399–404

[B] M. Sørensen, T. Hubing, and K. Jensen, "Study of the Impact of Board Orientation on Radiated Emissions due to Common-mode Currents on Attached Cables," *Electromagnetic Compatibility (EMC), 2016 IEEE International Symposium on*, Jul 2016, pp. 36-40

[C] M. Sørensen, S.K. Christensen, C. Vittarp, and H. Ebert, "Analysis and Measurement Investigation of the Workbench Faraday Cage Method, IEC 61967-5," *Submitted to IEEE Transactions on Electromagnetic Compatibility*, September 30, 2018

[D] M. Sørensen, O. Franek, G. Pedersen, K. Baltsen, and H. Ebert, "Perturbation of Near-field Scan from Connected Cables," *Electromagnetic Compatibility (EMC), 2012 IEEE International Symposium on*, Aug 2012, pp. 594–599

Nominated for best conference paper prize:

[E] M. Sørensen, O. Franek, G. Pedersen, A. Radchenko, K. Kam, and D. Pommerenke, "Estimate on the Uncertainty of Predicting Radiated Emission from Near-field Scan Caused by Insufficient or Inaccurate Near-field Data: Evaluation of the Needed Step Size, Phase Accuracy and the Need for all Surfaces in the Huygens' Box," *Electromagnetic Compatibility (EMC EUROPE), 2012 International Symposium on*, Sept 2012, pp. 1–6

[F] M. Sørensen, I. Bonev, O. Franek, G. Pedersen, and H. Ebert, "How to Handle a Huygens' Box Inside an Enclosure," *Electromagnetic Compatibility (EMC), 2013 IEEE International Symposium on*, Aug 2013, pp. 802–807

[G] M. Sørensen, I. Bonev, O. Franek, G. Pedersen, and H. Ebert, "Review of the Huygens' Box Method With Different Sources Near Obstacles," *Submitted to IEEE Transactions on Electromagnetic Compatibility*, September 30, 2018

[H] M. Sørensen, O. Franek, and G. Pedersen, "Recent Developments in using Measured Sources in Computational EMC," *Antennas and Propagation (EuCAP), 2015 9th European Conference on*, April 2015, pp. 1–5

[I] M. Sørensen, S. Marathe, D. Pommerenke, H. Kajbaf and J. Min "Design of TEM Transmission Line for Probe Calibration up to 40 GHz," *Electromagnetic Compatibility (EMC), 2018 IEEE International Symposium on*, Jul 2018

[J] M. Sorensen, H. Kajbaf, V. Khilkevich, L. Zhang, and D. Pommerenke, "Analysis of the Effect on Image Quality of Different Scanning Point Selection Methods in Sparse ESM," Accepted for publication in *IEEE Transactions on Electromagnetic Compatibility*, August 2^{th} 2018.

The thesis is based on the submitted or published scientific papers which are listed above. Parts of the papers are used directly or indirectly in the summary of the papers. As part of the assessment, co-author statements have been made available to the assessment committee and are also available at the faculty.

Preface

This thesis is submitted as partial fulfillment of the requirements for the degree of Doctor of Philosophy at Aalborg University, Denmark. The main part of the thesis is a collection of papers published in or submitted to peer-reviewed conferences and journals. It is mainly the results of research at Antennas, Propagation and Millimetre-wave Systems (APMS) section at the Department of Electronic Systems, Aalborg University, Denmark and Bang & Olufsen, Struer, Denmark. Most of the research was carried out as industrial PhD student in the innovation consortium "EMC Design – First Time Right" from July 2010 to June 2013. However some of the work continued after the mentioned period. The scientific contributions to this thesis were done under the supervision of Prof. Gert F. Pedersen, Assoc. Prof. Ondrej Franek and Assoc. Prof. Hans Ebert. The industrial contribution were done under the supervision of former Bang & Olufsen employees EMC Consultant Knud A. Baltsen and technology specialist Søren Kjærulff Christensen. I would like to express my sincere gratitude to all the supervisors for sharing their expertise and enthusiasm. Most of the work has been done within "Innovation Consortium EMC Design – First Time Right, co-sponsored by The Danish Agency for Science, Technology and Innovation, and The Danish Council for Technology and Innovation. Through this collaboration, the high quality knowledge of (in alphabetic order) Kim Jensen (former Bang & Olufsen), Anders P. Mynster (Force Technology), and Claus Vittarp (DEIF A/S) has been a great inspiration and lead to many of the presented results. I would also like to thank the Ivan Bonev Bonev (former Aalborg University) for his help with performing simulations at the hybrid Linux cluster Fyrkat at Aalborg Universit, and Jan Clausen (DEIF a/s) for his many module level measurements.

Morten Sørensen
Rolla, Missouri, USA, October 5, 2018

Part I

Introduction

Introduction

1 Introduction

1.1 Background for the Thesis

For many years, there has been an acceleration in time-to-market in the global electronics industry. Electronic apparatuses are typically made of several modules. For example a television can be pieced together from a power supply (PSU), a video engine, an audio engine, a LCD panel including a timing controller (T-Con), audio amplifiers etc. Some modules are developed in-house, while other modules are developed by a subcontractor. Finally, some modules are off the shell products. All sub projects run in parallel and often the final apparatus is not ready for EMC tests until three weeks before release for production.

Legal and regulatory requirements regarding radiated emissions from electrical apparatus have always been applied to the whole apparatus and not to the individual modules that are part of the apparatus [1, 2]. If the final apparatus fails EMC tests three weeks before release for production, it is most often extremely complicated, expensive, and time consuming to modify an otherwise completed apparatus. However, even more costly could be that the apparatus' intended launch time is delayed. It is a general experience that these late EMC problems occur frequently, especially problems with radiated emission, even for companies with extensive experience regarding EMC. In order to avoid those last minute and costly EMC rescue operations, EMC engineers tend to overdesign which also adds cost to the final product.

Hence methods that quantitatively evaluate a modules contribution to the final apparatus' radiated emission is needed.

1.2 Definitions

In this thesis a module is defined as an electronic device which, together with other modules, is a part of an apparatus. A module can, with the right software, operate on its own with respect to measurements of EMC characteristic,

(i.e., it will operates electromagnetically in the same way that it operates in the final apparatus with same current, voltage, clock frequencies etc.) Often a module is a printed circuit board (PCB) with components but in other cases more than one PCB are needed in order to operate on its own.

The apparatus is the electronic device, configured of modules, which has to fulfill the regulatory requirements.

In this thesis, an apparatus EMC architecture is defined as the conceptual structure and organization of the modules with respect to EMC. Some of the key components in EMC architecture, with respect to radiated emission, are chassis and grounding, shielding, mutual module placement and cabling.

1.3 What Does Radiate in an Apparatus?

The total radiated emission from an apparatus depends on many factors including [3–6]:

- Common mode currents induced on cables attached to PCBs.
- Radiation from the PCBs themselves, (i.e., traces, components, power-ground plane resonances, etc.)
- Unintended radiation from the signals on cables and connectors, (i.e., transfer impedance in cables and connectors).
- Resonances in chassis, cavities and the like.

All in all, a very complex system which is further complicated by the fact that the above mentioned factors are not independent and highly depend on the apparatus' EMC architecture, (i.e., the mutual module placement, cabling, grounding strategy etc.)

Coupling from IC to Cables

The coupling mechanisms by which the intentional signal induces common mode currents on cables can be divided into three categories: Current driven, voltage driven and I/O signal coupling. Current driven [7, 8] and voltage driven [9, 10] common mode emission are illustrated in Fig. 1.

When a PCB is mounted to a metal chassis, the cavity formed between the circuit board ground and the chassis can resonate at certain frequencies resulting in unintended radiated emissions.

Current driven common mode emission occur because the return plane is of finite size and the magnetic flux wraps around the plane. Hence the current return path has an effective inductance and a voltage across the return plane will occur and drive attached cables.

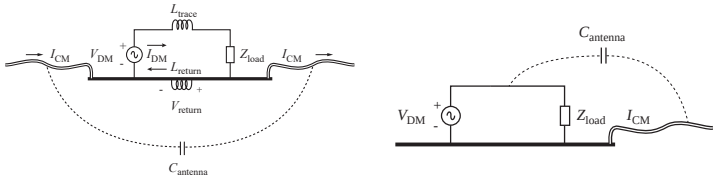

Fig. 1: (a) Current driven common mode emission. (b) Voltage driven common mode emission.

Voltage driven common mode emission arises because the voltage across the signal generator (VDM) drives the trace relative to the return plane with cables. If the signal trace couples capacitive to larger structures, (e.g., a heatsink,) the voltage-driven current can be significantly magnified.

I/O coupled common mode emission arises because of crosstalk between signal traces and traces that connect to wires that bring signals or power onto the board (I/O lines) [11]. This is most likely to be a problem when the cable is not designed to carry high-frequency signals, or if a low quality connector, with low transfer impedance from differential to common mode, is used.

Radiation from PCB Themselves

As the electrical length of current carrying structures approaches 1/10 of the wavelength, it starts to radiates by itself [12]. Unwanted antennas likes attached cables are not necessary. Starting at a few hundred MHz, power/ground plane cavities [13, 14], traces [15, 16], heat sinks [17] etc. start to radiate depending on physical size. An important factor in power plane resonances are via placement [18]. Splits in ground plane and changing reference plane [19] can effect the trace radiation.

Unintended Radiation from the Signals on Cables

Performance of cables can be expressed as transfer impedance, which is a measure for the coupling between domains internal and external to the shield. It is defined as the ratio of induced voltage on the inside of the shield over the current flowing on its outer surface [20]. Broken or insufficient shielding is one source for common mode current on cables, but more frequently the common mode current is caused by coax cables with pigtails [21, 22] or low transfer impedance in connectors [23].

Resonances in Chassis, Cavities and the like

When a PCB is mounted to a metal chassis, the cavity formed between the circuit board ground and the chassis can resonate at certain frequencies re-

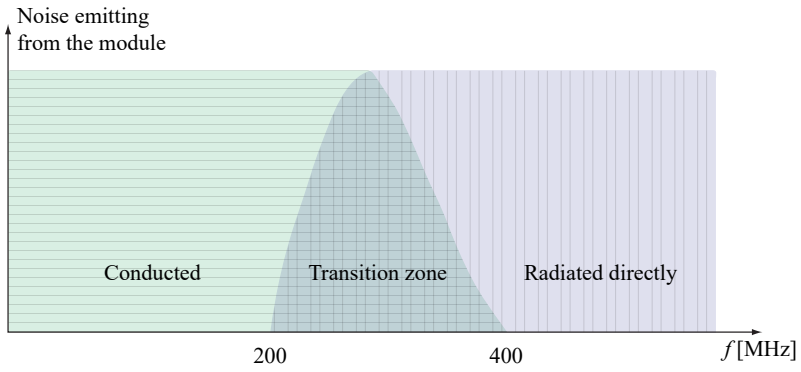

Fig. 2: Rule of thumb for conducted emission (common mode radiation from the cables) and radiation directly from PCBs.

sulting in unintended radiated emissions [24]. Also junction current which is the current flowing through screws connecting PCB ground to chassis can be the root cause of radiated emission [25]. A typical EMC guideline states that one should mount PCBs on chassis, preferable large metal planes. The idea is that it reduces susceptibility to transients and reduces radiated emission. However, chassis resonances are very complex and sometimes a chassis can even increase radiated emission [26].

1.4 Conducted emission vs. radiation directly from the PCBs

Assuming that the right cable and connectors are selected, (i.e., no radiation caused by low transfer impedance,) then it is possible to setup a rule of thumb for the radiation mechanisms vs. frequency as shown in Fig. 2.

Below 200 MHz, the dominant emission mechanism is conducted, (i.e., common mode currents flowing on the cables.) When the wavelength exceed 1/10 of the PCB length, the transition zone begins where the dominating radiation can originate from both the attached cables and from PCBs themselves depending on the cable length and termination impedance.

When the wavelength exceeds 1/2 of ground plane length, the transition zone ends, and the radiation originates solely from the PCB itself. In other words, if the PCB is large, PCB radiation becomes dominant in the low end of the transition zone, and if the PCB is small, PCB radiation becomes dominant in the high end of the transition zone.

The above rules on distinguishing between the relevant frequency ranges are only rules of thumb, and it is possible to find examples where it is not valid. However, a large number of apparatus from DEIF (power control units) and from Bang & Olufsen (audio and video products as well as loudspeakers) has been tested during the innovation consortium and the results were in

agreement with the above conclusion.

1.5 Module Level Measurement Methods

The IEC standard “Integrated circuits - Measurement of electromagnetic emissions, 150 kHz to 1 GHz” (IEC 61967) [27] describes five different methods to measure the noise emitted from an IC at module level. Among these the most widespread method is probably part II “TEM cell method”. Part 5, "Work Bench Faraday Cage" (WBFC) which was developed at Philips, Netherland, [28, 29] in 1994. Through the close cooperation between EMC engineers at Philips and Bang & Olufsen at that time, the method was introduced at Bang & Olufsen and later to Bang & Olufsen’s subcontractors. The WBFC assumes that radiated emission is dominated by common mode currents on cables, and therefore it is possible to predict the worst case by considering the apparatus signal cables as balanced dipole antennas.

Part 3, ”Measurement of Radiated Emissions – Surface Scan Method” provides a test procedure which defines an evaluation method for the near electric, magnetic or electromagnetic field components at or near the surface of an IC. The measurement method provides a mapping of the electric or magnetic near-field emissions over the IC which can be compared with measurements of other IC’s. However, the standard does not provide any method to relate measured near-field to radiated emission.

1.6 Repeatability of Measurements

A continuous challenge in EMC is to make repeatable measurements. The measurements of radiated emission in a semi anechoic chamber (SAC) at low frequencies in the range of 30 MHz up to the transition zone will, for vertical polarization, depend very much on terminating of the attached cables. In particular, the impedance of the cables leaving the room or passing through the reference plane affect the measurement. [30, 31].

Hence, radiated emission from (e.g., power cables) will vary with the impedance between the power line and the power source ground. Nine certified laboratories participated in a round robin test of radiated emission from a PC tower [30]. Between of the laboratories, the test of radiated emissions showed differences of up to 20 dB at frequencies below 100 MHz, with a standard deviation up to 8 dB.

After years of discussions on the CISPR meetings, the participants agreed on use of common mode absorbing devices (CMAD) on all lines [1], (i.e., power input and output as well communication and signal lines.) CMADs should stabilize the common mode impedance independently on the termination impedance of the line. Similar problems apply to the cable terminations when interconnecting different modules. According to [32] a calibrated

SAC is allowed to have a measurement uncertainty up to 6.3 dB from 30 MHz - 1000 MHz.

1.7 Numerical Methods and Near-field Scan

Through the past 15 years, there has been a significant increase in the possible applications of electromagnetic numerical methods within EMC-related problems. The development has been strong because it has benefited from both the computer's increased processing power, and new and improved numerical methods [33].

Numerical methods are used for all disciplines within EMC, (e.g., prediction of shielding effectiveness [34, 35], PCB layout [36, 37], signal and power integrity [38–40], radiation from integrated circuits [41, 42] and resonance phenomena [43].) The outcome of the simulations are mostly relative or absolute EMC properties of a component or a single module. However, by help of different numerical methods, it is also possible to do a full system EMC analysis and estimate the radiated emission [38, 44].

An automated near-field scan systems can be used for hot spot finding [45–49] and resonances [50]. It is also possible to estimate a module's far-field based on near-field measurements of the same. The scientific world has not yet agreed on a method. Still there are two different dominating approaches to the far-field prediction. One approach uses the near-field as a basis for source by help of an equivalent set of electric and/or magnetic dipoles [51–53]. In Cartesian coordinates, the dipoles can be reduced to one electric dipoles P_z representing voltage and two magnetic dipoles in M_x and M_y representing currents [54]. The locations, amplitudes, and phase of the dipoles are optimized by least square method combined with a regularization technique.

Another approach uses tangential near fields on a surface entirely enclosing the module [55–58]. According to the surface equivalence principle, these fields distributed on the closed surface, often named the Huygens' box (HB), then act as sources generating the same fields as the original module outside of this surface.

Because of the complexity, only in recent years have there been scientific attempts to combine near-field measurements and simulations for a whole system with obstacles and enclosures, (i.e., attempt to predict an apparatus' total radiated emissions based on measurements of module-level emission and the apparatus' architecture [56, 59, 60].) As described in Sec. 1.4, radiated emission will be dominated by common mode emission from attached cables at low frequencies while direct radiated emission from PCBs will dominate at higher frequencies. It has been suggested that to predict the radiated emission, common mode current measurements on cables and near-field to far-field transformation at higher frequencies can be combined [44].

1.8 Near-field Probes and Calibration

Various probe calibration methods suitable for different frequency ranges are published in the literature; the different calibration methods and their typical frequency ranges are mentioned in the IEEE Standard 1309-2013 [61] and IEC 61000-4-20 Annex E covers E-field probe calibration in TEM waveguides [27]. Previous work [62] has shown that referring a measured voltage to the known fields of a 50 Ω transmission line (TL) is an effective method for calculating the probe factor.

1.9 Emission Source Microscopy

As mentioned before, a common objective with near-field scan is to find sources for radiated emission. However, a high magnitude spot in the reactive near field could easily be evanescent and not be source for radiation. For example a differential microstrip pair will, in the near-field region, have a strong magnetic amplitude but this field is evanescent. The evanescent waves may cause misinterpretation of near-field scans.

Emission Source Microscopy (ESM) is a measurement method that can identify the radiating sources of a complex system [63]. The phase resolved tangential electric fields are measured on a plane above the device under test (DUT) and the plane wave spectrum is back propagated to the source plane, where the radiating field sources are reconstructed with a resolution down to a half wavelength. ESM directly reveals the sources for radiated emission. The measurements can be done automatically, with a near-field scanner a few wavelengths away from the DUT [63] with a step size fulfilling Nyquist's sampling rate. Sparse- and non-uniform sampling points further away have also been used [64]. Because the resolution is no better than a half wavelength, the method is only useful above a certain frequency, (e.g., at 10 GHz the resolution cannot be better than 1.5 cm.) Previous work has showed that the method can distinguish between multiple radiating sources on a complex PCB [65] above 5 GHz.

2 Aims of the Work

Available EMC literature [66–69] describes many qualitative methods for each noise source that makes it possible to suppress electromagnetic radiation and interference. Currently only few accurate quantitative methods are available that predict the effect on apparatus level through an effort made at module level or made by the architecture. Quantitative methods are the objective of this thesis. The very ambitious goal for much of EMC research is to combine module measurements and 3D full wave electromagnetic simulations to:

- Predicting an apparatus' complete radiated emissions in the far-field based on the characteristic of the used modules, and the architecture (modules, cabling, interconnection location, chassis, etc.)
- Converting emission requirements on apparatus level to requirements for each module and the apparatus' architecture.

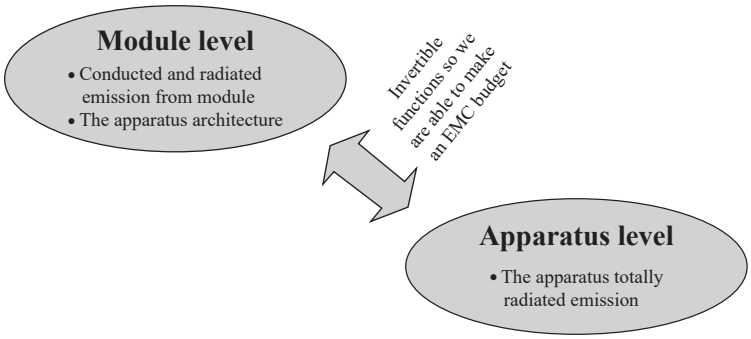

Fig. 3: The very ambitious goal.

No one is currently able to do that, and it is doubtful whether it ever will be possible. But with the great development in electromagnetic simulations and computing power in recent years, it is now well worth investigating the possibilities. This thesis will concentrate on predicting radiated emission of apparatus configured of modules by means of numerical methods and module level measurements. It is the projects objectives to investigate a concept where an apparatus' total radiated emission is predicted based on module measurements and 3D full wave electromagnetic simulations.

To achieve this, research in using measured data as a source for simulations has been carried out in combination with research in module measurement methods.

2.1 Common Mode Emission

Cables represent a distinct challenge for the prediction of the radiated emission. Cables often have lengths comparable with the wavelength of the noise, so that cables are the dominant emitter. Emission from PCBs couple inductive, capacitive, or conducted to the cables and can cause common mode currents, but leaks in connectors and cables also causes common mode currents.

As already mentioned in Sec. 1.6, common mode emission strongly depends on cabling and termination of power and auxiliary cables. In a specific setup, it is possible to measure the common mode current on attached cables and then assuming that the attached cables radiate like a half wavelength dipole, the measured common mode current can predict the radiated emission with approximately 6 dB uncertainty. [67]. However, as a module level assessment it is not adequate because the common mode emission can vary more than 20 dB with cabling and cable termination at frequencies below 100 MHz [30]. Hence a method is needed that estimates worst case contribution to radiated emission from a module in any conceivable EMC architecture.

IEC 61967, part 5, Workbench Faraday Cage Method [27] claims to be such a method. It is based on the assumption that both common mode sources and attached cables can be represented by a lumped element model with source and load impedance. The WBFC measurements provide a figure of merit that tends to correlate with radiated emissions measurements, however neither the standard [27] nor the original investigation [28] provides a rigorously theoretical basis for the method.

In the nineties, there was a close cooperation between Philips and Bang & Olufsen and the Workbench Faraday Cage Method has been used at Bang & Olufsen ever since that. However, no systematic investigation of the methods predictions has ever been made internally at Bang & Olufsen. A search in IEEE Explorer gives only three papers. Nether practical test nor theoretically investigation has been made of this standard approved by "The International Electrotechnical Commission". This thesis investigates the theory behind the WBFC method and its success as pre-compliance test with respect to different modules.

2.2 Direct Radiated Emission

According to the surface equivalent principle, an arbitrary structure containing sources of electric and magnetic fields is equated with electric and magnetic currents on a surface that encloses the structure so that the field within the surface is 0, while outside the surface the field is identical to the field caused by the initial sources. A prerequisite is that the electric and magnetic current densities satisfy boundary conditions on the surface. These current

densities can be deduced from the tangential electric and magnetic fields on the closed surface.

The thesis will investigate whether noise sources like PCBs in simulations can be characterized by their equivalent current densities on a surface that encloses the noise source. For practical reasons, a Cartesian coordinate system will be used so that noise sources can be equated with boxes.

The surface equivalence principle requires that the space outside the HB must be the same in the original problem and in the equivalent problem. If the space outside the HB changes from the original problem to the equivalent problem, the method is no longer valid, (i.e., the surface equivalence principle does not take HB interaction into account.) This issue is unexplored and hence will have high priority in the project, since Bang & Olufsen's products contain much metal.

Current density may, depending on the knowledge of the noise source, be provided either by near-field scan of the source or alternatively by 3D full-wave simulations.

Phase resolved near-field scanning of 4 components (H_x, H_y, E_x *and* E_y) on all 6 surfaces on a box will be very time consuming and impractical, so the thesis will briefly investigate the possibilities to reduce the measurements requirements, (i.e., whether it is possible to only measure H- or E-field and whether all 6 surfaces on the Huygens' box are required.)

Near-field Measurements

In order to use the HB's method, reliable phase resolved near-field scans are needed. Since near-field data often is obtained in the reactive near-field, probes and calibration of them are a challenge. In this thesis a small investigation of probe calibration and how to characterize unwanted field coupling is carried out.

2.3 Emission Source Microscopy

The traditional near-field scans often reveal the sources for radiation. However, as the measurements are done in the near-field, it is easy to make wrong conclusions based on evanescent waves. Emission source microscopy measurements are often done at least a few wavelength away, and in addition it makes use of the plane wave spectrum to exclude the evanescent waves. Hence the method reveals what is the source for radiation. In this thesis an analysis of the effect of selecting scanning points in sparse EMS is carried out. The objective is to reduce the number of measurement points and hence shorten the measurement time.

2.4 Industrial Aim

The industrial aim is to provide the industry methods so R&D departments become able to estimate radiated emission from the finished product early in the development. This makes it possible to do changes while the architecture has not yet been settled, and often before the individual modules are fully developed. It will also become more secure and predictable to reuse modules from apparatus to apparatus. Equally important is the spin off from the research. Through dissemination of the obtained knowledge it is the aim that electrical engineers will get a better understanding of the radiated emission mechanisms and how to mitigate them.

3 Thesis Contributions

This thesis investigates methods that make it possible to do precompliance tests regarding radiated emission very early in an industrial development project. In order to do that, it was necessary to understand the radiation mechanism in different frequency spans. Different methods are used for common mode emission and direct radiated emission. In addition, work was completed to optimize the scanning procedure for Emission Source Microsopy for source reconstruction.

3.1 Common Mode Emission

In paper A, an initial investigation of the WBFC method was carried out on a simple microstrip test PCB that was used throughout the whole project. Results were acceptable, so a more thorough analysis and measurement validation were done in Paper C. Different kinds of modules (a power supply, two digital boards and the simple microstrip test PCB) were tested. Also, the theoretical background was challenged. The paper unfortunately showed that the method has some theoretical problems and measurement could not validate the method.

As discussed in Sec. 1, several different papers describe voltage driven and current driven common mode emission. Typically the described models predict maximum radiated emission by modeling the PCB geometry and signals as a noise generator with attached cables. Paper B further developed a method to distinguish between voltage driven and current driven common mode emission and showed that the method also works for long microstrips. However, the paper also investigated whether it is possible to simplify PCBs to noise generators and lumped elements, and it was showed that common mode emission is more complicated than the simplification and must be considered as complicated antennas.

3.2 Direct Radiated Emission

The ambitious idea is to characterize modules as HBs, (i.e., represent modules by the tangential electrical and magnetic fields on a box enclosing the module.) In previous work, it has been shown that radiated emission from a single module in open boundaries can be predicted based on near-field to far-field transformation of a Huygens' box. However, placing a module close to obstacles can change the radiated emission more than 20 dB, so the simple near-field far-field method does not work as a precompliance test when the EMC architecture of the apparatus is included. Paper F investigated how to handle the HB's method inside two different enclosures. The enclosure changed the radiated emission up to 20 dB as compared to the free space

condition. By placing the main features of the PCB inside the HB, it was possible to predict the maximum radiated emission within a few dB. This investigation was extended with different PCB's and obstacles in paper G. The purpose with the work presented in paper G was to search for the limitations of the HB method. It was found that in most cases the maximum radiated emission is predicted within a few dB. However, far-field error will increase with the Q-factor of the resonances. If the ground planes are the radiator, e.g., plane resonances, it is also necessary to include the vias and ground fill.

From a practical point of view it is time consuming and difficult to obtain all 4 components on all 6 surfaces of the HB. In paper D it was (by help of simulations) shown that cables running through the surface of the HB does not perpetuate near-field to far-field results, but it is not possible to predict common mode emission based on near-field scan. Measurement difficulties will cause measurement uncertainty. Paper E estimated (by help of simulations) the uncertainty of predicting radiated emission from near-field scan caused by insufficient or inaccurate near-field data including phase measurement uncertainty and the effect of only measuring one plane above the PCB instead of all 6 surfaces.

3.3 Measurement Related

In the beginning of this project, no commercial EMC near-field scanners were capable of phase measurements, so in order to do experimental precompliance test and hot spot finding, an in-house near-field scanner was developed. Different phase measurement methods were investigated. The objective was to find a broad banded method that could obtain all frequencies of interest in one scan. A network analyzer in tuned receiver mode will only be able to measure a narrow bandwith while Fourier transformations of signals from a two channel oscilloscope gives broad banded results. Based on the fact that the majority of Bang & Olufsen's EMC challenges were between 30 and 1000 MHz, the sampling rate of a 4 GHz scope is sufficient. It should be noted the instrumental department at Bang & Olufsen did the robot programming.

Paper H gives an overview of the development in using measured data as a source for simulations. The inhouse scanner is briefly presented in paper H and used for near-field to far-field estimation based on only H-field measurement on top surface. By help of CST simulations as well as the measurement with the inhouse scanner, it was tested whether in practice it is possible to make the near-field to far-field transformation by only measuring the magnetic near-field on one surface and filling the HB with perfect magnetic conductor.

Reliable probes are essential for predicting far-field based on the HB-method. As frequencies increase, unwanted E-field coupling becomes a problem and it is important to characterize the unwanted coupling. Paper I

presents a small design study with an air trace that gives a true TEM line for probe calibration up to 40 GHz.

3.4 Emission Source Microscopy

EMS is closely related to near-field scanning and are able to reveal the sources for radiation. Paper J presents an analysis of the effects of choosing measurement points in sparse ESM. It is showed that for ESM purpose, it is possible to go sub Nyquist as long as the aliasing does not overlap the DUT image.

4 Summary of Papers

4.1 Common Mode Emission

Paper A

Assessment of the Usability of the Workbench Faraday Cage Method, *Electromagnetic Compatibility (EMC), 2011 IEEE International Symposium on, Aug 2011*

Motivation
The Workbench Faraday Cage Method (WBFC) is a time efficient module pre-compliance test regarding common mode emission. It has been standardized by IEC 61967 "*Integrated circuits – Measurement of electromagnetic emissions, 150 kHz to 1 GHz*". The Method has been used since the 1990s at Bang & Olufsen without any systematic validation of the method. Until now, there are no scientific publications presenting analysis or measurement validation of the method.

Paper
The paper presents a preliminary study of the usability of the WBFC method and its mode of operation. The investigation was performed on a simple 150 mm $\times$ 225 mm PCB with three 50 Ω microstrips with an unbroken ground plane. The analysis was done by help of full wave simulations in CST and an experimental measurement validation. This was done with a 20 MHz comb generator, (i.e., a signal generator that produces multiple harmonics of its input signal and looks like a comb when measured with a spectrum analyzer).

Main Results
For the tested PCB with a 20 MHz comb generator, the WBFC method was a fairly useful pre-compliance test up to 350 MHz regarding radiated emission because conducted emission was dominating. The radiated emission from the PCB was maximum 4 dB above the radiated emission predicted by the WBFC method. From 400 MHz and up radiation from the PCB itself was dominating and the WBFC method was of no use.

Paper B

Study of the Impact of Board Orientation on Radiated Emissions due to Common Mode Currents on Attached Cables, Electromagnetic Compatibility (EMC), *Electromagnetic Compatibility (EMC), 2016 IEEE International Symposium on, Jul 2016*

Motivation
Common-mode current on attached cables is a typical source for radiated emission. Several models have been made for conversion of the intended differential signal on a PCB to unwanted common-mode current on cables. For an electrical short microstrip, it is possible to distinguish between voltage driven and current driven common mode radiation by changing the voltage, the source impedance and the load impedance. However, as the trace length approach $1/10\ \lambda$ the methods fail. All models assume that it is possible to describe common mode emission by lump element models.

Paper
This paper present a method for identifying the radiation sources arising from a long microstrip by dividing the microstrip into electrical short traces with phase shift. The method was used to investigate radiated emission from the microstrip test board.

Main Results
By help of the proposed method, it was possible to distinguish between current and voltage driven common mode radiation caused by a 12 cm long microstrip. The method was used to show that radiated emission caused by common-mode current on attached cables is quite complex - even with a simple structure. It was shown that the maximum radiated emission differed up to 10 dB depending on the orientation of the traces. Voltage-driven sources had the highest radiation with traces facing up, while the current-driven sources had highest radiation with the traces facing down. This effect was confirmed by measurement. Hence the complexity of common mode emission cannot be fully described by lumped elements models.

Paper C

Analysis and Measurement Investigation of the Workbench Faraday Cage Method, IEC 61967-5, *Submitted to IEEE Transactions on Electromagnetic Compatibility, September 30, 2018*

Motivation
Paper A presented a preliminary investigation of the Workbench Faraday Cage Method. Maximum radiated emission from the test PCB was not more

than 4 dB larger than the maximum radiated emission predicted by the WBFC method. Whether paper A's conclusions are representative for contemporary PCB's used in electronic apparatus is the subject of this paper.

Paper
By help of simulations of the test PCB, the theoretical background for the method was analyzed. A power supply, two digital boards with micro controllers and ICs were measured by the WBFC method and compared with radiated emission measurements in a 3 m semi anechoic chamber.

Main Results
Except for PSU noise, the WBFC method fails as a precompliance test. Both in the simulations and measurements, there was a poor agreement between the radiated emission predicted from the WBFC and the actual radiated emission. At low frequencies, the WBFC tends to overestimate the radiated emission because of electrically short cables in the 3 m SAC measurements, but as the frequency increases, WBFC increasingly underestimates the radiated emission. The difference was explained by simulations that showed that the Faraday cage strongly affects the electric, magnetic, and direct coupling from a microstrip to the termination. However, there was a good agreement between the trends in the WBFC and 3 m SAC for PSU noise. The PSU noise source coupling is different from the microstrip coupling.

4.2 Direct Radiated Emission

Paper D

Perturbation of Near-field Scan from Connected Cables, *Electromagnetic Compatibility (EMC), 2012 IEEE International Symposium on, Aug 2012*

Motivation
Cables represent both a low-practically and a theoretically challenge in near-field scan. Low-practically, it is difficult to measure the tangential components of the near-field on the side where the cables are running out of the Huygens' box, (i.e., it is difficult to avoid collision between probe and cables.) Theoretically, attached cables will cause pertubation of the measured near-field. The question is whether it is possible to predict maximum radiated emission of a HB with cables but measured without cables.

Paper
A Huygens' box around the microstrip test PCB was extracted in CST and compared with a Huygens' box of same PCB with attached cables. A near-field to far-field transformation was made based on the different Huygens

Boxes and compared with a simulation of the physical model.

Main Results
If the Huygens' box is extracted with cables present in the same configuration as the final apparatus, it is theoretically possible from the surface equivalence principle to predict the radiated far-field also at cable resonances. However, it requires that the near-field can be measured very close to the cables. Away from the cable resonance frequencies, where direct emission from the PCBs dominates, a connected cable also causes perturbation of the near-fields, but the perturbation of near-field does not influence the far-field prediction. So for direct radiated emission from a PCB with cables, it is possible to make near-field to far-field transformation based on a Huygens' box measured without cables.

Paper E

Estimate on the Uncertainty of Predicting Radiated Emission from Near-field Scan Caused by Insufficient or Inaccurate Near-field Data: Evaluation of the Needed Step Size, Phase Accuracy and the need for all Surfaces in the Huygens' Box, *Electromagnetic Compatibility (EMC EUROPE), 2012 International Symposium on*, Sept 2012. (Nominated for best conference paper prize)

Motivation
Near-field scan on a Huygens' box can be used to predict the maximal radiated emission from a PCB. The objective of the work presented in this article is to estimate the importance of measurement step size, the need of all 6 surfaces, and accuracy of the phase representation.

Paper
With the purposes of increasing the credibility of the investigation's conclusions, a cross verification with two different structures simulated with two different numerical tools was carried out. The significance of step size and phase accuracy, as well as the importance of a full Huygens' box was investigated. CST Microwave Studio, which is based on Finite Integration Technology, was used to simulate the microstrip test board. EMCoS, which is based on Method of Moment, was used to simulate a scaled IC.

Main Results
The investigations showed that step size must be below $\frac{\lambda}{2}$. The near-field to far-field transformation is very robust for random phase noise. Even $\pm$ 15° random noise causes less than 1 dB error. The near-field to far-field transformation is also very robust to systematic phase shift. Also 30° across the PCB

causes less than 1 dB error. It was shown that it is very important to measure the E- and H-field phase with same reference. A phase shift between E- and H-field could cause up to 5 dB error. The results indicated that all 6 surfaces are needed. If only top surface was measured, there was several dB's underestimation of the maximal radiated emission – especially for frequencies below 300 MHz. However, the larger the scanning areas, the less error occurs.

Paper F

How to Handle a Huygens' Box Inside an Enclosure, Electromagnetic Compatibility (EMC), 2013 IEEE International Symposium on, Aug 2013, pp. 802–807

Motivation
Previous work has shown that it is possible in simulations of far-fields to replace PCBs with a HB representation obtained from a near-field scan. However, the surface equivalence theorem requires that the environment outside HB is the same in the near-field scan and in the apparatus. This is seldom the case in common types of apparatus. PCBs are often placed inside metal enclosures like racks and these enclosures can both attenuate the radiated emission and increase the maximum radiated emission because of resonances. Hence a simple near-field to far-field transformation is not useful as a precompliance test. This paper discusses how to handle a HB inside typical enclosures.

Paper
This paper investigates the error in the predicted far-field when a HB from a "free space" near-field scan is used inside an enclosure, that was not present when the near-field scan was carried out. In addition, how to reduce these far-field prediction errors was also investigated. The predicted far-field from the free space Huygens' box was compared with a full wave simulation of the physical model. The comparison was carried out for both the scenario where the PCB was floating inside the enclosure and the scenario where the PCB was galvanic connected to the enclosure. The simple microstrip test board was simulated with and without galvanic connections to ground in two different enclosures. A narrow box (only 20 mm high) open in one end as well as a larger more open box mimicking a loud speaker were used in the investigations.

Main Results
The paper showed that such replacement can cause a significant error in the far-field prediction. However, these errors can be almost removed if the main features of the PCB are included in the HB. Best results were obtained if both the ground plane and the substrate were included. Still, if there are other

sources of rescattering, ground plane and substrate may not be sufficient. If the model of the structure is converging to the full original model, excluding the sources, then the error can be made almost negligible and theoretically zero.

Paper G

Review of the Huygens' Box Method with Different Sources Near Obstacles, Submitted to IEEE Transactions on Electromagnetic Compatibility, September 30, 2018

Motivation
Paper F showed a HB replacement could cause a significant error in the far-field prediction, however these errors were below 2 dB, if the ground plane and dielectric of the PCB were included in the HB. In paper F, the method was validated with only one PCB and two enclosures. The method's success must have further rigorous testing to validate the results and make a trustworthy conclusion.

Paper
With the purpose of gaining better understanding of the method and especially its limits, the method was tested with several combinations of PCBs and environments. Three different types of boards were tested including the simple micrrostrip PCB, a PCB with plane resonances, and a PCB mimicking an IC. The models in previous work have predicted maximum far-field with less than 2 dB error, except for a few frequencies with strong resonances, so focus in this study was to search for the method's limitations.

Main Results
The results indicate, that generally, the HB method itself only introduces small errors (less than 1 dB) if the environment does not have strong resonances. The results also indicate that the far-field errors increase with the Q-factor of the resonances. The method finds a limit when the far-field are predicted from PCBs, with plane resonances, places in a resonant environment. In that case, the unacceptable far-field errors are not restricted to a few resonance frequencies.

4.3 Measurement Related

Paper H

Recent Developments in Using Measured Sources in Computational EMC, Antennas and Propagation (EuCAP), 2015 9th European Conference on, April

2015, pp. 1–5

Motivation
EuCAP had an special session on using measured sources in simulations. The authors were invited to give a perspective on the topic from an EMC point of view and an overview of recent developments in using measured sources in computational EMC. It is very time-consuming to measure both E- and H-fields on all 6 surfaces and, in addition, it is difficult to make a precise tangential E-field probe.

Paper
The paper starts with an overview of the development in using measured sources in EMC and gives a description of the Bang & Olufsen in-house scanner. It was investigated whether it is possible to predict far-field from measured H-field on the top and bottom surfaces only. The investigation was based on simulation and measurements of a simple PCB and measurement of a real signal board. The HB was filled with perfect magnetic conductor in order to compensate for the missing E-fields.

Main Results
There was a very good agreement between simulated and measured near-field 10 mm above the simple microstrip PCB, both regarding amplitude and phase. The evaluation based on a simulation of a simple PCB with a microstrip showed good results. Only 1-2 dB error was introduced, if the simulations were based on only the H-field at top and bottom of the PCB. The distance from PCB edge to scan area edge must be more than 40 mm, otherwise the fields on the side of the HB are still significant. The evaluation based on a measurement and a simulations of a real signal board showed poor to fair results. One possibility is that the scan areas were insufficient, or that the E-field and not the H-field was dominating, or that the phase on the bottom of the PCB was measured incorrectly relative to the phase on top of the PCB.

Paper I

Design of TEM Transmission Line for Probe Calibration up to 40 GHz, *Electromagnetic Compatibility (EMC), 2018 IEEE International Symposium on*, Jul 2018

Motivation
With the ongoing development of 5G wireless communication, frequencies as high as 40 GHz have become relevant for EMI near-field scanning. Previous work has shown that referring a measured voltage to the known fields of a 50 Ω transmission line is an effective method for calculating the probe factor.

A pure TEM mode is convenient for calibration since pure TEM is frequency independent and the field components are well defined, and that is needed for characterization of unwanted field coupling.

Paper
This paper goes through the design process of two transmission lines in air, i.e., homogeneous dielectric. The first method was a rod above a ground plane. The second method was an easier to manufacture air trace. S11 and S21 of both structures were simulated and compared with measurements.

Main Results
Simulations and measurements show that it is possible to obtain almost pure TEM, but reflections and loss increase while the frequency approaches 40 GHz. This can be improved by decreasing the PCB thickness. The design study also made it clear that every physical detail must be included in the simulation in order to obtain good agreement. This is very important since the calibration method strongly depends on reliable simulations.

4.4 Emission Source Microscopy

Paper J

Analysis of the Effect on Image Quality of Different Scanning Point Selection Methods in Sparse ESM, Accepted for publication in IEEE Transactions on Electromagnetic Compatibility, August 2^{th} 2018.

Motivation
Sparse Emission Source Microscopy is an efficient method to identity radiating sources from 5 GHz and up. A basic understanding of how the selection of measurement points affects image quality is required in order to make efficient sparse emission source microscopy with a low noise reconstructed image.

Paper
With the purpose to demonstrate the effect of scanning height, sampling rate and selection of measurement points on the image quality, a simple 1.4 mm two layer PCB with a few sources of radiation was simulated. The PCB had an 100 mm $\times$ 100 mm unbroken ground plane with two 20 mm long 50 Ω micro strips and a 20 mm $\times$ 20 mm metal box similar to a heat sink. By the simulated example and mathematical arguments, the effect of sampling rate vs. scanning height caused by 2D DFT was visualized.

Main Results

In a typical measurement setup, it is possible to go far below spatial Nyquist sampling rate because the spatial aliasing created is folded outside the area of interest. In the example where the distance between the sources were small compared to the distance to the measurement plane, measurement points on a lower plan could be projected to a higher plane given the same reconstructed image in the area of interest despite going sub-Nyquist. Contrary to observations in other research areas, uniform selection of measurement point is superior to nonuniform selection as aliasing away from the DUT does not effect the diagnosing of radiating sources. Previously, it has been suggested that an operator of a hand held scanner can make intelligent choices based on the real time reconstructed image, but the results of the study indicate that this is not possible as long as uniform 2D DFT is used. Regardless of the criteria for extra point selection, it seems that clustering of measurement points degrade the image quality.

5 Discussion

The work presented in this thesis has been made with the purpose to precompliance test on module level. Radiated emission from modules can be divided in to common mode emission from cables and direct emission from modules. Depending on PCB size, the transition from common mode emission to direct emission happens between 200 MHz and 400 MHz. The two radiation mechanisms are different and need different evaluation methods. Based on decades of use of the Workbench Faraday Cage at Bang & Olufsen and approved as IEC standard, the hypothesis was that this method would fulfill the requirements for common mode emission. For direct emission it has been investigated whether it is possible to used near-field scan as source for simulations. Both theoretical challenges and practical challenges has been investigated mainly by numerical methods.

In addition to the precompliance test, the thesis also looks into Emission Source Microscopy which is a method for identifying sources for radiated emission above 5 GHz.

5.1 Common Mode Emission

The ambition has been to find a method that can do precompliance test at module level early in an industrial development project before cabling is defined. IEC 61967 provide 5 methods for measurement of electromagnetic emissions from integrated circuits. The workbench Faraday cage method model the IC and the rest of the PCB as a noise generator and the attached cables as lumped elements. Hence it should be possible to measure the noise generator with 150 Ω load in the Faraday cage. A simple microstrip PCB has been used throughout the project as representative for a digital printed circuit board. The theoretical analysis showed that this assumption simplifies the physical world too much. In addition the simulations showed that the Faraday cage affects the coupling from microstrip to termination in the cage. The measurement campaign where one PSU and two digital boards were measured could not validate the method. The coupling mechanism are not the same when the module is placed in the WBFC with 150 Ω lump element load as when the module is placed in a setup with attached cables. Especially voltage driven common mode emission cannnot be modeled in a WBFC because of the disturbance from the Faraday cage.

However, there was a good agreement between the trends in the WBFC and 3 m SAC for PSU noise. The PSU noise source coupling is different from the microstrip coupling.

It was possible to distinguish voltage and current driven common mode emission for the 120 mm long simple microstrip PCB. However, the fact that maximum radiated emission differed up to 10 dB depending on the orienta-

tion of the traces shows that common mode emission is complex and only to some extend can be predicted by simple generator / lumped element methods.

5.2 Direct Emission

The very ambitious goal is to predict radiated emission of an apparatus configured of several modules based on near-field scan. Theoretically, if all 4 tangential components of the near-field on a box surrounding the module is known, the field outside the box is also known. This works in free space. Modules are not mounted in free space inside apparatus. Enclosures, nearby cables, chassis etc. can change the maximum radiated emission from a module tenths of dB compared to the module in free space, so the objective is to be able to predict the maximum radiated emission with the obstacles present. But if a Huygens' box measured in free space is used as source for simulation, this project work shows that the result can be several dB off.

According to an inverse version of the induction theorem, the field outside the box can be accurate predicted, if the full PCB is included in the Huygens' box. Including the full PCB inside the Huygens' box will in most cases be impossible and there would be no reason to measure the near-field, if the full PCB layout anyway should be included in the simulations. The simulated setups show, that if ground plane and substrate are included in the Huygens box, maximum radiated emission, in many cases, can be predicted with a few dB uncertainty. The cases include a nearby cable, a half open box and a narrow box. The limitations seems to be very resonance systems where for example highly resonant structures are placed inside a narrow enclosure. Also PCB with ground fill can in extreme cases be problematically. Finally it should be mentioned that if the ground plane is a part of the resonance, it is also necessary to include vias in the Huygens' box in order to induce the correct resonances.

On top of this theoretically challenges with the Huygens' box nearby obstacles there is off course the challenge to obtain reliable measurement results. Attached cables to required auxiliary equipment will make it difficult to scan all 6 surfaces, and there will be measurements uncertainty. Based on free space near-field to far-field transformation, the work shows that the methods is robust to both random and systematic phase shift caused by measurement inaccuracy. Even 45° random phase shift causes only a few dB error. But the magnetic field and electric field phase must be locked.

In order to reduce measurement time, measurements can be reduced to only top and bottom surface. The induced error because of this approximation can be reduced by increasing the scanning area. Hence the field on the omitted sides of the Huygens' box becomes weak and does not contribute much to the radiation. Theoretically it is possible to only measure the H-

field (or E-field) and then fill up the Huygens' box with perfect magnetic (electric) conductor. In practices this will require really good probes that reject unwanted fields and the measurement equipment must have a large dynamic range. A challenging example could be a PCB with a low voltage, high current trace and an IC with a heat sink. In that case the probe should be capable of measuring both the strong magnetic field above the microstrip and the weak magnetic field close to the heat sink while it rejects the strong E-field from the heat sink.

If it is required to place features from the PCB inside the Huygens' box because of scattering, it should be possible first to fill the Huygens' box with perfect magnetic conductor, then calculate / simulate a tiny larger Huygens box with magnetic currents, remove the perfect magnetic conductor and place the required PCB features inside the new Huygens' box.

5.3 Measurement Related

An in-house scanner was constructed by help of a six axis robot and a four channel 4 giga samples oscilloscope. The functionality of the scanner was controlled by comparing the magnetic near-field 10 mm above the PCB with simulations. As an experimental investigation of the Huygens' box method, an audio signal board was magnetic near-field scanned on top and bottom surface only. The predicted maximum radiated emission in 3 m distance differed up to 6 dB from the field measured in a 3 m semi anechoic chamber. Same experiment with only magnetic near-field on top and bottom was also done by help of CST simulations of the simple microstrip PCB. The maximum deviation between maximum radiated emission from a full model simulation and a Huygens' box simulations was only 1-2 dB.

The experimental validation show the importance of reliable near-field measurements. E.g., if the probe calibration is off a couple of dB, the predicted far-field will also be off. A strong E-field could couple to the H-field probe and cause false electrical currents on the Huygens' box. In order to exclude probe effects on the far-field prediction, it is important to make a correct probe calibration that gives correct probe factor and reveal in which frequency span the probe has large enough unwanted field rejection. Scanning a true TEM tranmission line can be one way to calibrate the probe and characterize the unwanted field coupling. Because of inhomogeneous dielectric, a co-planar waveguide will have non TEM-mode and it is not possible to determine whether an Hx loop probe measure the Hy-field or the Ex field.

With the in-house scanner the man hours needed to do a six surfaces phase resolved near-field scan did not commensurate with the outcome, so the method has not been implemented in everyday practice, but 3D scanners automatically measuring a full Huygens' box are now commercial available. However, a spin off has been that near-field scan at Bang & Olufsen nowadays

are used both qualitative and quantitative in the EMC architecture design.

5.4 Emission Source Microscopy

If a module fails the Huygens' box precompliance test, it helps the design engineer to mitigate the problem if the sources becomes visible. Emission source microscopy is closely related to near-field scan but typically the measurements are performed further away from the PCB compared to near-field scan. The measured field is Fourier transformed to the plane wave spectrum and back-propagated to the source plane. Eventually evanescent waves are nullified, and the inverse Fourier transform at the source plane reveal the radiating sources. Researchers refer to Nyquist sampling rate, i.e. stepsize shorter than $\frac{\lambda}{2}$ without further discussion. The thesis shows that the scanning method can be optimized with a little background knowledge. It is possible to do sparse sampling with a step sizes much longer than $\frac{\lambda}{2}$ on the expense of aliasing. But the spatial aliasing created is folded outside the area of interest and does no harm. Hence the number of measurement points can be reduced significantly. There is no theoretically limits on the scanning height, so the backpropagation method can be applied to a traditional near-field scan. However, the resolution is limited by the aperture angle, so a large scanning area exceeding the EUT is required.

6 Conclusion

The thesis describes methodS to do precompliance test at module level. Radiated emission was divided into two primary mechanisms: Common mode emission from attacbed cables and direct radiated emission from printed circuit boards. Based on decades use of Workbench Faraday Cage (IEC 61967-5) for precompliance test of printed circuit boards at Bang & Olufsens, this methods was chosen for the common mode emission. The presented work shows that the method does not have a strong theoretical background and the measurement validation was also poor– except for the amplifier test case. Common mode emission is rather complicated and a lumped element model is not enough.

The thesis gives a proof of concept for using measured near-field scan as source for simulation. If main features of the PCB responsible for scattering are included in the Huygens' box, it is possible to do near-field scan in free space and then use the measured near-field as source for simulations. Determination of what is main features regarding scattering must rely on electromagnetic understanding and experience, but ground plane and substrate are a good starting point. The method is robust to random or systematic phase inaccuracy, however, phase lock between H- and E-field is important.

It is possible to approximate the Huygens' box by measuring only top and bottom on the expense of a few dB's error in maximum radiated emission. It has only been tested with free space near- to far-field and it is a topic for further investigation how much error the approximations introduce nearby obstacles.

The measured attempt to use the Huygens' box method made it clear, that making reliable near-field scan, including reliable probe calibration, is a complex high-tech problem in itself.

Emission source microscopy can reveal the radiating sources above 5 GHz. It is possible to go below Nyquist sampling because the spatial aliasing is folded outside the area of interest.

The thesis partly confirmed the concept of precompliace test of direct radiated emission at module level but in order to make it profitable in industry, it requires more automation in the near-field measurement procedure.

Although the objective with precompliance test is only partly fulfilled, the obtained background knowledge has helped EMC engineers at Bang & Olufsen and the other consortium members with faster and more secure EMC design.

References

[1] CISPR, "CISPR 32:2015 Electromagnetic Compatibility of Multimedia Equipment - Emission Requirements," Standard, 2015.

[2] FCC, "C63.4-2014," Standard, 2014.

[3] J. L. Drewniak, T. H. Hubing, and T. P. V. Doren, "Investigation of fundamental mechanisms of common-mode radiation from printed circuit boards with attached cables," in *Proceedings of IEEE Symposium on Electromagnetic Compatibility*, Aug 1994, pp. 110–115.

[4] J. L. Drewniak, F. Sha, T. P. V. Doren, T. H. Hubing, and J. Shaw, "Diagnosing and modeling common-mode radiation from printed circuit boards with attached cables," in *Proceedings of International Symposium on Electromagnetic Compatibility*, Aug 1995, pp. 465–470.

[5] T. Hubing, "Printed circuit board EMI source mechanisms," in *Electromagnetic Compatibility, 2003 IEEE International Symposium on*, vol. 1, Aug 2003, pp. 1–3 vol.1.

[6] S. Deng, T. Hubing, and D. Beetner, "Estimating maximum radiated emissions from printed circuit boards with an attached cable," *Electromagnetic Compatibility, IEEE Transactions on*, vol. 50, no. 1, pp. 215–218, Feb 2008.

[7] G. Dash, J. Curtis, and I. Straus, "The "current driven model" -experimental verification and the contribution of I_{dd} delta to digital device radiation," in *Electromagnetic Compatibility, 1999 IEEE International Symposium on*, vol. 1, 1999, pp. 317–322 vol.1.

[8] D. Hockanson, J. Dreniak, T. Hubing, T. Van Doren, F. Sha, and C.-W. Lam, "Quantifying EMI resulting from finite-impedance reference planes," *Electromagnetic Compatibility, IEEE Transactions on*, vol. 39, no. 4, pp. 286–297, Nov 1997.

[9] H.-W. Shim and T. H. Hubing, "Model for estimating radiated emissions from a printed circuit board with attached cables due to voltage-driven sources," *IEEE Transactions on Electromagnetic Compatibility*, vol. 47, no. 4, pp. 899–907, Nov 2005.

[10] S. Deng, T. Hubing, and D. Beetner, "Characterizing the electric field coupling from IC heatsink structures to external cables using TEM cell measurements," *Electromagnetic Compatibility, IEEE Transactions on*, vol. 49, no. 4, pp. 785–791, Nov 2007.

[11] C. Su and T. H. Hubing, "Calculating radiated emissions due to I/O line coupling on printed circuit boards using the imbalance difference method," *IEEE Transactions on Electromagnetic Compatibility*, vol. 54, no. 1, pp. 212–217, Feb 2012.

[12] K. Kaiser, *Electromagnetic Compatibility Handbook*, ser. Electrical engineering handbook series. Taylor & Francis, 2004. [Online]. Available: https://books.google.com/books?id=nZzOAsroBIEC

[13] J. S. Pak, H. Kim, J. Lee, and J. Kim, "Modeling and measurement of radiated field emission from a power/ground plane cavity edge excited by a through-hole signal via based on a balanced TLM and via coupling model," *IEEE Transactions on Advanced Packaging*, vol. 30, no. 1, pp. 73–85, Feb 2007.

[14] H.-W. Shim and T. H. Hubing, "A closed-form expression for estimating radiated emissions from the power planes in a populated printed circuit board," *IEEE Transactions on Electromagnetic Compatibility*, vol. 48, no. 1, pp. 74–81, Feb 2006.

[15] R. G. Kaires, "Radiated emissions from printed circuit board traces including the effect of vias, as a function of source, termination and board characteristics," in *1998 IEEE EMC Symposium. International Symposium on Electromagnetic Compatibility. Symposium Record (Cat. No.98CH36253)*, vol. 2, Aug 1998, pp. 872–877 vol.2.

[16] A. M. Sayegh and M. Z. M. Jenu, "Prediction of radiated emissions from high speed PCB traces using travelling wave antenna model," in *2014 IEEE Asia-Pacific Conference on Applied Electromagnetics (APACE)*, Dec 2014, pp. 91–94.

[17] R. Georgerian and M. I. Montrose, "Product safety and the heat sink - dilemma of minimizing radiated emissions and maximizing thermal cooling," in *2003 IEEE Symposium on Electromagnetic Compatibility. Symposium Record (Cat. No.03CH37446)*, vol. 1, Aug 2003, pp. 134–137 vol.1.

[18] M. I. Montrose and E. X. Liu, "Radiated emission effects from multiple via stimulation within a printed circuit board," in *2008 Asia-Pacific Symposium on Electromagnetic Compatibility and 19th International Zurich Symposium on Electromagnetic Compatibility*, May 2008, pp. 176–179.

[19] M. van Doorn, "Radiated emission from signal traces changing reference planes," in *2014 International Symposium on Electromagnetic Compatibility*, Sept 2014, pp. 709–712.

[20] J. H. G. J. L. Rotgerink, H. Schippers, and J. Verpoorte, "Multi-conductor transmission line modelling of transfer impedance measurement methods," in *2017 International Symposium on Electromagnetic Compatibility - EMC EUROPE*, Sept 2017, pp. 1–7.

[21] F. Han, "Radiated emission from shielded cables by pigtail effect," *IEEE Transactions on Electromagnetic Compatibility*, vol. 34, no. 3, pp. 345–348, Aug 1992.

[22] M. Liu, J. Wang, and X. Wu, "Analysis of the radiation from a pigtail-terminated coaxial cable using the imbalance difference model," in *2016 Progress in Electromagnetic Research Symposium (PIERS)*, Aug 2016, pp. 2179–2183.

[23] J. Xu, G. Liu, and Z. Yu, "A fast method for measuring transfer impedance of bus connectors," in *2009 3rd IEEE International Symposium on Microwave, Antenna, Propagation and EMC Technologies for Wireless Communications*, Oct 2009, pp. 754–757.

[24] X. He, T. Hubing, H. Ke, N. Kobayashi, K. Morishita, and T. Harada, "Calculation of optimal ground post resistance for reducing emissions from chassis-mounted printed circuit boards," *IEEE Transactions on Electromagnetic Compatibility*, vol. 53, no. 2, pp. 475–481, May 2011.

[25] H. Funato and T. Suga, "An investigation on the reduction technique of radiated emission from chassis with PCB," in *2008 IEEE International Symposium on Electromagnetic Compatibility*, Aug 2008, pp. 1–6.

[26] ——, "A study on correlation between the PCB layout and EMI from chassis," in *2007 IEEE International Symposium on Electromagnetic Compatibility*, July 2007, pp. 1–5.

[27] "IEC 61967, Integrated Circuits - Measurement of Electromagnetic Emissions, 150 kHz to 1 GHz," Standard, 2005.

[28] M. Coenen, "EMC workbench: Testing methodology, module level testing and standardization," *Philips Journal of Research*, vol. 48, 1994.

[29] ——, "Common mode impedance measurements on cables in the frequency range 30 MHz – 1 GHz," *EIE92004, Philips Semiconductor*, 1994.

[30] S. Okuyama, K. Osabe, K. Tanakajima, and H. Muramatsu, "Investigation on effectiveness of very high frequency line impedance stabilization network (VHF-LISN) for measurement reproducibility," in *2013 International Symposium on Electromagnetic Compatibility*, Sept 2013, pp. 174–179.

[31] K. Osabe, N. Kuwabara, and S. Okuyama, "Termination impedance for AC mains cable leaving from EUT area in radiated emission measurement," in *2017 International Symposium on Electromagnetic Compatibility - EMC EUROPE*, Sept 2017, pp. 1–6.

[32] CISPR, "CISPR 16-4-2 Measurement Instrument Uncertainty, 2015,," Standard, 2015.

[33] H. D. Bruns, C. Schuster, and H. Singer, "Numerical electromagnetic field analysis for EMC problems," *IEEE Transactions on Electromagnetic Compatibility*, vol. 49, no. 2, pp. 253–262, May 2007.

[34] A. Tsaliovich, *"Electromagnetic Shielding Handbook for Wired and Wireless EMC Application*, ser. The Springer International Series in Engineering and Computer Science. Kluwer Academic Publishers, 1999.

[35] A. C. Scogna and M. Schauer, "EMC simulation of complex PCB inside a metallic enclosure and shielding effectiveness analysis," in *2007 18th International Zurich Symposium on Electromagnetic Compatibility*, Sept 2007, pp. 91–94.

[36] R. Rimolo-Donadio, X. Duan, H. D. Bruns, and C. Schuster, "Differential to common mode conversion due to asymmetric ground via configurations," in *2009 IEEE Workshop on Signal Propagation on Interconnects*, May 2009, pp. 1–4.

[37] M. I. Montrose, E.-P. Li, H.-F. Jin, and W.-L. Yuan, "Analysis on the effectiveness of the 20-H rule for printed-circuit-board layout to reduce edge-radiated coupling," *IEEE Transactions on Electromagnetic Compatibility*, vol. 47, no. 2, pp. 227–233, May 2005.

[38] A. C. Scogna and D. P. Johns, "Efficient methodologies to study the signal integrity of multi Gb/s interconnects and full system EMC," in *2009 IEEE International Symposium on Electromagnetic Compatibility*, Aug 2009, pp. 274–279.

[39] E.-P. Li, E.-X. Liu, L.-W. Li, and M.-S. Leong, "A coupled efficient and systematic full-wave time-domain macromodeling and circuit simulation method for signal integrity analysis of high-speed interconnects," *IEEE Transactions on Advanced Packaging*, vol. 27, no. 1, pp. 213–223, Feb 2004.

[40] W. D. Guo, G. H. Shiue, C. M. Lin, and R. B. Wu, "An integrated signal and power integrity analysis for signal traces through the parallel planes using hybrid finite-element and finite-difference time-domain techniques," *IEEE Transactions on Advanced Packaging*, vol. 30, no. 3, pp. 558–565, Aug 2007.

[41] T. Steinecke, D. Hesidenz, and E. Miersch, "EMI modeling and simulation in the IC design process," in *2006 17th International Zurich Symposium on Electromagnetic Compatibility*, Feb 2006, pp. 594–597.

[42] A. Barchanski, "Linking circuit simulation with full-wave solver for board-level EMC design," *IEEE Electromagnetic Compatibility Magazine*, vol. 4, no. 3, pp. 52–58, rd 2015.

[43] I. Kelander, M. Uusimaki, and A. N. Arslan, "EMC analysis on stacked packages," in *2006 17th International Zurich Symposium on Electromagnetic Compatibility*, Feb 2006, pp. 602–605.

[44] J. Shi, J. He, E. Chan, K. Slattery, J. Zhao, J. Fejfar, and F. Zanella, "Equivalent radiation source extraction method for system level EMI and RFI prediction," in *2008 IEEE International Symposium on Electromagnetic Compatibility*, Aug 2008, pp. 1–5.

[45] S. Kuehn, M. Wild, P. Sepan, E. Grobelaar, and N. Kuster, "Automated near-field EMC/EMI scanning system with active electro-optical field probes," in *2012 IEEE Electrical Design of Advanced Packaging and Systems Symposium (EDAPS)*, Dec 2012, pp. 109–112.

[46] S. Kühn, N. Kuster, M. Wild, E. Grobbelaar, P. Sepan, B. Kochali, A. Fuchs, and J. Lienemann, "Automated EMC/EMI near-field testbed," in *2014 International Symposium on Electromagnetic Compatibility, Tokyo*, May 2014, pp. 513–516.

[47] D. Deschrijver, F. Vanhee, D. Pissoort, and T. Dhaene, "Automated near-field scanning algorithm for the EMC analysis of electronic devices," *IEEE Transactions on Electromagnetic Compatibility*, vol. 54, no. 3, pp. 502–510, June 2012.

[48] T. Harada, N. Masuda, and M. Yamaguchi, "Near-filed magnetic measurements and their application to EMC of digital equipment," *IEICE Trans. Electron., C*, vol. 89, no. 1, pp. 9–15, jan 2006. [Online]. Available: https://ci.nii.ac.jp/naid/110003485780/en/.

[49] D. Baudry, C. Arcambal, A. Louis, B. Mazari, and P. Eudeline, "Applications of the near-field techniques in EMC investigations," *IEEE Transactions on Electromagnetic Compatibility*, vol. 49, no. 3, pp. 485–493, Aug 2007.

[50] G. Muchaidze, H. Wei, J. Min, S. Peng, J. Drewniak, and D. Pommerenke, "Automated near-field scanning to identify resonances," in *2008 International Symposium on Electromagnetic Compatibility - EMC Europe*, Sept 2008, pp. 1–5.

[51] X. Tong, D. W. P. Thomas, A. Nothofer, P. Sewell, and C. Christopoulos, "Reduction of sensitivity to measurement errors in the derivation of equivalent models of emission in numerical computation," in *IET 8th International Conference on Computation in Electromagnetics (CEM 2011)*, April 2011, pp. 1–2.

[52] Y. Vives-Gilabert, C. Arcambal, A. Louis, F. de Daran, P. Eudeline, and B. Mazari, "Modeling magnetic radiations of electronic circuits using near-field scanning method," *IEEE Transactions on Electromagnetic Compatibility*, vol. 49, no. 2, pp. 391–400, May 2007.

[53] M. Hernando, A. Fernandez, M. Arias, M. Rodriguez, Y. Alvarez, and F. Las-Heras, "EMI radiated noise measurement system using the source reconstruction technique," *Industrial Electronics, IEEE Transactions on*, vol. 55, no. 9, pp. 3258–3265, Sept 2008.

[54] Z. Yu, J. A. Mix, S. Sajuyigbe, K. P. Slattery, and J. Fan, "An improved dipole-moment model based on near-field scanning for characterizing near-field coupling and far-field radiation from an IC," *IEEE Transactions on Electromagnetic Compatibility*, vol. 55, no. 1, pp. 97–108, Feb 2013.

[55] J. Shi, M. Cracraft, J. Zhang, R. DuBroff, and K. Slattery, "Using near-field scanning to predict radiated fields," in *Electromagnetic Compatibility, 2004. EMC 2004. 2004 InternationalSymposium on*, vol. 1, Aug 2004, pp. 14–18 vol.1.

[56] H. Weng, D. G. Beetner, and R. E. DuBroff, "Prediction of radiated emissions using near-field measurements," *IEEE Transactions on Electromagnetic Compatibility*, vol. 53, no. 4, pp. 891–899, Nov 2011.

[57] X. Gao, J. Fan, Y. Zhang, H. Kajbaf, and D. Pommerenke, "Far-field prediction using only magnetic near-field scanning for EMI test," *Electromagnetic Compatibility, IEEE Transactions on*, vol. PP, no. 99, pp. 1–9, 2014.

[58] L. Foged, L. Scialacqua, F. Saccardi, F. Mioc, D. Tallini, E. Leroux, U. Becker, J. Araque Quijano, and G. Vecchi, "Bringing numerical simulation and antenna measurements together," in *Antennas and Propagation (EuCAP), 2014 8th European Conference on*, April 2014, pp. 3421–3425.

[59] F. S. de Adana, M. F. Cátedra, J. M. Gómez, R. Mittra, J. Berkowitsch, F. Gutiérrez, and M. Alfonsea, "A systematic approach for radiated system-level verification of unknown sources inside satellites from unit-level measurements," *IEEE Antennas and Propagation Magazine*, vol. 52, no. 2, pp. 71–85, April 2010.

[60] K. W. Kam, A. Radchenko, and D. Pommerenke, "On different approaches to combine cable information into near-field data for radiated-field estimation," *IEEE Transactions on Electromagnetic Compatibility*, vol. 56, no. 2, pp. 276–285, April 2014.

[61] "IEEE standard for calibration of electromagnetic field sensors and probes (excluding antennas) from 9 kHz to 40 GHz," *IEEE Std 1309-2013 (Revision of IEEE Std 1309-2005)*, pp. 1–111, Nov 2013.

[62] J. Zhang, K. W. Kam, J. Min, V. V. Khilkevich, D. Pommerenke, and J. Fan, "An effective method of probe calibration in phase-resolved near-field scanning for EMI application," *IEEE Transactions on Instrumentation and Measurement*, vol. 62, no. 3, pp. 648–658, March 2013.

[63] P. Maheshwari, H. Kajbaf, V. V. Khilkevich, and D. Pommerenke, "Emission source microscopy technique for EMI source localization," *IEEE Transactions on Electromagnetic Compatibility*, vol. 58, no. 3, pp. 729–737, June 2016.

[64] L. Zhang, V. V. Khilkevich, X. Jiao, X. Li, S. Toor, A. U. Bhobe, K. Koo, D. Pommerenke, and J. L. Drewniak, "Sparse emission source microscopy for rapid emission source imaging," *IEEE Transactions on Electromagnetic Compatibility*, vol. 59, no. 2, pp. 729–738, April 2017.

[65] P. Maheshwari, V. Khilkevich, D. Pommerenke, H. Kajbaf, and J. Min, "Application of emission source microscopy technique to EMI source localization above 5 GHz," in *2014 IEEE International Symposium on Electromagnetic Compatibility (EMC)*, Aug 2014, pp. 7–11.

[66] C. Paul, *Introduction to Electromagnetic Compatibility*, ser. Wiley Series in Microwave and Optical Engineering. Wiley, 2006. [Online]. Available: https://books.google.com/books?id=6P2Wyram310C.

[67] H. W. Ott, *Electromagnetic Compatibility Engineering*. John Wiley & Sons, Inc., aug 2009. [Online]. Available: https://doi.org/10.1002/9780470508510.

[68] P. Chatterton and M. Houlden, *EMC: Electromagnetic Theory to Practical Design*. Wiley, 1992. [Online]. Available: https://books.google.com/books?id=uHpxQgAACAAJ.

[69] M. Coenen and J. Goedbloed, *Electromagnetic Compatibility*. Mybusinessmedia, 2010. [Online]. Available: https://books.google.com/books?id=QYeHtgAACAAJ

Part II

Papers

Paper A

Assessment of the Usability of the Workbench Faraday Cage Method

Morten Sørensen[1,2], Ondrej Franek[1], Søren K. Christensen[2], Gert Frølund Pedersen[1], Hans Ebert[1]
[1]Antennas, Propagation and Radio Networking section, Aalborg University, Niels Jernes Vej 12, 9220 Aalborg, Denmark, {mos, of, gfp, heb}@es.aau.dk
[2]Bang & Olufsens a/s, Peter Bangs Vej 15, 7600 Struer, Denmark, skn@bang-olufsen.dk

The paper has been published in the *IEEE International Symposium on Electromagnetic Compatibility (EMC)*, Aug 2011, pp. 399–404.

Assessment of the Usability of the Workbench Faraday Cage Method

Morten Sørensen[#1], Ondrej Franek[#2], Søren K. Christensen[*3], Gert Frølund Pedersen[#4], Hans Ebert[#5]

Antennas, Propagation and Radio Networking section, Aalborg University,
Niels Jernes Vej 12, 9220 Aalborg, Denmark

[1] mos@es.aau.dk
[2] of@es.aau.dk
[4] gfp@es.aau.dk
[5] heb@es.aau.dk

[*] *Bang & Olufsens a/s, Peter Bangs Vej 15, 7600 Struer, Denmark*

[3] skn@bang-olufsen.dk

***Abstract*—The workbench Faraday Cage method (WBFC) is a time efficient module pre-compliance test regarding radiated emission. This work investigates the method's usability and credibility and concludes that for this particular case the WBFC perform a tolerable compliance test for frequencies below 360 MHz while it is essentially useless for higher frequencies.**

I. Introduction

Electrical engineers have for years been interested in performing pre-compliance tests regarding radiated emission on IC or PCB level. The international standard IEC 61967 "*Integrated circuits – Measurement of electromagnetic emissions, 150 kHz to 1 GHz*" describes five different methods for measuring conducted and radiated electromagnetic emissions from integrated circuits. Part 5 "*Measurement of conducted emissions – Workbench Faraday Cage method*" [1] (WBFC method) describes a method to measure the conducted electromagnetic emission of integrated circuits either applied on the standardized test-board or on a final printed circuit board (PCB).

The WBFC method is a time efficient method which allows the engineer to do trial and error work at his workbench, i.e. he can do some changes in e.g. the filtering and immediately get a figure of the effect regarding radiated emission by measuring in the WBFC. Therefore the method is widely used in private companies where the objective is to pass the radiated emission requirements as fast and cheapest as possible. Although the method was developed in the beginning of the nineties [2] and first edition of the standard is from 2003, there has been no scientific investigation of the method's usability and credibility.

In this paper, we investigate the mode of operation of the WBFC method. Based on some impedance considerations supported by measurements and simulations of a rather simple test setup, we show in which frequency span the method is useful and fairly credible and where, conversely it makes no sense to do measurement with the WBFC.

In section II the WBFC method is introduced and some impedance considerations are given. In Section III the test setup and simulations are described. The results are presented and discussed in Section IV. Finally Section V draws the conclusions.

II. The WBFC method

A. Sources of Radiation

In contemporary audio/video products switched circuits like switched-mode power supplies (SMPS) and digital circuits are the primary sources of unintentional radiated electromagnetic emissions from electronic products in the frequency span from 30 MHz to 1 GHz.

However, SMPS and digital circuits are most likely too small to radiate significantly on their own. In order to radiate fields strong enough to cause regulatory problems, power must be coupled from the small noise source to larger structures that act as antennas such as circuit board planes, heatsinks, cables or chassis.

The conducted emission depends on the filtering and in practice you need a full operational PCB in order to have a full operational IC with associated unintentional electromagnetic emission. Therefore it is the PCB's conducted emission the WBFC method measures rather than the IC's emission.

PCB's can radiate by itself (at high frequencies, from large planes or long traces) or by coupling to cables and surrounding structures. There are three modes of coupling:

- Conducted coupling,
- Electric field coupling,
- Magnetic field coupling.

Assuming that the WBFC measures the conducted coupling correctly, the usability of the WBFC method depends on whether the conducted coupling in a certain frequency span is dominating.

Another source of radiated emission is EMI leaky connectors and cables but these are not possible to measure with the WBFC. We also assume that the desired signal – single ended or differential – does not radiate. In this paper, we concentrate on the common mode noise.

B. The Workbench Faraday Cage Method

The WBFC method assumes that supply and signal cable(s) are attached to an electrically small PCB, with dimensions $<\lambda/2$, i.e. 0.15 m at 1 GHz. The hypothesis is that connected cables become the dominant antennas, so RF emission takes

place via these antennas. It is suggested that the maximum conducted emission carried by a wire emerging from DUT can be estimated by loading the common-mode port with 150 Ω resistance and measuring the absorbed power. 150 Ω is widely used in RF emission and immunity standards as average common mode impedance and the justification for this value as a representation for the radiation resistance of long cables arises from empirical data [3].

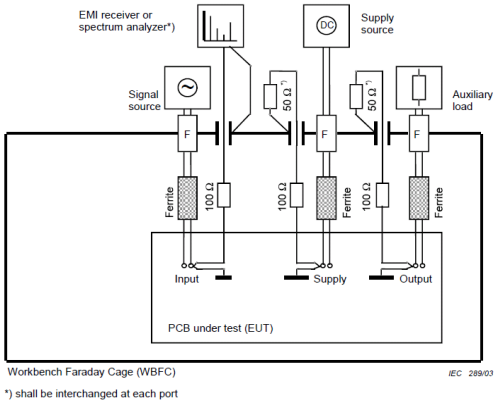

Fig. 1. Test setup for measuring emission with the WBFC [1].

The test setup is shown in Fig. 1. The PCB under test is placed on an insulating support 30 mm above the bottom plate. All functional connections, e.g. the power supply and auxiliary equipment, to the PCB under test are fed through dedicated filters mounted on the wall of the cage. All wires from these filters need to be wrapped on ferrite ring cores to create impedances much higher than 150 Ω at the frequencies of interest.

The assumption is that the worst case arises when the measured absorbed power in the load impedance (150 Ω) of the WBFC, in the final apparatus is radiated from a matched dipole. This assumption gives the following conversion between the limit for radiated emission in 3 m distance according to CISPR 13 and the voltage limit across 50 Ω in WBFC [2]:

$$V_{\mathrm{WBFC,\ limit}}\ [\mathrm{dB\mu V}] = E_{\mathrm{3m,\ limit}}\ [\mathrm{dB\mu V/m}] + 4.8\ \mathrm{dB} \quad (1)$$

C. Some Considerations About the Impedance

The purpose of using the Faraday cage is (with reference to the inventors [2]) only to shield the measurements from the irrelevant noise from outside. Under the assumption that the cage does not influence the measurements of the conducted emission it is reasonable to make a schematic of the equivalent circuit representing the EUT and the common-mode impedance as shown in Fig. 2. It is assumed that the source of the conducted emission inside the module has a form of non-ideal physical source with internal impedance in series (represented by the voltage source and Z_s in Fig. 2).

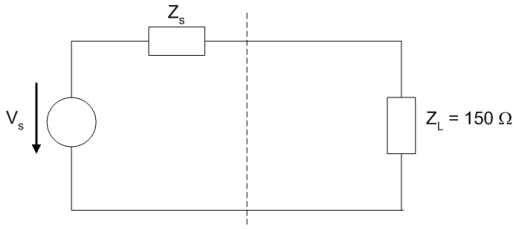

Fig. 2. Equivalent circuit representing the module and the common-mode impedance. The left side represents the EUT with a common mode noise source and the right side represents the 150 Ω load that we measure on.

The 150 Ω common-mode impedance forms the load impedance, Z_L, of this source for the particular connection that we want to measure. In addition to the 150 Ω load impedance, Z_L includes also the impedance of the return path, i.e. all the others 150 Ω connection terminations in parallel with the impedance between the EUT and the WBFC (see Fig. 1), so in practice Z_L in Fig. 2 can be higher than 150 Ω.

It is well-known that maximum transfer of power occurs when the source and the load impedances are matched

$$Z_S = Z_L^* \quad (2)$$

while all other combinations result in non-optimal transfer.

The objective of a module test such as the WBFC method is to perform a modular pre-compliance test, i.e. the WBFC must predict the worst case in order to be sure to pass the final test, when the module is placed in the apparatus. To fulfil the worst case assumption we must actually assume that a) the common-mode load impedance in the apparatus is always 150 Ω, or b) the internal impedance of the source (Z_S in Fig. 2) is equal to 150 Ω and unchanged when you move the PCB from the Faraday cage to the apparatus. In the first case, if we use the 150 Ω load as suggested by the standard, then we measure the same power as in real situation (because it is assumed always to be 150 Ω) and the measurement is therefore representative and valid. In the second case, we allow the common-mode impedance in the apparatus to vary from 150 Ω, but we assume that the internal impedance, Z_s, is fixed to 150 Ω, and so measuring with Z_L = 150 Ω results in the best matching cf. (2) and, consequently, the upper bound of power transfer.

But what if the source and load impedances are both other than 150 Ω? Then, with 150 Ω load, we measure less power than may actually be emitted. This situation is quite likely to happen, because the internal source of emission may be similar to a voltage source (low internal impedance) and the cable running outside of DUT will often be close to the ground plane (low characteristic impedance, low load). These low impedances will likely be better matched and allowing for higher power coupling than with the 150 Ω load. The WBFC method will then show lower than maximum power.

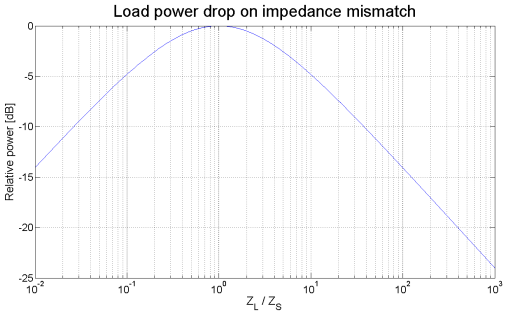

Fig. 3. Load power drop on impedance mismatch.

Let us assume, for simplicity, that both the source and the load impedances are real. If the load impedance happens to be the same as the internal impedance of the source ($Z_L = Z_S$), then the power measured on such load is indeed the maximum possible. However, when the load impedance is, e.g. ten times higher (or lower) than the internal impedance of the source, the measured power will be 5 dB lower (see Fig. 3). This means that if we do not measure the output power on the same impedance as the internal impedance of the source, the estimated power will always be lower than what the source could actually deliver.

D. Radiater directivity

The directivity of the radiating element (antenna), be it the cable itself or another structure it couples to (e.g. the chassis), is assumed as that of a matched dipole by the standard. This might be sufficient approximation for most of the situations, although higher directivity is theoretically possible. The most likely radiating elements are wires and slots in the chassis. Slots behave similarly to wires and dipoles, but they can occur in rows, increasing the overall directivity. A high directivity can cause the situation where a module passes the WBFC test but fail the radiated emission when placed in the final apparatus.

III. The Experimental Setup

A. The Objective of the Experiment

It emerges clearly from the impedance and directivity considerations that there is a lot of sources of error when you want to compare measurements in the WBFC and measurements in a 3 m semi anechoic (3 m SAC). Is the common mode impedance 150 Ω in the apparatus? Is the return path impedance low in the WBFC? Does the apparatus radiate with a high directivity? In addition, the WBFC is of no use if the dominating coupling is via electric and/or magnetic fields or if the PCB radiates by itself. Many questions arise and, as a result, some engineers and scientist question the usefulness and credibility of the method. A simple test setup was made with the purpose of investigating the considerations mentioned in the first two sections.

B. The Test Setup

A comb generator with fundamental frequency of 20 MHz and a flat frequency response up to 1 GHz was used as a noise generator. It was mounted on the back of a 150 x 225 mm PCB with a 120 mm long, 50 Ω micro strip, terminated with 4 parallel 200 Ω resistors. The common mode noise on the PCB ground was measured in the WBFC. Next, the radiated emission from the PCB with an 80 cm angled cable soldered to the PCB ground was measured. With the purpose of distinguishing conducted coupling and field coupling it was also measured with no galvanic connection between the cable and the PCB ground.

With the purpose of estimating the common mode source impedance the current through the cable connection to the PCB was measured, see Fig. 5.

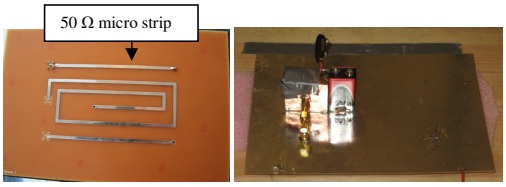

Fig. 4. The PCB and the comb generator used in the experiment.

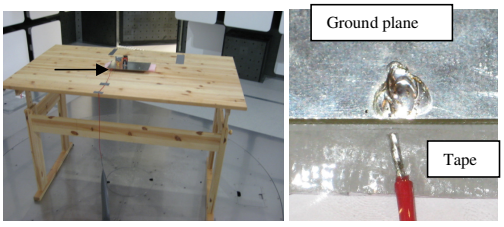

Fig. 5. The test setup in the 3 m semi anechoic chamber and a close-up photo of the setup with no galvanic contact between the cable and the PCB. In addition the current through the cable connection (marked by the arrow) was measured with a current probe.

C. The Simulations

With the purpose of understanding the measured results, 3D full wave FIT simulations of the experiment were set up [4]. The model has perfect lumped elements without parasitic capacitance and inductance.

Also the radiated emission from PCB and cable and the common mode impedance of the cable was simulated. (See Fig. 6.)

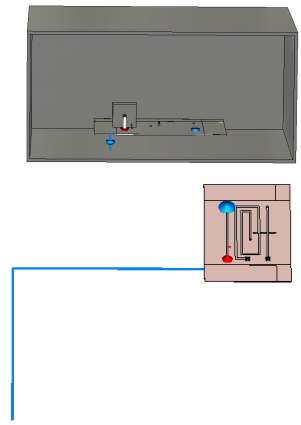

Fig. 6. Models for the 3D full wave simulations.

IV. Results and Discussion

In Fig. 7 the measured voltage across the 50 Ω input resistance in the spectrum analyser is compared with the simulated results. The simulations and measurements are in agreement up to 450 MHz, above 450 MHz they have similar trends. The difference above 450 MHz can be caused by the fact that the component used in the measurement has parasitic capacitance and inductance. In addition, there can be loss in cables and connectors when the frequency increases. Last but not least, cavity resonances of the box arise after 450 MHz. Both simulations and measurements have a quite flat frequency response up to 400 MHz after which they rise to a peak at approx. 500 MHz. Above 550 MHz the common mode noise decreases and the response is no longer flat.

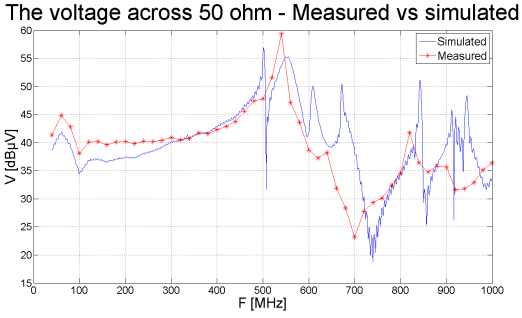

Fig. 7. Simulated and measured common mode noise obtained by the WBFC method. The red markers indicate the measured comb generator frequencies.

In Fig. 8 the WBFC measurement is compared with the measured radiated emission according to (1) in the setup where the cable has galvanic contact to the PCB. Except for 120, 280 and 300 MHz the comparison shows that up to 360 MHz the WBFC predict worse case, i.e. $E_{WBFC} \geq E_{3m\ SAC}$. At 120 and 280-300 MHz the measured radiated emission is 2 dB and 4 dB higher respectively than the predicted. Due to the large measurement uncertainty it is hard to draw firm conclusions. But the suggested WBFC limit from the standard [1] does not take into account the effect of the conducting reflecting floor in the semi anechoic chamber. A simulation of the far-field at 120 and 300 MHz including the conducting floor gives a directivity of 5.5 dBi and 8.8 dBi respectively, so it is not unlikely that this is an example of a setup where the standard's WBFC limit is not sufficient because of high directivity, in this example mainly caused by the conducting floor.

Above 560 MHz the WBFC measurement is considerably below the measured radiated emission.

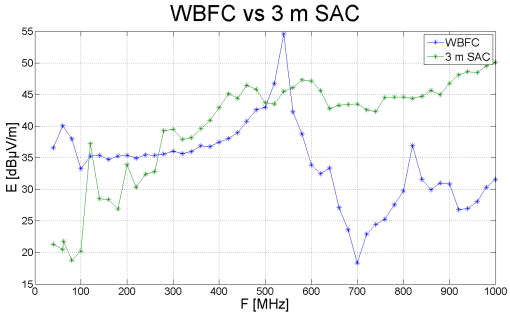

Fig. 8. Worst case predictions of the radiated emission based on WBFC measurement compared to the 3 m semi anechoic chamber measurements of the setup with galvanic contact between PCB and cable. The markers indicate the measured comb frequencies.

In Fig. 9 the simulated radiated emission is compared with the measured, both for the setup with galvanic contact between the cable and the PCB and for the setup without galvanic contact. The simulated radiated emission is the maximum electric far-field evaluated at all points in the upper half of the hemisphere in a 3 m radius. The simulated radiation pattern is quite inhomogeneous at high frequencies. The measurement is done according to CISPR 13 with a 1.5 m broad biconical antenna which in several ways differs from a precise far-field measurement, so the measurement and simulation are not completely comparable. For example according to CISPR 13 we only measure the field from theta = 45° to theta = 90° in traditional spherical coordinates.

Because the measurement uncertainty in a 3 m SAC is up to 6 dB it is hard to draw conclusions based on differences of the same magnitude between two measured values. But if both simulations and measurements show the same difference it is reasonable to trust that the difference is real.

Fig. 9 shows that at about 120 MHz and 300 MHz the radiation from the setup with galvanic contact between the cable and the PCB is considerably higher than from the setup with no galvanic contact. At 200 MHz it is only the measurement that shows a significant difference, which is why we attribute this difference to measurement inaccuracy.

At frequencies above 400 MHz both simulations and measurements show that it does not matter whether the cable has galvanic contact or not, i.e. the PCB radiates by itself or the dominating coupling above 400 MHz is via magnetic and electric fields and not via conducted coupling.

Here it must be mentioned that simulations and measurements of the radiation from the PCB and comb generator alone, i.e. without the cable, shows the same level of radiated emission compared to the setups with the cable, so above 400 MHz the radiation is mainly caused by radiation from the PCB itself.

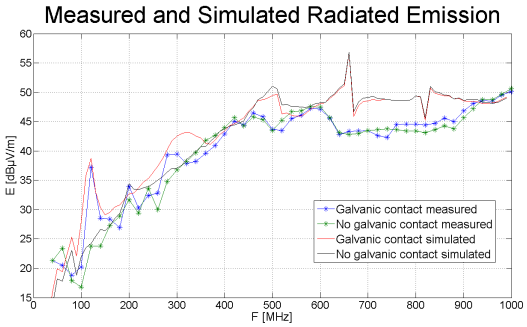

Fig. 9. Simulated and measured radiated emission from the PCB and the cable, with and without galvanic connection. The markers indicate the measured comb frequencies.

Fig. 10 shows the measured current at the cable connection in the setup with galvanic contact between the cable and the PCB (see Fig. 5). In same figure on a secondary axis the simulated common mode impedance of the attached cable at the same point is plotted (see Figs. 5 and 6).

By comparing the two plots it becomes clear, that there is a connection between currents peaks/dips and the common mode impedance. When the common mode impedance is low, there is a current peak, and conversely high common mode impedance causes a current dip. Therefore we can conclude that the common mode noise source is a voltage source with comparatively low internal impedance. This is also in agreement with the fact that low common mode load impedance causes effective conducted power transfer according to the 120 and 300 MHz peaks in Fig. 9.

Above 600 MHz the measured cable current at the connection decreases in accordance to the WBFC measurements in Fig. 7, i.e. the lower conducted emission level above 600 MHz. For some reason the 500 MHz current peak has lower amplitude in contrast to the WBFC measurement, which peaks at approx. 500 MHz. But the low current is in agreement with Fig. 9 that shows that in the radiated emission test setup, field coupling is dominating above 400 MHz. Hence the broad WBFC peak around 500 MHz is probably due to some resonance caused by the measurement method which does not occur in the radiated emission test setup.

.

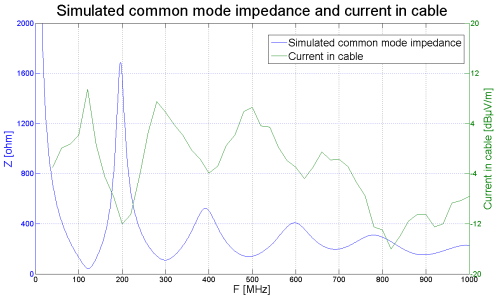

Fig. 10. On left y-axis the simulated common mode impedance of the attached cable (see Fig. 5). On right y-axis the measured current at the cable connection (see Fig. 5) in the setup with galvanic contact between cable and PCB.

To sum up, below approximately 360 MHz the conducted coupling dominates the emission. Hence if the module passes the WBFC test it will likely also pass the final radiated emission test. But high directivity (e.g. caused by reflecting waves from the conducting floor in a semi anechoic chamber) or impedance mismatch can cause excesses.

Whether the PCB/cable setup radiates depends on the common mode impedance of the cable, i.e. whether there is impedance match between the common mode noise generator and the cable. The common mode noise generator acts like a voltage source with comparatively low source impedance.

Above 400 MHz field coupling or radiation from the PCB itself dominates although the WBFC measurement has its maximum values around a broad peak at about 500 MHz. This peak indicates a resonance that occurs in the WBFC set-up but not in the apparatus

V. Conclusions

The usability of the WBFC method and its mode of operation have been investigated. With a 4 dB safety margin the WBFC method is a fairly useful pre-compliance test up to 350 MHz regarding radiated emission where conducted coupling is dominating. Above 400 MHz field coupling or radiating from the PCB itself is dominating and the WBFC method is essentially useless.

Whether the above conclusions are representative for contemporary PCB's used in electronic apparatus is a subject of ongoing work.

ACKNOWLEDGMENT

Authors wish to thank Mr. Claus Vittarp and Mr. Jan Clausen, both from DEIF A/S, for their valuable help in performing the measurements.

REFERENCES

[1] IEC/EN 61967-5:2003, Integrated circuits - Measurement of electromagnetic emissions, Part 5: Measurement of conducted emissions – Workbench Faraday Cage method

[2] M.J. Coenen, "EMC Workbench: Testing methodology, module level testing and standardization" Philips Journal of Research vol.48 1994.

[3] M.J. Coenen, "Common Mode Impedance Measurements on Cables in the Frequency Range 30 MHz–1 GHz," EIE 92004, Philips Semiconductors 1992.

[4] CST Microwave Studio (www.cst.com).

Paper B

Study of the Impact of Board Orientation on Radiated Emissions due to Common-Mode Currents on Attached Cables

Morten Sørensen[1,3], Todd H. Hubing[2], Kim Jensen[3]
[1]Antennas, Propagation and Radio Networking section, Aalborg University, Niels Jernes Vej 12, 9220 Aalborg, Denmark, mos@es.aau.dk
[2]LearnEMC, P.O. Box 729, Stoughton, WI 53589, USA, hubing@learnemc.com
[3]Bang & Olufsens a/s, Peter Bangs Vej 15, 7600 Struer, Denmark, kjn@bang-olufsen.dk

The paper has been published in the
Electromagnetic Compatibility (EMC), 2016 IEEE International Symposium on, Jul 2016, pp. 36-40.

The layout has been revised.

Study of the Impact of Board Orientation on Radiated Emissions due to Common-Mode Currents on Attached Cables

Morten Sørensen*, Todd H. Hubing†, Kim Jensen‡
*Antennas, Propagation and Radio Networking, Department of Electronic Systems,
Faculty of Engineering and Science, Aalborg University
Niels Jernes Vej 12, 9220 Aalborg st, Denmark
Email: mos@es.aau.dk
†LearnEMC, P.O. Box 729, Stoughton, WI 53589, USA
Email: hubing@learnemc.com
‡Bang & Olufsen a/s, Peter Bangs Vej 15, 7600 Struer, Denmark
Email: kjn@bang-olufsen.dk

***Abstract*—Common-mode current on attached cables is a typical source for radiated emission. Several models have been made for conversion of the intended differential signal to unwanted common-mode current on cables. In this paper we refine a method for identifying the radiation sources arising from a long microstrip. This method is used to show that the radiated emission from a PCB with attached cable(s) caused by a long trace depends on whether the trace is facing up or down with different result for voltage and current sources.**

I. Introduction

Structures with maximum dimension much smaller than the wavelength are called electrical small and are inefficient as antennas [1]. Hence printed circuit boards (PCB) by itself do not radiate below 300-500 MHz – depending on PCB size. But cables attached to the PCB are comparable with wavelength and common-mode currents on cables are a typical reason for failing radiated emission test.

Four main mechanisms by which intentional signals induce- or transfer to common-mode current on attached cables are well described in the literature [2]–[5]:

- Current driven (magnetic field coupling)
- Voltage driven (electric field coupling)
- Conducted
- Low transfer impedance in cables and connectors

Several models for predicting maximum radiating emission from cables attached to PCB's with traces, ICs and heatsinks have been developed. A model for magnetic field coupling from a trace to an attached cable is shown in Fig. 1a. The return plane is of finite size and the magnetic flux will wrap around the plane. Hence the current return path has an effective inductance and a voltage across the return plane will arise. This voltage drives cables attached at different positions like a dipole antenna. The amplitude of the predicted maximum radiated emission is a function of current amplitude and the geometry of the current-loop, i.e. trace length, trace distance to edge, return plane size etc. [6]–[8].

A model for electric field coupling from trace to attached cables is shown in Fig. 1b. The voltage across the signal generator (V_{DM}) drives the trace relative to the return plane with cables. If the signal trace couples capacitive to larger structures, e.g. a heatsink, the voltage-driven can be significantly magnified. In order to estimate the maximum radiated emission, the PCB and attached cables can be modeled by placing equivalent common-mode voltage generators between the return plane and the attached cable. The amplitude of this equivalent common-mode voltage source is determined by the ratio of the self-capacitance of the trace and the self-capacitance of the board [9]–[11].

Shim et al. [9] developed a method for identifying the nature of the radiation sources arising from a short microstrip with an unbroken ground plane by modifying the source and load impedance.

The imbalance difference model [12]–[14] is another model for conversion of differential-mode signal currents to common-mode noise currents. It is based on a parameter called imbalance factor which is defined by the degree of imbalance of a transmission line. One advantage of this method is, that it models the coupling between the differential signals on the board and the common-mode currents on attached cables without specifying a particular field coupling mechanism.

All the above mentioned methods and models are very useful in most situations, but they have also their limitations. The models, by their very nature, make a lot of simplifications and assumptions and the models must be used with caution.

In this paper we further develop the above mentioned method to identify the nature of the source [9], so it is able to handle long traces. The method is used to show that radiated emission caused by common-mode current on attached cables is quite complex - even with a simple structure. It is shown that the maximum radiated emission depends on the orientation of the traces, i.e. whether the traces are facing up or down in a setup with the PCB parallel to a large ground plane and

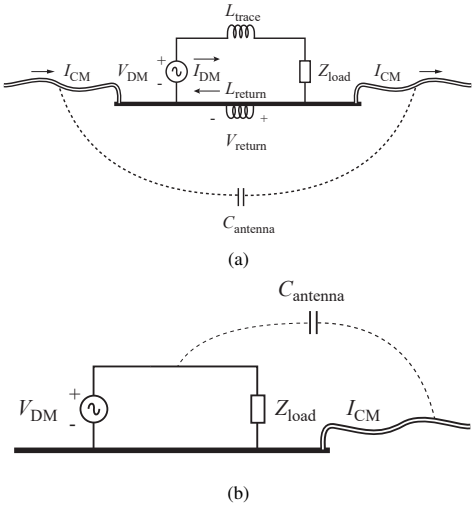

Fig. 1: Illustration of typical coupling mechanisms for common-mode current on attached cables: (a) current driven and (b) voltage driven.

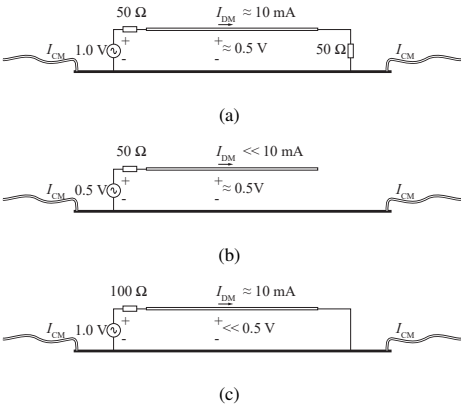

Fig. 2: Illustration of the method for identifying radiation source. (a) original configuration with perfect match microstrip (b) voltage driven source with low current and same voltage as original configuration (c) current driven source with low voltage and same current as original configuration.

cable(s) attached to the floor of the chamber, see Fig. 4. To our knowledge, no models or expert systems for predicting radiated emission consider this phenomena.

The paper is organized as follows. In Section II the enhanced method for identifying radiation sources is presented. Section III describes the test setup. Results are shown and discussed in Section IV. Finally, conclusions are drawn in Section V

II. Identifying the Radiation Sources for Long Traces

Shim et al. proposed a simulation method for identifying the radiation sources for a PCB with a short microstrip and cable(s) attached [9]. Assume that an electrical short 50 Ω microstrip is driven by a 50 Ω 1 V voltage generator. The microstrip is terminated with 50 Ω. If perfectly match, the current is 10 mA and the voltage between trace and return plane is 0.5 V as illustrated in Fig. 2a. If the generator voltage is halved to 0.5 V and the 50 Ω termination is removed, no significant current runs along the trace and hence the voltage between trace and return plane is ∼0.5 V. The voltage-driven source is still present but the current-driven source is removed. This is illustrated in Fig. 2b.

If the source impedance is doubled and the termination is shorted, the current is ∼10 mA, but now the voltage drop is over the source impedance and there is no significant voltage between trace and return plane. The current-driven source is still present, but the voltage-driven source is removed. This is illustrated in Fig. 2c.

All the above claims are only valid as long as the trace is electrical small, i.e. trace length ≪ wavelength. As the trace length increases, standing waves arise and the microstrip becomes a transmission line.

Using FR4 with $\epsilon_r = 4.3$ the propagation speed is approximately $c_0/\sqrt{\epsilon_r} \approx c_0/2$. Let us assume that the microstrip begins to behave like a transmission line when the trace length is longer than $\frac{1}{10}$ of the wavelength, then the model is valid up to 300 MHz for a 5 cm trace but only up to 125 MHz for a 12 cm long trace.

In order to enhance the model to longer traces or higher frequencies, we suggest to divide the trace into a number of subtraces with a length shorter than $\frac{1}{10}$ wavelength, see Fig. 3. Each subtrace is excited with a port at the beginning of the trace and terminated at the end. The excitation of the ports is time shifted with the time it takes the signal to propagate from one generator to the next generator, i.e. time shift δ = subtrace length / propagation speed. Hence when the signal reach the end of subtrace 1, port 2 begins and then when the signal reach the end of subtrace 2, port 3 begins etc.

In this way the current and the voltage along the divided trace should be approximately equal to the current and the voltage along the non-divided trace – except for the very thin split between the 3 subtraces. Since the subtraces is electrical short, the idea is that the above described method to identify the radiation sources can be used. Voltage sources can be identified if the load impedance (Z_L) is infinite. Current sources can be identified if the source impedance is doubled and load impedance is 0.

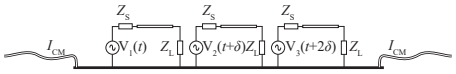

Fig. 3: Subtrace model: The long trace is divided into a number of subtraces with its own port and termination.

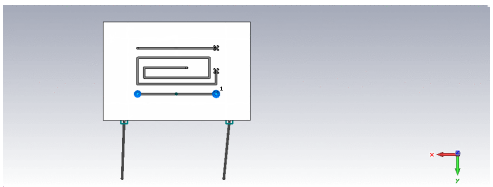

(a)

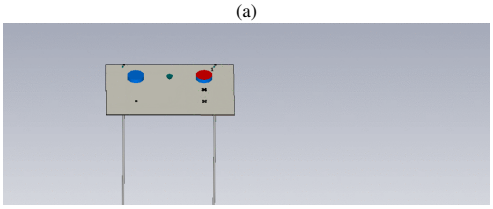

(b)

Fig. 4: The test PCB: A simple 150 x 225 mm PCB with three 50 Ω traces on the top layer with a full ground plane on the bottom layer. Only one trace was excited and terminated. Both source impedance and load impedance was 50 Ω. One and two 1 m long cables were attached to the ground plane of the PCB. The cables were terminated to an infinite ground plane representing the floor of a chamber. In (a) the traces are facing up relative to the cables and the floor of the chamber. In (b) the traces are facing down relative to the cables and the floor of the chamber.

III. Test Setup

A. The Simulation Models

The PCB with a 12 cm long trace shown in Fig. 4 was used as test case for the proposed method. All the metal was perfect electric conductor (PEC) and lossy FR4 was used as substrate. All simulations were done both without cables and with one and two 1 m long cables attached to the PCB. The PCB was placed 1 m above an infinite ground plane and the attached cables were terminated to this ground plane. The PCB was simulated in CST Microwave Studio with the transient solver (Finite Integration Technique) [15]. There was a far-field monitors for every 10 MHz and additional far-field monitors for every 1 MHz around cable resonances. The electric field was evaluated at all points in the upper half of the hemisphere in a 3 m radius and the maximum electric-field vs. frequency was found – similar to a radiated emission test like CISPR 22.

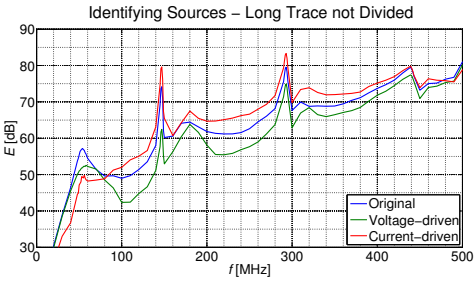

Fig. 5: First attempt to identify the radiation sources with the trace undivided.

In order to test the proposed, the 12 cm long trace was divided in 3 subtraces as illustrated in Fig. 3. In the original setup the signal arrived at the termination 0.76 ns after excitation at the port. Hence the signal on port 2, in the divided model, was time shifted $\frac{1}{3}\cdot 0.76$ ns and the signal on port 3 was time shifted $\frac{2}{3}\cdot 0.76$ ns.

B. Measurements

The effect of the orientation of the traces was also investigated by help of measurements. A comb generator with fundamental frequency of 1 MHz and a flat frequency response up to 1 GHz was used as a noise generator. It was connected with a short cable to a PCB like the one in the simulations: 150 x 225 mm PCB with a 120 mm long, 50 Ω micro strip, terminated with 4 parallel 200 Ω SMD resistors.

C. Workflow of the Experiments

First we tried to identify the radiation sources without dividing the traces into subtraces. Next we tested whether the divided trace model can reproduce the electromagnetic properties of the original setup. After that we identified the radiation source by help of the divided trace model. Voltage driven sources were identified by reducing all 3 generator voltages to 0.5 V and with all 3 traces open ($Z_L = \infty$). Current-driven sources were identified by doubling all 3 sources impedances to 100 Ω and with all 3 traces shorted ($Z_L = 0$). Finally we compared maximum radiated emission from PCB with attached cables with the traces facing up and down.

IV. Results and Discussion

A. Comparison of Methods for Identifying Radiation Sources

Fig. 5 shows the result of the original method for identifying radiation sources, i.e. with an undivided trace as shown in Fig. 2.

The figure shows clearly that it is not possible to identify the sources. Voltage and current monitors along the trace in the simulations show, that standing waves arise and hence the voltage-driven configuration has significant current and the current-driven configuration has significant voltage between trace and return plane.

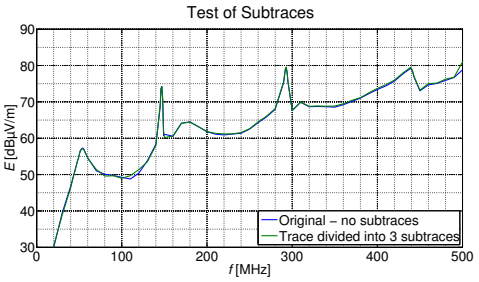

Fig. 6: Test of the subtraces model.

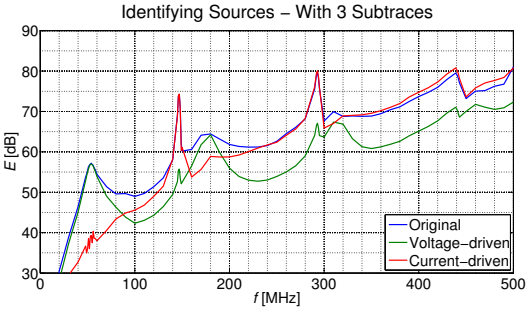

Fig. 7: Source identification with trace divided in 3 subtraces.

Fig. 6 shows a comparison of the original (i.e. undivided trace) simulation of the PCB with two cables attached and the result for a PCB with the trace divided in 3 subtraces. Each voltage generator is time shifted as shown in Fig. 3. The agreement is very good and there is only small deviations at some specific frequencies between the cable resonance frequencies. We conclude that the subtrace model can reproduce the electromagnetic properties of the original model.

Fig. 7 shows maximum radiated emission from the undivided unchanged PCB with two cables vs. the maximum radiated emission from the voltage-driven and current-driven configuration shown in Fig 3. It is clear from the figure that it is possible to identify the nature of radiation source. The cable resonances at 54 MHz and 175 MHz are voltage-driven and the other cable resonances are current-driven.

B. Orientation of the trace

Basically all the models and expert systems described in Section I are trying to predict maximum radiated emission based on the PCB geometry. This geometry does not include the orientation of the traces, i.e. whether they are facing up or down, see Fig. 4. Fig. 8 shows a comparison of maximum radiated emission of the PCB with one and two cables and with the traces facing up and down. At a glance there is no pattern in the differences. Most of the peaks are strongest when the traces are facing down, a few peaks are strongest with traces facing up and finally the resonance peak for one cable attached

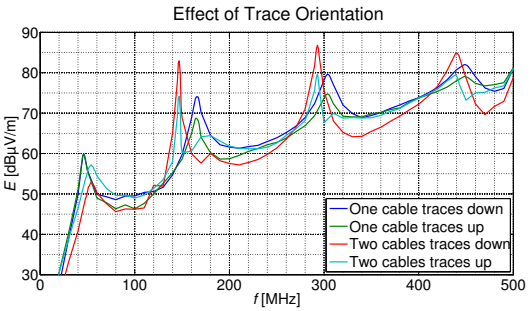

Fig. 8: Comparison of maximum radiated emission from the PCB with one and two cables attached and with traces facing up and down.

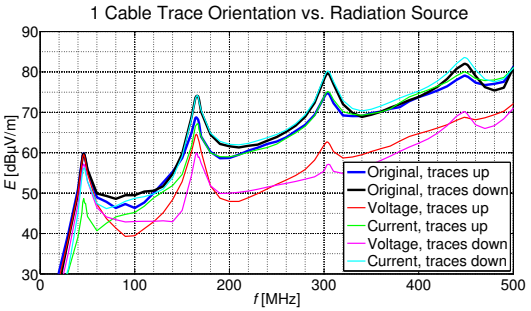

Fig. 9: Effect of board orientation on maximum radiated emission from PCB with one cable attached.

at 46 MHz seams indifferent to the board orientation. It is clear that board orientation matters and the difference can be up to 10 dB.

In Fig 9 maximum radiation emission from the PCB with one cable attached vs. radiation source vs. board orientation is shown. The peak at 46 MHz with traces down is a combination of current- and voltage-driven. With the traces up, the peak is clearly voltage-driven.

Fig. 10 shows the same results for the PCB with two cables attached.

In Table I and Table II the nature of radiation source and the effect of board orientation are summarized.

The summary in the tables shows, that both with one and two cables, voltage-driven peaks are highest with the traces facing up, while it is the other way around with current-driven peaks.

C. Measurement

Fig. 11 shows the results of the measurements vs. simulations with two cables attached. In spite of small deviations in amplitude and resonance frequencies, the measurements strongly support the simulations with regard to the effect of

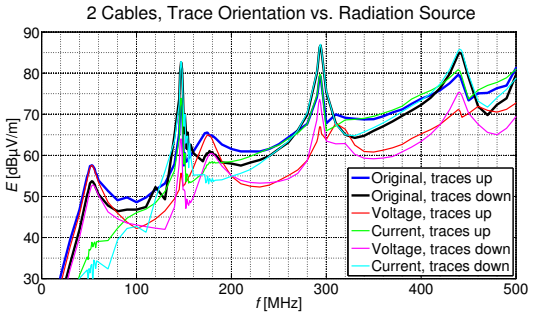

Fig. 10: Effect of board orientation on maximum radiated emission from PCB with two cables attached.

TABLE I: One Cable Attached: Nature of Radiation Source vs. Effect of Trace Orientation

f[MHz]	Radiation Source	Max. radiation
46	Voltage-driven (with traces up), combination (with traces down)	Voltage-driven increases with traces up, current-driven increases with traces down
166, 306, and 450	Current-driven	Traces down

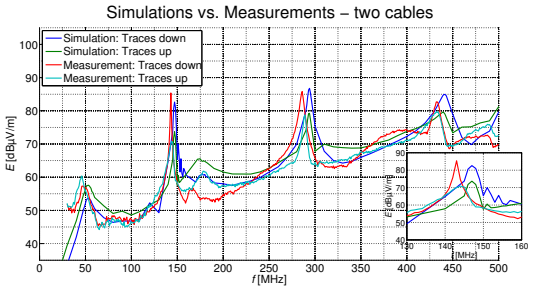

Fig. 11: Comparison of measurements and simulations. Zoom in from 130 - 160 MHz in the "plot in plot".

the orientation of the traces as concluded in Table II. Board orientation can significantly affect the radiated emissions.

V. Conclusion

A method for identifying radiation sources was enhanced by dividing a long trace into 3 electrical short traces. Each trace had its own termination and voltage generator, which was time shifted in order to reproduce the signal on the undivided trace. The enhanced method was used to identify voltage- and current-driven sources for radiated emission from a PCB with a 12 cm long trace with one and two 1 m long vertical cables attached and terminated to ground. The investigation showed that maximum radiated emission differed up to 10 dB depending on the orientation of the traces. Voltage-driven sources had highest radiation with traces facing up while current-driven sources had highest radiation with the traces facing down. This effect was confirmed by measurement.

TABLE II: Two Cables Attached: Nature of Radiation Source vs. Effect of Trace Orientation

f[MHz]	Radiation Source	Max. radiation
54 and 175	Voltage-driven	Traces up
147, 293, and 439	Current-driven	Traces down

The investigation did not explain the difference in the effect of orientation between voltage– and current-driven radiation sources. This requires detailed studies of the electric and magnetic field lines and is a subject of ongoing work.

References

[1] J. Kraus and R. Marhefka, *Antennas for all applications*.

[2] J. Drewniak, F. Sha, T. Van Doren, T. Hubing, and J. Shaw, "Diagnosing and modeling common-mode radiation from printed circuit boards with attached cables," in *Electromagnetic Compatibility, 1995. Symposium Record., 1995 IEEE International Symposium on*, Aug 1995, pp. 465–470.

[3] D. Hockanson, J. Drewniak, T. Hubing, T. Van Doren, F. Sha, and M. Wilhelm, "Investigation of fundamental EMI source mechanisms driving common-mode radiation from printed circuit boards with attached cables," *Electromagnetic Compatibility, IEEE Transactions on*, vol. 38, no. 4, pp. 557–566, Nov 1996.

[4] T. Hubing, "Printed circuit board emi source mechanisms," in *Electromagnetic Compatibility, 2003 IEEE International Symposium on*, vol. 1, Aug 2003, pp. 1–3 vol.1.

[5] J. Goedbloed, *Electromagnetic compatibility*.

[6] D. Hockanson, J. Dreniak, T. Hubing, T. Van Doren, F. Sha, and C.-W. Lam, "Quantifying emi resulting from finite-impedance reference planes," *Electromagnetic Compatibility, IEEE Transactions on*, vol. 39, no. 4, pp. 286–297, Nov 1997.

[7] F. Leferink, "Reduction of printed circuit board radiated emission," in *Electromagnetic Compatibility, 1997. IEEE 1997 International Symposium on*, Aug 1997, pp. 431–438.

[8] G. Dash, J. Curtis, and I. Straus, "The "current driven model" - experimental verification and the contribution of I_{dd} delta to digital device radiation," in *Electromagnetic Compatibility, 1999 IEEE International Symposium on*, vol. 1, 1999, pp. 317–322 vol.1.

[9] H.-W. Shim and T. Hubing, "Model for estimating radiated emissions from a printed circuit board with attached cables due to voltage-driven sources," *Electromagnetic Compatibility, IEEE Transactions on*, vol. 47, no. 4, pp. 899–907, Nov 2005.

[10] S. Deng, T. Hubing, and D. Beetner, "Characterizing the electric field coupling from ic heatsink structures to external cables using tem cell measurements," *Electromagnetic Compatibility, IEEE Transactions on*, vol. 49, no. 4, pp. 785–791, Nov 2007.

[11] ——, "Estimating maximum radiated emissions from printed circuit boards with an attached cable," *Electromagnetic Compatibility, IEEE Transactions on*, vol. 50, no. 1, pp. 215–218, Feb 2008.

[12] Y. Toyota, T. Matsushima, K. Iokibe, R. Koga, and T. Watanabe, "Experimental validation of imbalance difference model to estimate common-mode excitation in pcbs," in *Electromagnetic Compatibility, 2008. EMC 2008. IEEE International Symposium on*, Aug 2008, pp. 1–6.

[13] T. Matsushima, T. Watanabe, Y. Toyota, R. Koga, and O. Wada, "Prediction of emi from two-channel differential signaling system based on imbalance difference model," in *Electromagnetic Compatibility (EMC), 2010 IEEE International Symposium on*, July 2010, pp. 413–418.

[14] C. Su and T. Hubing, "Imbalance difference model for common-mode radiation from printed circuit boards," *Electromagnetic Compatibility, IEEE Transactions on*, vol. 53, no. 1, pp. 150–156, Feb 2011.

[15] "CST MicroWave Studio, http://www.cst.com."

Paper C

Analysis and Measurement Investigation of the Workbench Faraday Cage Method, IEC 61967-5

Morten Sørensen[1], Søren Kjærulf Christensen[2], Claus Vittarp[3], and Hans Ebert[4]
[1]EMC Laboratory, Missouri University of Science and Technology, Rolla, MO 65401, USA, sorensenmo@mst.edu
[2]Terma Group, 8520 Lystrup, Denmark, skch@terma.com
[3]DEIF A/S, 7800 Skive, Denmark, cvi@deif.com
[4]Antennas, Propagation, and Millimeter-Wave Systems Section, Department of Electronic Systems, Aalborg University, 9220 Aalborg, Denmark, heb@es.aau.dk

Submitted to IEEE Transactions on Electromagnetic Compatibility, September 30, 2018

The layout has been revised.

Analysis and Measurement Investigation of the Workbench Faraday Cage Method, IEC 61967-5

Morten Sørensen, *Member, IEEE,* Søren Kjærulf Christensen, Claus Vittarp, and Hans Ebert

***Abstract*—The Workbench Faraday Cage Method (WBFC), IEC 61967 Part 5, is a method to measure the conducted electromagnetic emission of integrated circuits either applied on a standardized test-board or on a final printed circuit board (PCB). The presented work analyzes the method by help of simulations of a simple microstrip board with two attached cables connected to ground. In addition a measurement test based on three real PCBs are done. The analysis shows that the theoretical foundation of the method is weak and that the WBFC method gives a poor prediction of the radiated emission. However, for power supply noise the WBFC and 3 m radiated emission measurements follows each other with a constant amplitude difference.**

***Index Terms*—Radiated Emisson, Common Mode Noise, Work-Bench Faraday Cage.**

I. Introduction

THE sooner potential EMI problems are discovered, the more ways there are to solve the problems. Therefore it is of great interest to electrical engineers to perform pre-compliance tests regarding radiated emission at integrated circuit (IC)- or printed circuit board (PCB) level.

The international standard IEC 61967 "Integrated circuits Measurement of electromagnetic emissions, 150 kHz to 1 GHz" describes five different methods for measuring conducted and radiated electromagnetic emissions from integrated circuits. Part 5, "Measurement of conducted emissions – Workbench Faraday Cage method" [1] describes a method to measure the conducted electromagnetic emission of integrated circuits either applied on a standardized test-board or on a fully functional PCB. According to the standard, "*it has a high repeatability and a good relationship to the measured RF emission of final applications with the integrated circuits used*".

The WBFC method was invented at Philips, Netherland in 1994 [2], [3] and became an IEC standard in 2003 with 2019 as the current stability date, (i.e., the publication will be either reconfirmed, withdrawn, replaced by a revised edition or amended in 2019.) Although it is an official IEC standard, there are only a few studies of the method. To the authors' knowledge, there are few scientific publications with theoretical- or measurement validation of the method.

M. Sørensen is with the EMC Laboratory, Missouri University of Science and Technology, Rolla, MO, 65401 USA (e-mail:sorensenmo@mst.edu).

S. K. Christensen is with Terma Group, 8520 Lystrup, Denmark (e-mail: skch@terma.com).

Claus Vittarp is with DEIF A/S, 7800 Skive, Denmark (e-mail: cvi@deif.com).

Hans Ebert is with the Antennas, Propagation, and Millimeter-Wave Systems Section, Department of Electronic Systems, Aalborg University, 9220 Aalborg, Denmark (e-mail: heb@es.aau.dk)

In [4] the common mode current caused by Vcc/Vss voltage fluctuations from a microcomputer was investigated by the WBFC method. At some frequencies there was a good correlation between WBFC measurements and 3 m semi anechoic chamber (SAC) measurements while other frequencies showed large differences. In [5] the effect of the position of the WBFC measurement points were investigated.

A preliminary study of the method was done in [6]. The radiated emission from a simple microstrip PCB was estimated by help of the WBFC method and compared with 3 m SAC measurements. The conclusion was that with a 4 dB safety margin the WBFC method was a fairly useful common mode emission pre-compliance test up to 350 MHz. However, the method overestimated the radiation at low frequencies.

This paper analyzes and discusses the WBFC method with respect to electric and magnetic coupling mechanism and direct I/O coupling. It is done by help of simulations of the simple microstrip PCB used in [6]. After that, WBFC measurements and 3 m SAC measurements for three real PCBs are compared. The three chosen test boards were a power supply unit (PSU) and two different boards both with DC-to-DC converters and various digital circuits with microprocessors, RAM, Ethernet, etc.

The paper starts with an introduction to common mode emission in Section II followed by Section III that describes the WBFC Method and the theoretical background. Section IV describes the simulation setup for the analysis, and the results are discussed in Section V. Section VI describes the setup for the measurement validation which results are presented in Section VII and discussed in Section VIII. Finally the conclusions are drawn in Section IX.

II. Common Mode Emission

Below a few hundred MHz, ICs and PCBs are electrically small and do not radiate by themselves. Instead IC signals couple, e.g. by help of microstrips, to attached cables that have a significant electrical length [7], [8]. The coupling induces common mode currents on the cables which cause unwanted radiated emission. In this paper, common mode emission should be understood as radiated emission caused by common mode current running on attached cables.

A. Coupling Mechanism

The coupling mechanisms by which the intentional signal induces common mode currents on cables can be divided into three main categories: current driven, voltage driven and direct signal to I/O coupling.

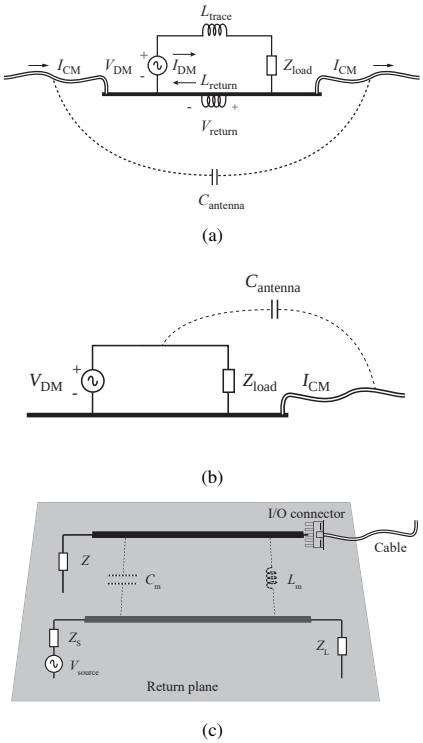

Fig. 1: (a) Current driven common mode emission. (b) Voltage driven common mode emission. (c) I/O coupled common mode emission.

Current driven common mode emission is illustrated in Fig. 1(a). It occurs because the return plane is of finite size and the magnetic flux wraps around the plane [9]–[11].

Voltage driven common mode emission is illustrated in Fig. 1(b). The voltage across the signal generator (V_{DM}) drives the trace relative to the return plane with cables [12]–[14].

Direct I/O coupled common mode is illustrated in Fig. 1(c). Emission occurs because of crosstalk between signal traces and traces that connect external wires to the board (I/O lines) [15].

Basically all the models described above are trying to predict the maximum radiated emission based on the PCB geometry. This geometry does not include the orientation of the traces, (i.e., whether the traces are facing up or down,) in a setup with the PCB parallel to a large ground plane and cable(s) going to the floor of a chamber. In [16] it was shown that the maximum radiated emission differed up to 10 dB depending on the orientation of the traces. Hence, even with a simple structure, common mode emission is quite complex and cannot fully be described by equivalent noise generators based on board geometry.

B. Cable Termination

Radiated emission from, for example power cables, will vary with the impedance between the power line and the ground in the power source. Nine certified laboratories participated in a round robin test of radiated emission from a PC tower [17]. The measurement results from the laboratories varied more than 20 dB at frequencies below 100 MHz with a standard deviation up to 8 dB. In another study [18], similar differences in maximum radiated emission were observed, but if the attached cables was resistive terminated to ground with 150 Ω, there was no strong resonances and maximum radiated emission vs. frequency was slightly increasing with frequency.

The use of common mode absorbing devices (CMAD) on all lines are now included in standards like CISPR32 [19], (i.e., power input and output as well communication and signal lines.) CMADs should stabilize the common mode impedance independently on the termination impedance of the line.

III. The WBFC Method and the Theoretical Background

The WBFC method [1] assumes that the supply and signal cable(s) are attached to an electrically small PCB with largest dimensions smaller than $\frac{\lambda}{2}$. Hence, attached cables are the dominant antennas and the RF emission is caused by common mode current on the cables. The method suggests that the maximum common mode emission can be estimated by loading the test points with 150 Ω resistance and then measuring the absorbed power. 150 Ω is a representation for the radiation resistance of long cables and comes from empirical data [2].

The PCB is placed in a small Faraday cage in order to limit the influence of the ambient noise on the test results, and in order to have defined coupling parameters to the PCB surroundings.

According to the standard's appendix A the coupling mechanisms inside the cage are described as electric field coupling between the PCB and the cage and magnetic field coupling between areas on the PCB with the loop area formed between the Faraday cage wall and the common-mode impedances, Z_{CM}, at both sides of the PCB. Note: the standard's description of the coupling was written years before the more stringent description from Section II-A.

A. Limits

The standard's annex C relates the measured voltage in the cage to the radiated emission limits. Several standards' limits (e.g., CISPR 32 and IEC 61000-6-3 light industrial) correspond to an effective radiated power of 2 nW in a matched dipole and the limit in the WBFC can be set as maximum 2 nW absorbed in the 150 Ω termination. Corrected for the 50 Ω measurement equipment the limits for a 3 m SAC measurement becomes:

$$U_{\text{limit, WBFC}}[\text{dB}\mu\text{V}] = E_{\text{limit, 3 m SAC}}[\text{dB}\mu\text{V/m}] + 5.3 \text{ dB}. \quad (1)$$

For CISPR 32 [19] the voltage limits in the WBFC is given by:

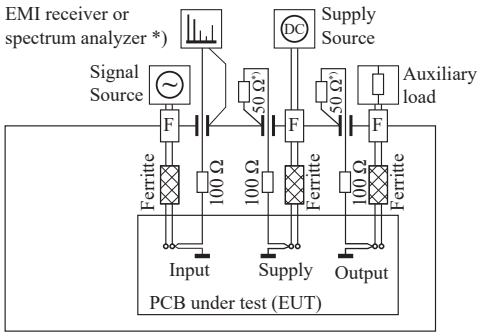

*) shall be interchanged at each port

Fig. 2: Workbench Faraday Cage setup [1].

30 - 230 MHz: 45 dBμV
230 - 1000 MHz: 52 dBμV

These limits do not take reflections from the chamber's floor into account. Also the common impedance of the attached cables could be different from 150 Ω causing weaker or stronger radiation compared to [1]. The original work [3] suggested a 6 dB safety margin.

The standard's suggested limits are for each individual I/O termination. It is not suggested in the standard, however, one could argue that the limit should be based on the total absorbed power in all I/O termination resistors as an average superposition of radiated emission from different attached cables. In that case U in (1) becomes the root sum square of the individual measured voltages across the I/O terminations.

B. Test Procedure

The common mode current is typically evaluated at the DC- (or AC-) power supply connector, at the in- and output connectors, and at ground. All these common mode points must be terminated with 150 Ω. All functional connections, like power supplies and auxiliary equipment, to the PCB must be fed through the dedicated filters and wrapped around ferrite cores to create impedance much larger than 150 Ω. The test setup is shown in Fig. 2. The DUT must be placed 30 mm above the bottom with the IC(s) to be tested facing the bottom plate. When measurements were done on one point, the other test points must be terminated with 150 Ω

IV. Simulation Setup for Analysis

A. Identifying the Sources in the Simulations

As mentioned in Section II-A, it has been shown that common mode emission can be divided into voltage and current driven sources and direct I/O coupling. In simulations it is possible to investigate the different coupling mechanism behavior inside the WBFC.

For an electrically short trace with a voltage generator, and with source- and load impedances, it is possible to divide the noise source into a voltage and current source [12]. The voltage driven source can be excited by halving the voltage and removing the termination. A current driven source can be excited by doubling the source impedance and shorting the termination.

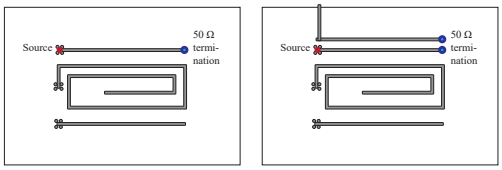

(a) (b)

Fig. 3: The simple microstrip for test. (a) Voltage and current driven. (b) I/O coupling.

This method works as long as the trace is electrically short. The method was further developed in [16]. The electrically long trace was divided into a number of subtraces with a length shorter than $\frac{1}{10}$ wavelength.

B. The test PCB

A simple 150 mm × 225 mm two layer PCB with three 50 Ω traces was modeled as shown in Fig. 3(a). The substrate was lossy FR4. Only one trace was excited and terminated. The active trace was 120 mm long and 3 mm wide and both source and load impedances were 50 Ω.

The PCB was placed 30 mm above the bottom of a WBFC with the dimensions 460 mm × 310 mm × 240 mm. Two test points placed 32 mm from the edges were terminated with 150 Ω to the bottom of the WBFC. The setup was simulated in CST Microwave Studio with the transient solver (Finite Integration Technique) [20]. The model is shown in Fig. 4. The voltage across the 150 Ω WBFC terminations were monitored and adjusted to a 50 Ω measurement system. The sources were identified as current or voltage sources as described in Section IV-A.

The simulated WBFC measurements were compared with a simulated 3 m SAC radiated emission, where the PCB was placed 1 m above an infinite ground plane. Two 1 m long cables were attached 32 mm from the edges, (i.e., same position as in the WBFC) and terminated to the infinite ground plane, both directly to the ground and through a 150 Ω resistor. There were far-field monitors for every 10 MHz and additional far-field monitors for every 1 MHz around cable resonances. The electric field was evaluated in 3 m distance corresponding to a radiated emission test like CISPR 32.

The I/O-coupling was simulated by placing an identical trace 10 mm away, parallel to the signal trace, as illustrated in Fig. 3(b). The I/O trace was the test point in the WBFC simulation. In the 3 m SAC simulations, a 1 m long cable was attached to the I/O trace and terminated at ground in the same way as the simple microstrip board.

V. Result and Discussion of Analysis

The standard states that the IC(s) to be tested shall be facing the bottom of the cage. However, it is not the IC(s) itself

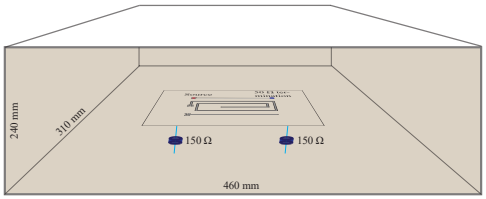

Fig. 4: The WBFC with the simple microstrip (with traces up) inside.

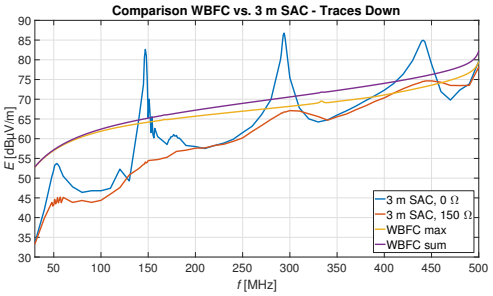

(a)

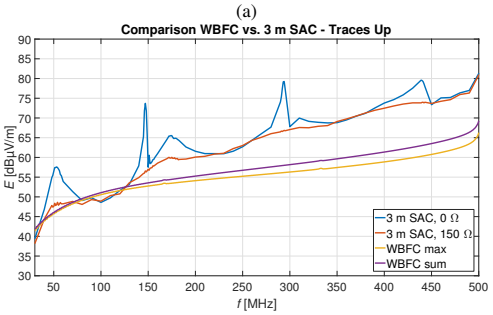

(b)

Fig. 5: (a) WBFC vs. 3 m SAC for traces down. (b) WBFC vs. 3 m SAC for traces up.

that couples to the attached cables but rather signal traces. These can be both on the top and bottom layer. Fig. 5 shows the WBFC simulations vs. the 3 m SAC simulations of the reference PCB with the traces facing down and up respectively, (i.e., whether the traces are facing up or down in a setup with the PCB parallel to the bottom of the WBFC and the chamber floor respectively.) The radiated emission, according to the WBFC, was found by using (1). Only results up to 500 MHz are present. Above the PCB size becomes comparable with the wavelength and the dominating antenna is the PCB itself and not the cables.

The 3 m SAC simulations show that when the cables are connected directly to ground, there are strong resonances. In contrast, a 150 Ω termination to ground almost completely suppresses the resonances. There is up to 30 dB difference between a 0 Ω termination and a 150 Ω termination. Hence it

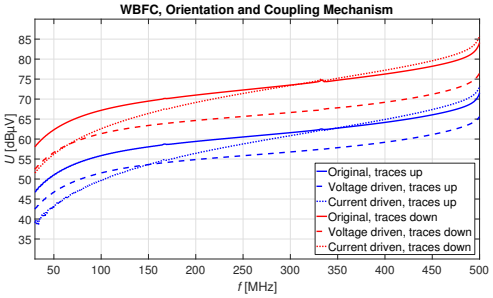

Fig. 6: WBFC traces up and down with voltage and current driven noise.

is highly arguable, how the WBFC measurement and 3 m SAC should be compared. The comparison can only be qualitative. Depending on the used CMAD device, measured values will be between those two extreme terminations.

The WBFC simulations show the (simulated) maximum voltage across the 50 Ω measurement equipment as suggested by the standard. In addition, the root square sum of both terminations is also plotted corresponding to adding the absorbed power from both terminations as discussed in Section III-A.

With the traces facing up and down, the trends are the same. Both WBFC values and 3 m SAC values increase with frequency, but the 3 m SAC values increase faster than the WBFC values. For traces facing down, this means that at low frequencies the WBFC overestimates the radiated emission, but as frequency increases, the WBFC underestimates the 3m SAC radiated emission. For traces facing up, the WBFC method underestimates the radiated emission over the whole frequency span. At 50 MHz, the radiated emission is within a 6 dB margin but at 439 MHz, the WBFC prediction is up to 20 dB below the 3 m SAC simulations. Even if the power absorbed in the two terminations are added and compared with the 150 Ω termination, the WBFC prediction is more than 10 dB below the 3 m SAC simulation.

In Fig. 6, WBFC simulations with traces up and down are compared. All over the frequency span, the WBFC simulations increase approximately 13 dB with the traces facing down compared to facing up. A typical PCB can have signal traces both on the top and bottom layer, so the accuracy of WBFC prediction will strongly depend on the orientation of the traces. Fig. 6 also shows that distinction between voltage and current driven coupling is also valid in the WBFC.

Fig. 7 shows the H-field on a plane orthogonal to the traces. The plane cut is in the center of the traces. The plot shows the H-field with the traces facing up and down inside the WBFC and in free space. It is clear from the figure, that the Faraday cage interferes with the H-field coming from the microstrip. The fields on both sides of the PCB interfere with the cage wall. According to [9] the EMI resulting from a finite ground plane is a function of both the flux wrapping around the trace and the flux wrapping around the ground plane. Hence, it is clear that the metal cage has strong influence on the WBFC measurements. There was a better agreement between WBFC

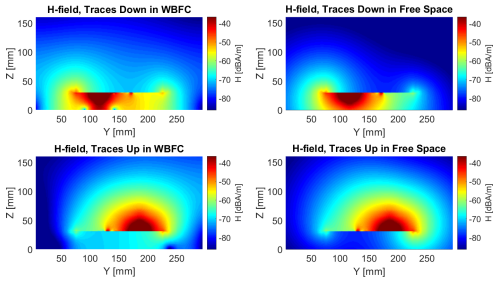

Fig. 7: H-field inside WBFC and in free space

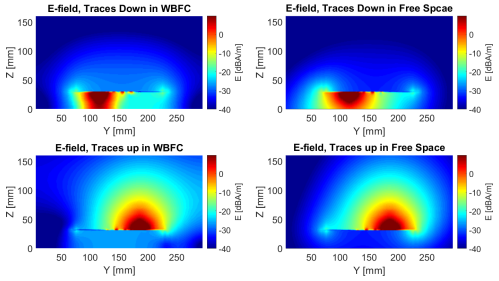

Fig. 8: E-field inside WBFC and in free space

and 3 m SAC for traces facing down than traces facing up. However, this improved agreement cannot be explained by the coupling mechanism inside the cage. There is no good physical argument why placing microstrip 30 mm above the cage floor facing down should mimic the coupling to cables better than with the traces facing up. Actually, in the specific 3 m SAC setup with the test microstrip PCB in open surrounding, (i.e., no product chassis, enclosure etc.,) traces up in the WBFC is physical more like the far-field setup.

Fig. 8 shows the same comparison for the E-field. Again, it is clear that the cage strongly affects the E-field on both sides of the ground plane. Hence, prediction of the voltage driven common mode emission will depend on the trace orientation in the WBFC. According to [12], the voltage driven EMI is a function of the ratio between the self-capacitance of the trace and the ground. The self-capacitance of the trace will increase with the traces down and the voltage driven common mode current will increase. Again, there is no good physical argument why traces facing down in the WBFC should be in better agreement with 3 m SAC simulations than traces facing up in the WBFC.

The comparison between WBFC and 3 m SAC for the I/O coupling reference PCB is shown in Fig. 9. The radiated emission in 3 m distance with cables attached does not change significantly with the trace orientation. However, the WBFC predicted radiated emission differs up to 6 dB whether the traces are facing up or down. Again, the difference between trace up and down in the WBFC can be explained by disturbance of the magnetic- and electric near-field of the active trace. Overall there is a better agreement between the WBFC

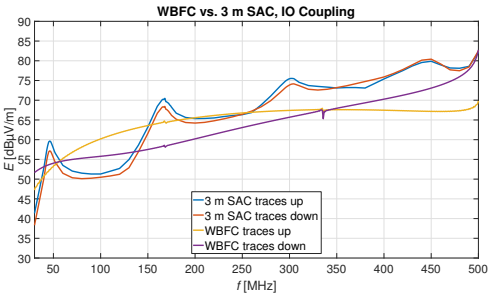

Fig. 9: WBFC vs. 3 m SAC for traces up.

predictions and the 3 m SAC values compared to the reference PCB where the EMI is voltage and current driven.

The above analyses were done based only on simulations. This choice is justified by previous work where there has been a small gap between simulations and measurements. In [6] WBFC simulations and measurements of the microstrip test PCB were in very good agreement. In [16] 3 m SAC simulations and measurements of the microstrip test PCB with 1 m long cables attached to ground were in very good agreement.

VI. Test Setup for Measurement Validation

A. Module Description

Three real boards were chosen for measurement validation: A power supply unit (PSU) and two measurement boards with both DC/DC converters, several microprocessor and RAM.

1) PCM5.1, Microprocessor and Power Supply Module: The PCM5.1 module is a microprocessor and power supply module for an advanced wind turbine controller. The controller is assembled with one PCM5.1 module and several other modules in a custom made rack system. All the modules are connected through a backplane mounted inside the rack system. Board size is 160 mm $\times$ 233 mm with 8 layers. Four test points were chosen: the ground of the power supply, ground of backplane, ground of Ethernet and finally ground of a RS422 connector.

2) GPM5.1, Voltage and Current Measurement Module: The GPM5.1 module is a voltage and current measurement module for an advanced wind turbine controller. The main function is to measure the three phased voltage on the mains and generator side, and the current trough all 3 phases. GPM5.1 is mounted in the controller rack. Board size is 160 mm $\times$ 233 mm with 6 layers. Five test points were chosen: power supply input and four I/Os for current and voltage measurements. Each of the three phase I/O was connected with a 300 Ω resistor to a star point resulting in 100 Ω common mode resistance.

3) PB50, Power Supply Unit: The PB50 module is a mains isolated power supply for audio equipment with build in loudspeakers. It has two flyback converters, one for standby and general electronic circuits and the other to supply the amplifiers. In general, the module has a low noise level from

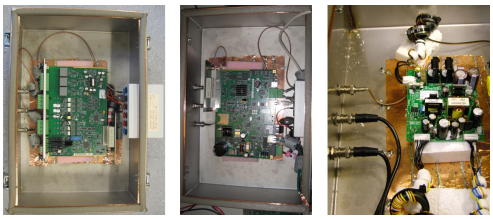

Fig. 10: WBFC test setup. Left: GPM5.1, center: PCM5.1, and right: PB50.

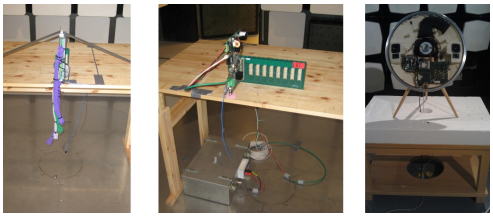

Fig. 11: 3 m SAC test setup. Left: GPM5.1, center: PCM5.1 mounted in backplane, and right: PB50.

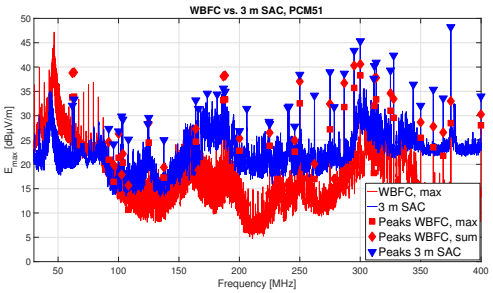

(a)

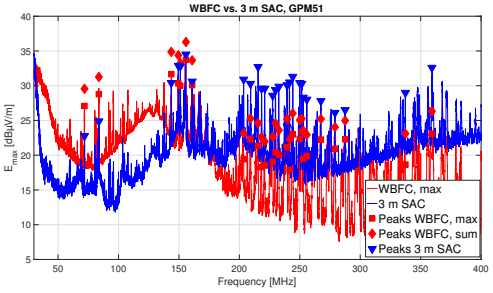

Fig. 12: Comparison of WBFC and 3 m SAC measurements. (a) PCM5.1, (b) GPM5.1

80 MHz upward so it will not disturb FM and TV signals. The only test point was the power line input.

B. General Test Setup

1) WBFC: The different DUTs were placed in a WBFC 30 mm above the cage floor and filtered according to the standard. All the PCB I/Os were terminated with 100 Ω (resistor) + 50 Ω (measurement equipment). The auxiliary signals were filtered and wrapped around a ferrite core in order to make the high impedance connection. A picture of the three WBFC test setups is shown in Fig. 10.

2) 3 m SAC: GPM51 and PCM51 were both measured alone in a 3 m SAC according to the EN 61000-6-3 light-industrial. Excess cable was organized according to the standard. For common mode absorbing, a ferrite bead was clamped on cables going out of the chamber, (i.e., the power cord and Ethernet cables.)

The PB50 was mounted in an active loudspeaker and measured according to CISPR 32. Only the PB50 was active with the same test software and power absorbers as used in the WBFC. Four ferrite beads were clamped on both the power cord and the Ethernet cable leaving the chamber.

The test setup is shown in Fig. 11

VII. Result of Measurement Validation

WBFC and 3 m SAC measurements are shown in the same plot. The WBFC voltage measurements are converted to 3 m SAC radiated emission measurements by (1). The maximum of the test points in the WBFC is plotted against the maximum of vertical and horizontal polarization in the 3 m SAC. For a more clear comparison, the peaks are marked. For the peaks, both the maximum and the power sum of all test points in the WBFC are plotted. The same test software is used in both WBFC and in 3 m SAC measurements. Hence, the measurements should be comparable with respect to clock frequencies.

A. PCM5.1 and GPM5.1

The comparison of WBFC and 3 m SAC measurements for PCM5.1 and GPM5.1 is shown in Fig. 12. For both boards the noise source from 30 - 60 MHz is the power supply (DC/DC converter) and the dominant test point in the WBFC is the power supplies ground pins. In this frequency span, WBFC and 3 m SAC measurements have the same trends, however, the amplitude of the WBFC measurements are 5-10 dB above the 3 m SAC measurements. From 60-300 MHz, the noise sources are digital, (i.e., microprocessors, Ethercat controller, AD converters etc.) and the dominant test points in the WBFC is the RS422 for PCM5.1 and the backplane ground and the generator voltage I/O for GPM5.1. From 60-140 MHz, the WBFC underestimates the radiated emission from a few dB up to 20 dB. The WBFC measurements have a few dips that is not seen in the 3 m SAC measurements, (e.g., PCM5.1 has a dip at 215 MHz and 265 MHz.) Above 400 MHz, the radiated emission was strongest with the ICs pointing directly to the measurement antenna which indicates that the module itself starts to radiate rather than attached cables.

If the power is added from all four test points, the WBFC predicting radiated emission increases between 1 and 5 dB and the underestimation of the radiated emission is reduced.

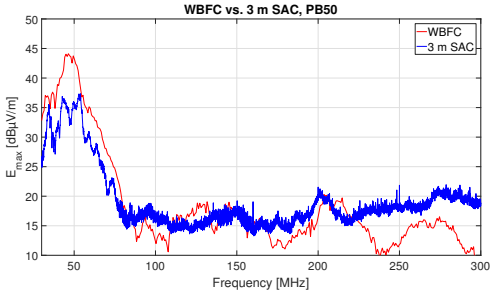

Fig. 13: Comparison of WBFC and 3 m SAC measurements of PB50.

-

B. PB50, Power Supply Unit

The comparison between WBFC and 3 m SAC measurements is shown in Fig. 13. In the WBFC measurements there was only one test point, the power supply. The PSU is generally low noise from 80 MHz and up, which also is clear from the WBFC measurement. There is good agreement between the trends in the WBFC and the 3 m SAC measurements. However, the WBFC measurements overestimate the radiated emission up to 8 dB.

VIII. Discussion of Measurement Results

A. Digital IC Noise

The radiation caused by IC noise, (e.g., micro processor and RAM,) couples to the cables by help of microstrips. The trends in the measurements were alike the trend in the simulations of the simple microstrip test board. As the frequency increases, the measured radiated emission increases more than the WBFC predicted radiated emission. In the 3 m SAC measurements, the cables were terminated with a ferrite bead preventing strong resonances. However, the WBFC still underestimate the radiated emission. The simulations showed that all three coupling mechanisms (i.e., voltage and current driven and direct coupling) are affected by the metal cage used in the WBFC measurements. Hence, it is not surprising that the agreement between the WBFC and 3 m SAC measurements is poor. In addition, previously work [16] has shown that the coupling between microstrip and cables cannot fully be described by noise generators and lumped elements.

If 3 m SAC measurements are compared with the WBFC prediction based on the power addition of all test points, the underestimation is reduced 1-5 dB, but it does not change the trend with increasing underestimation vs. frequency.

B. Power Supply Noise

For all three modules, WBFC and 3 m SAC measurements have the same trend regarding power supply noise. The noise is typical switch mode noise, (i.e., switch noise from diodes and MOSFETs.) The coupling from noise source to the power line is not like a simple microstrip but rather complicated. The coupling is properly from one loop on the board to another loop connected to the power line input. This coupling path seems to be undistorted by the cage used in the WBFC measurements contrary to electric field coupling, magnetic field coupling, and direct coupling as described in Section II-A.

One of the reasons is that there normally is a high impendent filter in the power line connection and the board react as a current source independent of the impedance of the wires connected in 3m SAC.

Both the radiated emission caused by the PSU and the ICs below 100 MHz is overestimated in the WBFC. (1) was determined based on the assumption that the power absorbed by the resistors in the WBFC is radiated in a match dipole. At 100 MHz, the wavelength is 3 m and a match dipole is slightly shorter than 1.5 m. Hence, at low frequencies, the cables are too short to radiate effectively.

IX. Conclusion

IEC 61967 part 5, the WBFC method, has been analyzed by simulations of a simple microstrip PCB and by measurements of three real modules. Both in the simulations and measurements, there was a poor agreement between the radiated emission predicted from the WBFC and the actual radiated emission. At low frequencies, the WBFC tends to overestimate the radiated emission because of electrically short cables in the 3 m SAC measurements, but as the frequency increases, WBFC increasingly underestimates the radiated emission.

The simulations showed that the Faraday cage strongly affects the electric, magnetic, and direct coupling from a microstrip to the termination. In the specific test case, traces facing the bottom of the cage measured 13 dB higher than traces facing up. For a real digital PCB, there can be signal traces on both the top and bottom layer, and, hence, the WBFC prediction becomes arbitrary depending on the orientation of the DUT in the WBFC.

The conclusions from the simulations were supported by the measurements of the three real PCBs. The measurements could not validate the method. However, there was a good agreement between the trends in the WBFC and 3 m SAC for PSU noise. The PSU noise source coupling is different from the microstrip coupling. WBFC overestimated the radiated emission, but it could be a topic for further studies to find a correction factor depending on cable length and termination.

In general, the noise generator and lumped elements model are too simple for common mode emission prediction. Placing the DUT in a Faraday cage, which affects the coupling path from trace to cables, makes prediction errors larger.

Except for PSU noise, the WBFC method fails as a pre-compliance test. It has not been investigated whether the method is useful for comparative measurements, (i.e., whether the relative effect of a layout or filter change in the WBFC gives the same relative effect in 3 m SAC measurements.)

Acknowledgment

The authors would like to thank Mr. Jan Clausen (DEIF A/S) for his valuable help in performing the measurements. The present work has been supported by the Danish Agency for Science, Technology and Innovation.

REFERENCES

[1] IEC, "IEC 61967-5:2003 Integrated circuits - Measurement of electromagnetic emissions, 150 kHz to 1 GHz - Part 5: Measurement of conducted emissions - Workbench Faraday Cage method," Standard, 2003.

[2] M. Coenen, "Common mode impedance measurements on cables in the frequency range 30 MHz - 1 GHz," *EIE92004, Philips Semiconductor*, 1994.

[3] ——, "EMC workbench: Testing methodology, module level testing and standardization," *Philips Journal of Research*, vol. 48, 1994.

[4] A. Nakamura and Y. Mabuchi, "Common mode voltage evaluation for choosing quiet MCU and optimizing PCB design: Electromagnetic emissions measurement for integrated circuits," in *2007 IEEE International Symposium on Electromagnetic Compatibility*, July 2007, pp. 1–7.

[5] V. Rek, J. Dnovsk, Z. Kejk, and J. Zachar, "Influence of the probe position to disturbance measurement in the workbench Faraday cage," in *Proceedings of 21st International Conference Radioelektronika 2011*, April 2011, pp. 1–4.

[6] M. Sørensen, O. Franek, S. K. Christensen, G. F. Pedersen, and H. Ebert, "Assessment of the usability of the workbench Faraday cage method," in *2011 IEEE International Symposium on Electromagnetic Compatibility*, Aug 2011, pp. 399–404.

[7] D. Hockanson, J. Drewniak, T. Hubing, T. Van Doren, F. Sha, and M. Wilhelm, "Investigation of fundamental EMI source mechanisms driving common-mode radiation from printed circuit boards with attached cables," *Electromagnetic Compatibility, IEEE Transactions on*, vol. 38, no. 4, pp. 557–566, Nov 1996.

[8] T. Hubing, "Printed circuit board emi source mechanisms," in *Electromagnetic Compatibility, 2003 IEEE International Symposium on*, vol. 1, Aug 2003, pp. 1–3 vol.1.

[9] D. Hockanson, J. Dreniak, T. Hubing, T. Van Doren, F. Sha, and C.-W. Lam, "Quantifying emi resulting from finite-impedance reference planes," *Electromagnetic Compatibility, IEEE Transactions on*, vol. 39, no. 4, pp. 286–297, Nov 1997.

[10] F. Leferink, "Reduction of printed circuit board radiated emission," in *Electromagnetic Compatibility, 1997. IEEE 1997 International Symposium on*, Aug 1997, pp. 431–438.

[11] G. Dash, J. Curtis, and I. Straus, "The "current driven model" - experimental verification and the contribution of I_{dd} delta to digital device radiation," in *Electromagnetic Compatibility, 1999 IEEE International Symposium on*, vol. 1, 1999, pp. 317–322 vol.1.

[12] H.-W. Shim and T. Hubing, "Model for estimating radiated emissions from a printed circuit board with attached cables due to voltage-driven sources," *Electromagnetic Compatibility, IEEE Transactions on*, vol. 47, no. 4, pp. 899–907, Nov 2005.

[13] S. Deng, T. Hubing, and D. Beetner, "Estimating maximum radiated emissions from printed circuit boards with an attached cable," *Electromagnetic Compatibility, IEEE Transactions on*, vol. 50, no. 1, pp. 215–218, Feb 2008.

[14] ——, "Characterizing the electric field coupling from ic heatsink structures to external cables using tem cell measurements," *Electromagnetic Compatibility, IEEE Transactions on*, vol. 49, no. 4, pp. 785–791, Nov 2007.

[15] C. Su and T. H. Hubing, "Calculating radiated emissions due to I/O line coupling on printed circuit boards using the imbalance difference method," *IEEE Transactions on Electromagnetic Compatibility*, vol. 54, no. 1, pp. 212–217, Feb 2012.

[16] M. Sørensen, T. H. Hubing, and K. Jensen, "Study of the impact of board orientation on radiated emissions due to common-mode currents on attached cables," in *2016 IEEE International Symposium on Electromagnetic Compatibility (EMC)*, July 2016, pp. 36–40.

[17] S. Okuyama, K. Osabe, K. Tanakajima, and H. Muramatsu, "Investigation on effectiveness of very high frequency line impedance stabilization network (VHF-LISN) for measurement reproducibility," in *2013 International Symposium on Electromagnetic Compatibility*, Sept 2013, pp. 174–179.

[18] K. Osabe, N. Kuwabara, and S. Okuyama, "Termination impedance for AC mains cable leaving from EUT area in radiated emission measurement," in *2017 International Symposium on Electromagnetic Compatibility - EMC EUROPE*, Sept 2017, pp. 1–6.

[19] CISPR, "CISPR 32:2015 Electromagnetic Compatibility of Multimedia Equipment - Emission Requirements," Standard, 2015.

[20] "CST MicroWave Studio, http://www.cst.com."

Morten Sørensen (M'08) received the M.S. degree in physics from Aarhus University, Aarhus, Denmark, in 2005. From 2006 to 2017, he was an Antenna and Electromagnetic Compatibility (EMC) specialist with Bang & Olufsen, Struer, Denmark, including three years (2011-2014) as a Researcher and Technical Project Manager in the innovation consortium, EMC Design First Time Right. In 2017, he joined the EMC Laboratory, Missouri University of Science and Technology, Rolla, MO, USA, where he is a visiting Assistant Research Professor. Since 2018 he has been working part time with Amber Precision Instruments, San Jose, CA, USA. His current resarch interests include near-field scanning, emission source microscopy, electrostatic discharge, and system-level radiated emission.

Søren Kjærullf Christensen received the B.S degree in electronic engineering from Aarhus Technical College, Denmark, in 1988. From 1990 to 2016 he worked with power and EMC at Bang & Olufsen, Struer, Denmark. From 2011 to 2014 he did research in the EMC Design First Time Right. In addition he has also done research in two EFP-projects Energy efficient mains powered standby power supplies and Energy-saving rectifier. He is a part of patent, US7656691B2, "Charge mode control of a serial resonance converter." From 2016 employed as senior engineer at Terma, Lystrup, Denmark. His current research interest include EMC related to power supplies.

Claus Vittarp received his B. Sc. in electrical engineering from Aarhus University, Herning. Denmark, in 1997. From 1997 to 2008 he worked with RF and EMC at Bang & Olufsen in Struer, Denmark. Since 2008 he has been working with high speed digital electronics and EMC at DEIF A/S in Skive Denmark, where he did research in the innovation consortium EMC Design, First Time Right from 2011-2014. His current research interest include EMI related to digital electronics.

Hans Ebert received his M.Sc. in Electrical Engineering from Aalborg University in 1984, and his PhD in 1991. Since 1984 he has been working with research and education in electromagnetic, antennas, cables, EMC and radio technology at Aalborg University. His current research interests include EMC, antenna design and simulation of wave propagation.

Paper D

Perturbation of Near-field Scan from Connected Cables

Morten Sørensen[1], Ondrej Franek[1], Gert Frølund Pedersen[1],
Knud A. Baltsen[2], Hans Ebert[1]
[1]Antennas, Propagation and Radio Networking section, Aalborg University,
Niels Jernes Vej 12, 9220 Aalborg, Denmark, {mos, of, gfp, heb}@es.aau.dk
[2]Bang & Olufsens a/s, Peter Bangs Vej 15, 7600 Struer, Denmark,
kbl@bang-olufsen.dk

The paper has been published in the
Electromagnetic Compatibility (EMC), 2012 IEEE International Symposium
on, Aug 2012, pp. 594–599.

The layout has been revised.

Perturbation of near-field scan from connected cables

Morten Sørensen[#1], Ondrej Franek[#2], Gert Frølund Pedersen[#3], Knud A. Baltsen[*4], Hans Ebert[#5]

[#]Antennas, Propagation and Radio Networking, Department of Electronic Systems, Faculty of Engineering and Science, Aalborg University,
Niels Jernes Vej 12, 9220 Aalborg, Denmark

[1] mos@es.aau.dk, [2] of@es.aau.dk, [3] gfp@es.aau.dk, [5] heb@es.aau.dk

[*] Bang & Olufsens a/s, Peter Bangs Vej 15, 7600 Struer, Denmark

[4] kbl@bang-olufsen.dk

***Abstract*—The perturbation of near-fields scan from connected cables are investigated and how to handle the cables is discussed. A connected cable induced small but theoretical detectable changes in the near-field. This change can be seen in Huygens' box simulations (equivalent source currents on a box) at the cable resonance frequencies while there is no change away from the resonance frequencies.**

I. Introduction

Near-field scanning has become a popular measurement technique in the field of EMI/EMC. For some years near-field scan has been used in the development phase in order to find EMI hotspots on PCBs (Printed Circuit Boards), but in recent years attempts to predict radiated emission using near-field measurement have also been carried out.

There are two different dominating approaches to far-field prediction. One approach uses the near-field as basis for source reconstruction by help of an equivalent set of dipoles [1,2] and one approach uses the tangential electrical and magnetic fields on a closed surface often named a Huygens' box [3,4].

The very ambitious idea is that an apparatus´ radiated emissions in the far-field can be simulated based on near-field scan of the modules comprising the apparatus and the influence of the architecture (module's relative position, cables, chassis and other environments).

The work with predicting far-field radiated emission from near-field scan is still in embryo and the attempts until now have been carried out on very simple structures without long cables and often only for a single frequency.

If near-field scanning shall become an effective tool for engineers in R&D, it is necessary to be able to near-field scan advanced PCBs with (galvanically) connected cables. But no one has yet investigated how connected cables can be handled in the near-field scan and the subsequent simulations. Do the cables perturb the near-field significantly? Is it best to establish fixed common mode impedance for connected cables? Is it possible to predict common mode currents on connected cables from near-field scan? It is many questions and they are not yet answered in the literature.

The objective of the work presented in this article is to start the investigation and discussion about this important topic by studying a simple PCB with connected long cables. Mainly based on simulations we will find the absolute and relative perturbation caused by a cable on the near-field.

Section II gives a very short introduction to the surface equivalence principle (the Huygens' box) and the challenges we face in using the principle for predicting far-fields based on measured near-field for real PCBs and apparatuses. In section III the test setup and simulations are described. Then the results are presented and discussed in Section IV. Finally Section V draws the conclusions.

In Fig. 1.a a PCB is enclosed in a surface S. The electric and magnetic fields on this surface are denoted $\{\boldsymbol{E_1(r)}\ \boldsymbol{H_1(r)}\}$ According to the surface equivalence principle an arbitrary structure containing sources of electric and magnetic fields is equated with electric and magnetic currents on a surface that encloses the structure so that the fields within the surface all are 0, while outside the surface the fields are identical to the fields caused by the initial sources provided that the outer region is homogeneous and source free [5,6]. A rectangular box with equivalent currents on the surface is often denoted a Huygens' box. This means that electric and magnetic fields at a general observation point outside S in Fig. 1.a, denoted $\{\boldsymbol{E(r)}\ \boldsymbol{H(r)}\}$, are equal to the electric and magnetic fields at the same

II. Huygens' Box

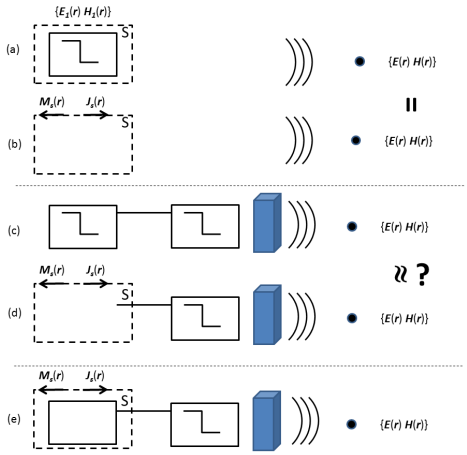

Fig. 1. Representation of the Huygens' box: (a) Original problem for a single radiating PCB, (b) equivalent sources on a Huygens' box, (c) original problem for a more complicated system with 2 PCBs, a cable and a scattering surface (the blue box), (d) an approximation of the surface equivalence principle where the region outside the surface is not homogenous nor source free, (e) a probably better solution where a ground plane approximates the coupling between the PCB and devices outside S.

observation point in Fig. 1.b where the equivalent electric and magnetic currents are given by $\boldsymbol{J_s(r)} = \boldsymbol{n} \times \boldsymbol{H_1(r)}$ and $\boldsymbol{M_s(r)} = -\boldsymbol{n} \times \boldsymbol{E_1(r)}$. These current densities can be deduced from the tangential electric and magnetic field on the closed surface, which in practice may be found using near-field measurements.

In real apparatuses configured of several PCBs, chassis, cables etc. the region outside the surface is not homogenous nor source free. This is indicated in Fig. 1.d. If we use the equivalent sources from Fig. 1.a in order to predict the electric and magnetic fields in Fig. 1.d, we do not know how well the electric and magnetic fields in a general observation point in Fig. 1.c and 1.d are in agreement.

As long as the coupling between devices outside the Huygens' box and the radiating device is weak, good results can probably be achieved by this approximation. To improve the results of a simulated model, one can approximate the first order effects of the coupling by replacing the radiating device inside the Huygens' box by an approximate model, e.g. the ground plane of a PCB (Fig. 1e). This is possible because the equivalent sources acting alone produce a null field inside the box.

Connected cables, e.g. LVDS cables or power cables represent a distinct challenge for the prediction of the radiated emission, because the coupling between the near-field scanned radiating device and the cables is strong and cables often have lengths comparable with the wavelength of the unintended radiated emission and hence common mode current on cables becomes the dominant emitter. In addition the cables go through the walls of the Huygens' box.

III. Test Setup

A. *The objective of the experiments*

It emerges clearly that the model for predicting radiated emission based on near-field measurements described in section II violates the surface equivalence principle when cables are connected. Does that mean that near-field measurements are useless if cables are connected or is the deviation small or can we perhaps compensate for the violation?

In order to answer these questions some simple setup were simulated and measured with and without connected cables. In each setup the approach was as illustrated in Fig. 2.

a) Physical models of the PCB alone and the PCB with a cable connected to the PCB ground plan. The PCB alone model represents a near-field scan where all connected cables have been terminated with perfect ferrites in order to remove the effect of the cables. The near-fields of the two models were compared with the objective to estimate whether it is possible to measure the differences with a near field scanner or the differences are below the measurements uncertainty.

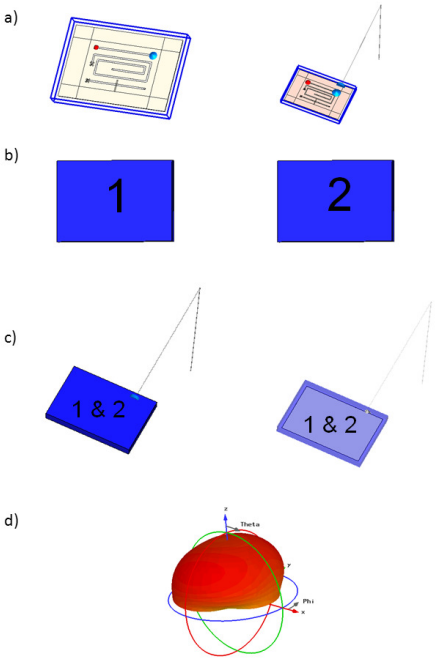

Fig. 2. Simulation workflow.

b) Huygens' box extraction: The tangential near-fields on a Huygens' box surrounding each model (i.e. with and without cable) were extracted. The Huygens' box exceeded the PCB by 10 mm in all directions and hence included a part of the cable (10 mm).

c) Huygens' box source simulations: The two Huygens' boxes were used as source for simulations of a 3 m semi-anechoic chamber (3 m SAC) measurement. For both cases a cable was added and in another simulation a ground plane inside the Huygens' box was also added in order to approximate the coupling between the PCB and the cable.

d) Comparison of far-fields: The predicted maximum far-fields from the physical models (reference) and the two different Huygens' boxes models were compared.

B. *Simulations*

The simulated PCB is shown in Fig. 3. A simple 150 x 225 mm PCB with three 50 ohms traces on the top layer and full unbroken ground plane were chosen. Only one trace were excited and terminated. Both source impedance and load was 50 Ω. The simulations were carried out in CST Microwave Studio with the transient solver (Finite Integration Technique).

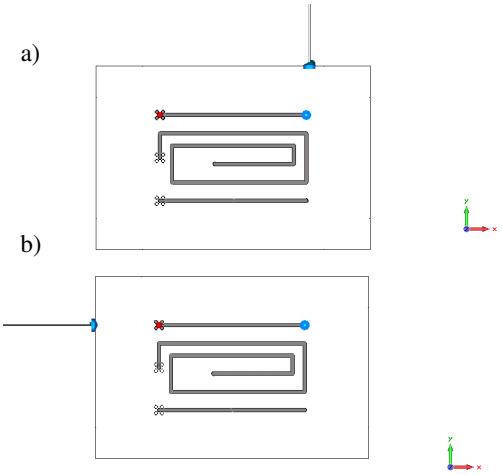

Fig. 3. Layout of the test PCB and position of the connected cables.

Three different cables setups were simulated. In all setups an infinite ground plane was placed 80 cm below the PCB in order to simulate a 3 m SAC.

1) An 80 cm long cable was connected 5 cm from the edge (Fig. 3.a). After 40 cm the cable made a 90° bend towards the ground and hence the cable end is 40 cm above the ground plane.

2) A 100 cm long cable was connected at the same position (Fig. 3.a). After 20 cm the cable made a 90° bend towards the ground and the end is connected to the ground plane 80 cm below the PCB.

3) A 100 cm straight cable was connected at another side of the PCB (Fig. 3.b).

The cable setups was chosen so that they represent a variety (floating vs. terminated cables) of typical setups in apparatus.

C. Measurements

With the purpose to perform a basic validation of the simulations, a near-field scan and a 3 m SAC measurement were carried out on setup 1. A comb generator (a signal generator that produces multiple harmonics of its input signal) with fundamental frequency of 20 MHz was mounted on the back of the PCB and used as a noise generator. The output voltage from the generator measured across 50 Ω was about 85 dBµV up to 1 GHz.

The near-field scanner was a home-made scanner consisting of a robot that moves a Langer RF 50-1 near-field probe across the PCB. Through an Agilent 8447D pre-amplifier the probe was connected to a Rohde Schwartz ZVB8 VNA acting like a spectrum analyser. In other words it was only the amplitude that was measured. The step size in the measurement was 5 mm and the scan height was 10 mm.

IV. Results and Discussion

The simulation results from all 3 setups were similar and therefore we will only present the results from setup 1. The simulation results will be presented in a way that represents a hypothetical state-of-the-art near-field scanner, which means that all data are plotted with a dynamic range of 60 dB. The input power in the simulation is scaled to 0 dBm.

A. Near-field comparison metric

In the next section we will compare the near-field on the Huygens' box for two different frequencies. Two different metrics for the difference between near-fields are chosen. In the "absolute difference" the near-fields (in linear scale) for with- and without cables are subtracted and then plotted in a dB-scale, e.g.:

Absolute diff. = 20*log10(abs($H_{x\ \text{without cable}}$ (linear) - $H_{x\ \text{with cable}}$ (linear)).

This gives an absolute measure of the perturbation from the cable.

In the "relative difference" the near-fields in dB scale are subtracted, e.g.:

Relative diff. = abs($H_{x\ \text{without cable}}$ (dB) - $H_{x\ \text{with cable}}$ (dB)).

If the near-field in a point is below the dynamic range the field value is set to the lowest value in the dynamic range in order to represent a real near-field scan where the field value is in the noise floor. It is reasonable to assume that a state-of-the-art near-field scanner would have a log-scaled measurement uncertainty and hence this relative difference will indicate whether it is possible to measure the difference, or whether it is below the measurement uncertainty. The color bar scale in the relative plots are set to 0-4 dB, which means that with this state-of-the-art scanner, the cable perturbation surely will be measurable in areas, where the difference is over 4 dB (the dark areas), while it goes below the measurement uncertainty when the difference come close to 0 dB (the blue areas).

B. Near-field comparison

In the simulations there was a cable resonance at 118 MHz and at 286 MHz. The results for 118 MHz and 286 MHz are similar and only the results for 286 MHz are shown. As a representative for a non-resonance frequency 800 MHz was chosen.

In Fig. 4.a the magnetic near-field at 286 MHz 10 mm above the PCB (xy-plane) is shown. The PCB is 225x150 mm and we have plotted the field 10 mm extra in both x- and y-direction (see PCB layout and coordinate systems in Fig. 3). In Fig. 4.b the H-field at 286 MHz on the xz-plane (at the cable side) 10 mm from the PCB is shown. The PCB was 1.6 mm thick and the ground plane is placed in z = 0 mm. The near-field data was exported with 1 mm resolution.

With the naked eye it is difficult to see any difference in Fig. 4a while even though the H-field level is weaker at the y-normal surface the cable emerge clearly in Fig. 4b (the dark spot at x = 175 mm, z = 0 mm).

In Fig. 5 the difference is plotted according to section IV A. At the xy-plane the absolute differences show that the cable resonance causes currents to run in the ground plane (especially at the edge on the cable side) although these are small compared to the currents running on the microstrip.

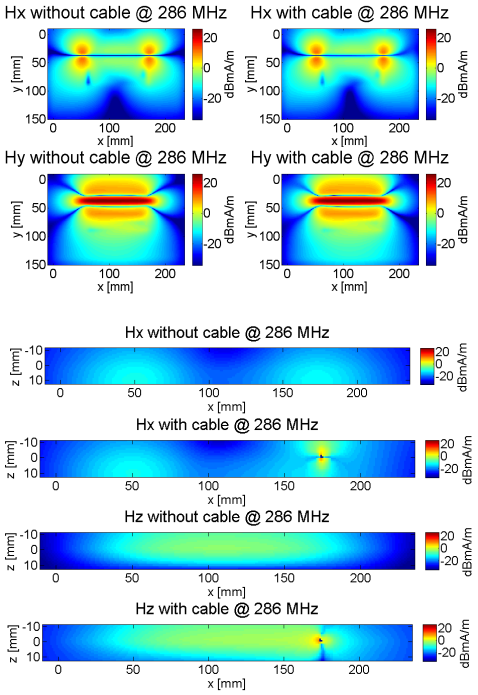

Fig. 4. The magnetic near-field at the top surface and the cable surface. See Fig. 3 for PCB layout and cable position.

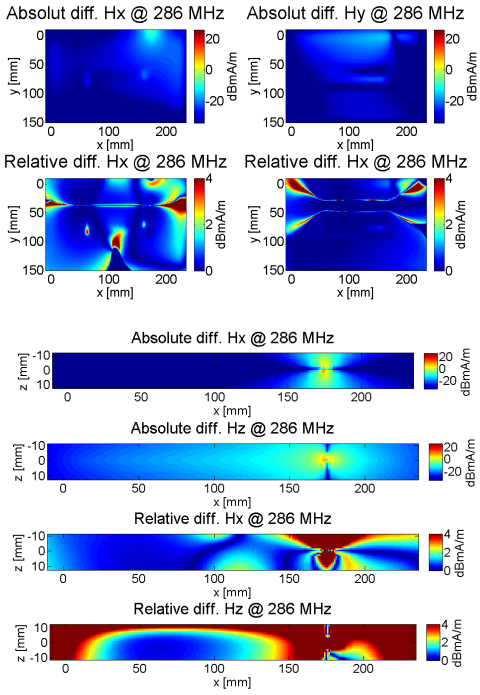

Fig. 5. The difference in magnetic near-field at the resonance frequency 286 MHz. See Fig. 3 for PCB layout and cable position.

The relative difference plot shows that with a measurement uncertainty of 1 dB and a dynamic range of 60 dB it is only possible to measure the difference at some low radiating spots. At the xz-plane the difference is larger - both absolute and relative. The common mode current on the connected cable is mainly induced by the fields on this plane.

The difference plot for the E-field at 286 MHz in figure 6 shows that the cable causes a voltage difference across the PCB´s ground plane. It also shows that the electric field caused by this voltage is small compared to the electric field from the microstrip.

In Fig. 7 the difference plot for the H-field at 800 MHz is shown. Even though the 800 MHz is not a resonance frequency, the perturbation of the near-field is at the same level as at the resonance frequencies.

C. Prediction of 3 m SAC measurement

In Fig. 8 the validity of the Huygens' box method is tested. In the simulation the full model of the PCB without cable is replaced by the Huygens' box and the radiated emission in 3m SAC is simulated. We have used two different mesh cell sizes, 2.5 mm and 5.0 mm (representing two different step sizes in a near-field scan), and both simulated Huygens boxes are in very good agreement with the full model simulation.

Fig. 9 shows the simulation of the maximum E-field in a 3 m SAC for the two different Huygens' boxes. When we added only a cable to the Huygens' box extracted from the model without cable connected and simulated the far-field, the simulations did not predict the resonances at 118 MHz and 286 MHz. When we inside the Huygens' box added a ground plane connected to the cable, the resonances was predicted but the amplitude of the resonance was far below the full model resonance.

Above 450 MHz the PCB itself was the dominating radiator and the connected cable did not change the far-field significantly. When we used the Huygens' box extracted from the model with cable connected (Fig. 9.b) and made the same simulations of the far-field, the simulations predicted the correct resonance frequencies at the right amplitude for both cases, i.e. only cable and cable plus ground plane.

For both Huygens' boxes a weak but wrong resonance at 190 MHz was also predicted (the enlarged part of Fig. 9) if only the cable and not the ground plane was added to the Huygens' box.

It is outside the scope of this paper to give a detailed explanation, but it is obvious that the cable alone in the 3 m SAC has another resonance than the cable together with the PCB ground plane.

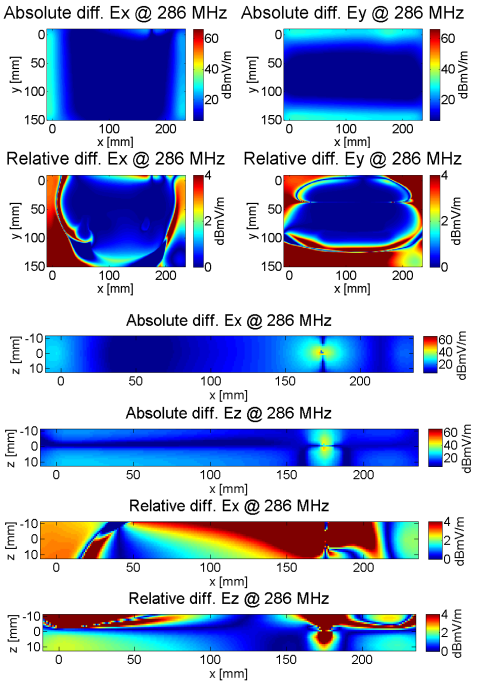

Fig. 6. The difference in electric near-field at the resonance frequency 286 MHz. See Fig. 3 for PCB layout and cable position.

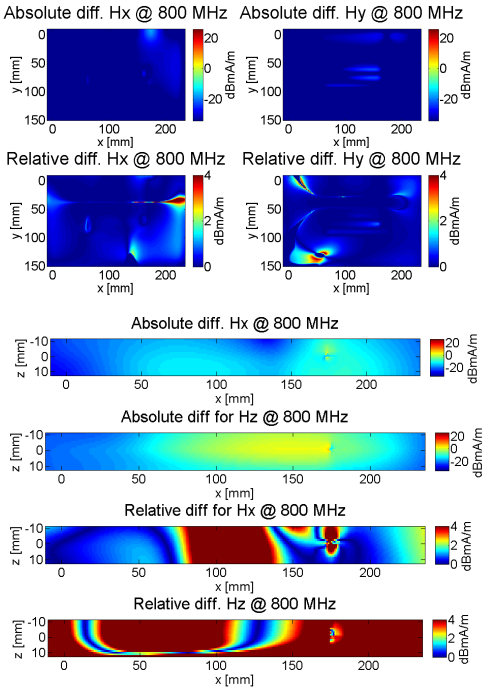

Fig. 7. The difference in electric near-field at the non resonance frequency 800 MHz. See Fig. 3 for PCB layout and cable position.

The field on top of the PCB (xy-plane), which does not change much with the cable attached, is able to induce a small current on the cable (with resonance frequency of 190 MHz) and cable plus ground plane (with resonance frequency of 118 and 286 MHz), but only the fields on the y-normal side of the Huygens' box are able to induce a large current. In practice it will be very difficult physically to make a near-field scan in the area close to cables which seems to be necessary in order to measure the near-field that induced the common mode current on cables.

A. Comparison between simulation and measurement

In Fig. 10 the measured and the simulated near-field is compared. The simulated near-field is scaled to the output power of the comb generator. The plot shows that our measurement did not have 60 dB dynamic range. The maximal amplitude in the simulation was 3.3 dBmA/m and –0.5 dBmA/m in the measurement. The step size in the measurement was 5 mm while data is extracted with a resolution of 1 mm from the simulation.

Beside that there is not used probe compensation in the measurement. At the scanned surface it was not possible to measure a systematic difference between the PCB without cable and the PCB with a cable connected, i.e. the difference was below the measurement uncertainty or the areas with relative large difference was in the noise floor.

Fig. 11 shows the full model simulated E-field inside the 3 m SAC compared with the 3 m SAC measurement - with and without cable. Here it must be pointed out that an EMC 3 m SAC measurement carried out after the CISPR standard does not give the correct E-field. Nevertheless simulation and measurement predict the same cable resonances and almost the same amplitude level.

The sharp resonances at approximately 500 MHz and 660 MHz are not reflected in the measurement but it is possible that the resonances were between two comb frequencies.

V. Conclusion

In this paper we have investigated the perturbation of near-field scan from connected cables. In order to measure the perturbation a very good near-field scanner with large dynamic range and small measurement uncertainty is needed. If we hypothetically assume that such a state-of-the-art scanner is available and it is physically possible to measure the near-field close to cables, it should be possible from the surface equivalence principle to predict the radiated far-field if we measure the near-field on a Huygens' box enclosing the PCB when the cable is present and connected and if we include a ground plane inside the Huygens' box in the simulations.

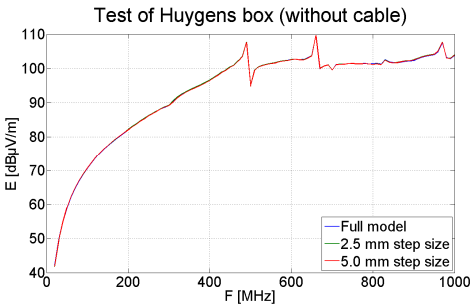

Fig. 8. Simulations of the E-field in a 3 m SAC chamber for the full model, a Huygens' box model with coarse mesh and fine mesh reflecting the step size in a near-field scan. The differences is within a few tenths dB and hence the curves overlap.

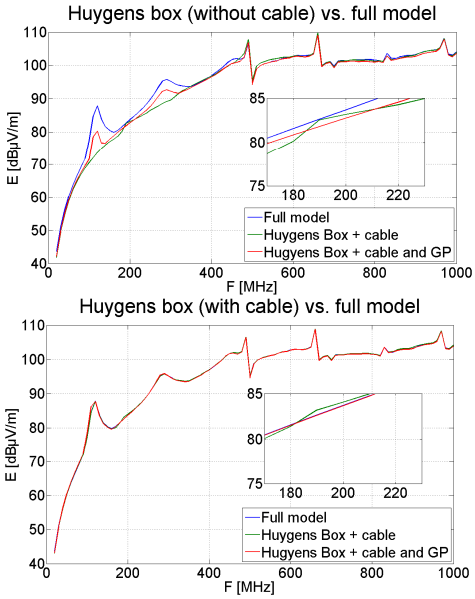

Fig. 9. Simulations of the E-field in a 3 m SAC chamber: (a) for the Huygen box source simulated without cable, (b) for the Huygne box source simulated with cable. In (b) the differences is within a few tenths dB and hence the curves overlap. The plot in a frequency span around 190 is enlarged in order to show the weak but wrong cable resonance at 190 MHz.

But this will require that the cable common mode impedance is the same in the near-field scan than in the final apparatus.

Away from the cable resonance frequencies a connected cable also causes perturbation of the fields, but the perturbation of near-field does not influence the far-field prediction. To be on the safe side one could of course add ferrites on the cables in the near-field scans.

In other words the near-fields on Huygens' boxes are useful for predicting radiated fields from the PCB itself even though cables are connected, but it could be difficult in practice to predict the radiation from common mode currents on cables based on near-field scan.

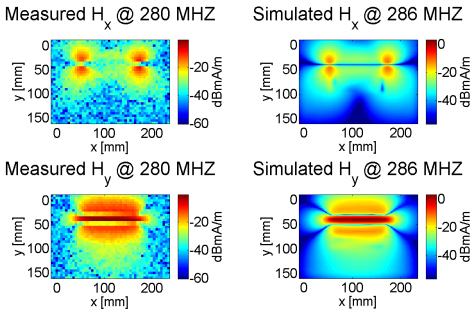

Fig. 10. Comparison between measured and simulated near-field at 286 MHz. See Fig. 3 for PCB layout.

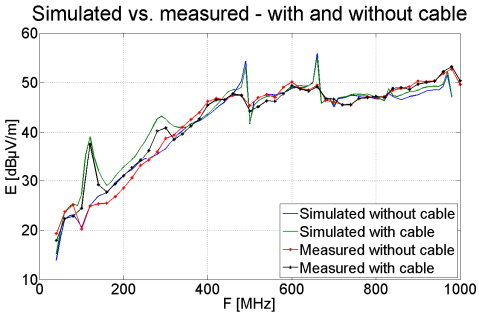

Fig. 11. Comparison between measured and simulated 3 m SAC measurement.

REFERENCES

[1] J-R Regué, M. Ribó, J-M Garrell, A. Martín, "*A Genetic Algorithm Based Method for Source Identification and Far-Field Radiated Emissions Prediction From Near-Field Measurements for PCB Characterization*", IEEE Transactions on Electromagnetic Compatibility, Volume 43, No 4, Nov. 2001

[2] Vives-Gilabert, Y.; Arcambal, C.; Louis, A.; Eudeline, P.; Mazari, B.; "*Modeling Magnetic Emissions Combining Image Processing and an Optimization Algorithm*" IEEE Transactions on Electromagnetic Compatibility, Volume 51, No 4, Nov. 2009

[3] Shi, J.; Cracraft, M.A.; Zhang, J.; DuBroff, R.E.; Slattery, K.; "*Using near-field scanning to predict radiated fields*, "Proceedings of IEEE International Symposium on Electromagnetic Compatibility, Silicon Valley, 2004.

[4] H. Weng, D. G. Beetner, R.E DuBroff, "*Prediction of Radiated Emissions Using Near-Field Measurements*" IEEE Transactions on Electromagnetic Compatibility, Volume 53, No 4, Nov. 2011

[5] C. A. Balanis, *Advanced Engineering Electromagnetics*, New York: John Wiley & Sons, Inc., 1989, chapter 7

[6] Rengarajan, S.R.; Rahmat-Samii, Y., "The field equivalence principle: illustration of the establishment of the non-intuitive null fields", Antennas and Propagation Magazine, IEEE, Volume 42, Issue 4, Aug 2000

Paper E

Estimate on the Uncertainty of Predicting Radiated Emission From Near-field Scan Caused by Insufficient or Inaccurate Near-field Data

Morten Sørensen[1], Andriy Radchenko[2], Keong Kam[2], David Pommerenke[2], Ondrej Franek[1], Gert Frølund Pedersen[1]
[1]Antennas, Propagation and Radio Networking section, Aalborg University, Niels Jernes Vej 12, 9220 Aalborg, Denmark, {mos, of, gfp}@es.aau.dk
[2]EMC Laboratory, Missouri University of Science and Technology, Rolla, MO 65401, USA, {ar8r3, kwkx8d, davidjp}@mst.edu

The paper has been published in the
Electromagnetic Compatibility (EMC EUROPE), 2012 International Symposium on, Sept 2012, pp. 1–6.

The layout has been revised.

Estimate on the uncertainty of predicting radiated emission from near-field scan caused by insufficient or inaccurate near-field data

Evaluation of the needed step size, phase accuracy and the need for all surfaces in the Huygens' box

Morten Sørensen, Ondrej Franek, Gert Frølund Pedersen
Antennas, Propagation and Radio Networking section,
Aalborg University
Aalborg, Denmark
mos@es.aau.dk, of@es.aau.dk, gfp@es.aau.dk

Andriy Radchenko, Keong Kam, David Pommerenke
EMC Laboratory
Missouri University of Science and Technology
Rolla, MO 65401, USA
ar8r3@mst.edu, kwkx8d@mst.edu, davidjp@mst.edu

***Abstract*—Near-field scan on a Huygens' box can be used in order to predict the maximal radiated emission from a Printed Circuit Board. The significance of step size and phase accuracy, and the importance of a full Huygens' box are investigated by simulation of two different models with two different numerical methods. The prediction of maximal radiated emission is quite robust but the results also show that a full scan on all six surfaces is probably needed.**

Keywords-component; near-field scan; Huygens' box; predicting radiated emission; simulation

I. INTRODUCTION

In the antenna society, near-field scan has been used to determine the far-field radiation from antennas since the 1960s[1]. In the EMC society, the aim of near-field scan has more been to find EMI hotspots on Printed Circuit Boards (PCBs), but in recent years, attempts to predict radiated emission using near-field measurement have also been carried out.

Near-field to far-field transformation based on antenna near-field scan is often done by plane- or spherical wave spectrum[2], but in EMI/EMC related problems, nearby PCBs, chassis, cables or other structures complicate the prediction of radiated emission, and therefore, numerical methods as MoM or FDTD/FIT are often used[3,4,5]. From a theoretical point of view, it is straight forward to make the near-field to far-field transformation if the complex tangential electrical and magnetic fields on a closed surface are known based on Huygens' principle. But in practice, a lot of difficulties arise when you want to measure unintentional emission in a large frequency span from a PCB.

We must measure close to the PCB to get highest SNR of the often weak fields, and, as a side effect, this is usually in the reactive field. This requires a fine measurement grid and since the EMC requirements cover a broad frequency spectrum, the measurement time can be overwhelming and the phase measurement itself represents a challenge.

Connected cables also make it difficult to measure the near-field on all 6 surfaces.

The objective of the work presented in this article is to estimate the importance of the issues mentioned above, i.e. measurement step size, the need of all 6 surfaces and accuracy of the phase representation. Section II gives a very short introduction to the surface equivalence principle, also called Huygens' principle. The objective with the simulations and a description of the models and simulations methods are given in section III. The results are presented and discussed in Section IV and finally Section V draws the conclusions.

II. HUYGENS' BOX

In Figure 1a a PCB is enclosed in a surface S. $\{\boldsymbol{E_1}(\boldsymbol{r})\,\boldsymbol{H_1}(\boldsymbol{r})\}$ represents the electric and magnetic fields on this surface. The Huygens' principle states that an arbitrary structure containing sources of electric and magnetic fields can be represented by electric and magnetic currents on a surface that encloses the structure such that they produce the same field outside the surface while producing null field inside [6,7]. Such a rectangular box with equivalent currents on the surface is often denoted as Huygens' box. This is illustrated in Figure 1a and 1b where the equivalent electric and magnetic currents are given by $\boldsymbol{J_s}(\boldsymbol{r}) = \boldsymbol{n} \times \boldsymbol{H_1}(\boldsymbol{r})$ and $\boldsymbol{M_s}(\boldsymbol{r}) = -\boldsymbol{n} \times \boldsymbol{E_1}(\boldsymbol{r})$. These current densities can be deduced from the tangential electric and magnetic field on the closed surface, which in practice may be found using near-field measurements.

A near-field scan with a finite number of points gives only an approximation of the equivalent currents on the Huygens´ box surfaces so the question is how many measurements points is needed as illustrated in Figure 1c.

Advanced contemporary PCB´s will often have a lot of cable connections that go through the Huygens' box. These cables will make it very difficult to measure the sides of the

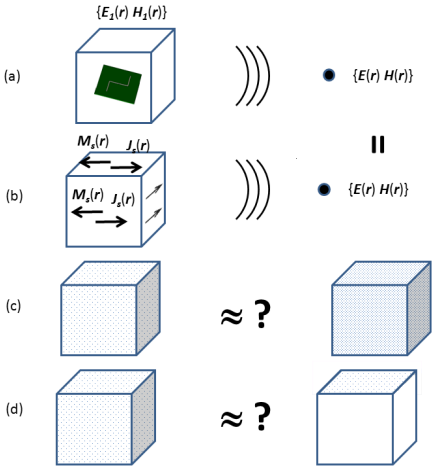

Figure 1: The surface equivalence principle and its representation by measured near-fields on a Huygens' box.

Huygens' box, where the cables go through. In addition, measuring the side of the Huygens' box requires an advanced robot or special perpendicular probes. It is therefore of interest how much accuracy is lost if only the field on the surface above the active part of the PCB is measured as illustrated in Figure 1d.

III. Test Setup

A. *The objective of the experiments*

As mentioned in the introduction, there are a lot of issues regarding the accuracy of the predicted radiated emission from a near-field scan.

The near-field measurement technics is still in embryo, so this paper will investigate the issues by means of simulations. With the purpose to increase the credibility of this investigation's conclusions a cross verification with two different structures simulated with two different numerical tools was carried out.

The work flow in the simulation is described in Figure 2.

a) A full model of the structure was simulated and the tangential components on a Huygens' box were exported. In addition, the maximal electric far-field in 3 m distance was calculated for reference as representative for a radiated emission test like CISPR 22.

b) The exported Huygens' box was now manipulated in different ways

c) and the maximum far-field in 3 m distance was simulated based on the manipulated Huygens' box. The different data manipulations are listed below:

- Reduction of the number of data points be equivalent to different step sizes in a near-field scan (see Figure 1c).

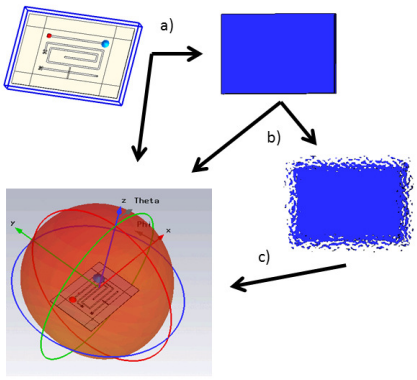

Figure 2: The simulation workflow

- Removing data from the sides and bottom of the Huygens' box in order to represent the situation, where only the surface above the PCB is measured (see Figure 1d). This was done for different scan heights and different scan areas.
- Random phase noise added to the data representing a random measurement uncertainty. For each field component and each frequency a random angle in different intervals was added (see Figure 3a).
- The H-field was unchanged but the phase of the E-field was shifted in order to equate a probe calibration, where the relative phase between the E-field probe and H-field probe was not considered and thereby random.
- A systematic phase error across the PCB. As mentioned before, the probe is in the reactive near-field in EMI near-field scan and hence complex interactions can take place. For example the probe could interact with the PCB and change the impedance of the traces and hence change the phase of the reference signal depending of the measurement probe position. Worst case is probably a case where the phase change is continuous across the scanned surface as illustrated in previous conducted near-field scan of one of the test PCBs (see Figure 3b).

B. *The models*

The two simulated models are shown in Figure 4. Model 1 was a simple 150 x 225 mm PCB with three 50 ohms traces on the top layer with a full ground plane on the bottom layer. Only one trace was excited and terminated. Both source impedance and load was 50 Ω. The simulations were carried out in CST Microwave Studio with the transient solver (Finite Integration Technique) [8].

Model 2 was a scaled IC consisting of two printed-circuit boards and ten vertical pin-headers, which were used to mimic the die substrate, the lead-frame package and foot print of an IC. There are few loads applied within the scaled IC. It was placed right on an infinite ground plane, which is in general

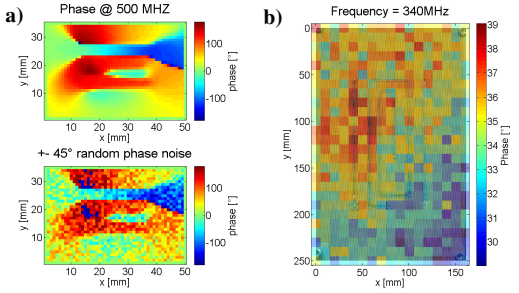

Figure 3: a) Introduced random +- 45° phase noise error., b) a real near-field scan of the PCB where the phase of the reference probe is plotted vs. the measurement probe position. The phase should be independent of the measurement probe position, but it looks like the phase decrease linearly across the PCB.

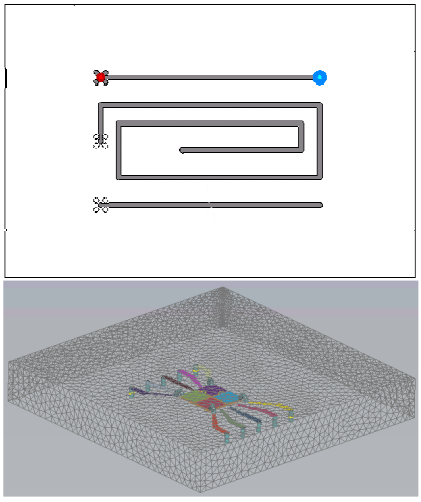

Figure 4: Model 1 (top), Model 2 (bottom)

similar to normal IC placed on PCB. The simulations were carried out in EMCos based on MoM [9].

In model 1 the radiated emission was evaluated on a sphere with a radius of 3 m (see Figure 2). In model 2 the maximal electric field was evaluated on a cylinder with radius 3 m simulating a 3 m semi anechoic chamber measurement.

IV. Results and Discussion

In most cases, the cross validation was successful. The trends in model 1, simulated with FIT, and the trends in model 2, simulated with MoM, was similar and for reason of space only result from one model is shown.

A. Stepsize

Figure 5 gives an indication of the necessary step size in near-field scan. Different step sizes were used on a full Huygens' box (all 6 surfaces) 10 and 20 mm from the PCB. For low frequencies (<50 MHz), the full model and the Huygens' box model differs some dB even for the smallest step size, which probably is caused by insufficient distance to the boundary in the FIT simulation. Above 50 MHz, the difference is below a few tenths of dB as long as the step size is less than or equal to the scan height divided by 2. With higher scan height, less number of measurements points is necessary, but in practice the dynamic range is also reduced due to weaker signal. It is likely that a smaller step size is needed if the simulation also must take interaction with nearby structures into account.

B. Top only scan

As mentioned in section II, it is often difficult and very time consuming to measure all 6 surfaces of the Huygens' box. Figure 6 compares the predicted radiated emission from model 2 based on the full model, a full Huygens' box (i.e. equivalent sources on all 6 surfaces) and the top only Huygens' box where the equivalent currents on all sides except the dominating top surface was set to 0. Three different step sizes were used for two different scan heights. The scan area was constant 20 x 20 cm. There is no visible difference between step size at given height – curves are matching each other in agreement with the step size result.

The full Huygens' box matches the full model within 0.1 dB (see Figure 6.a). The 10 mm scan height, top only box was within 0.8-2.5 dB and the 20 mm scan height, top only box was within 1.2-3.8 dB. Figure 6.b shows that all kinds of sources become better at higher frequencies, especially above about 600 MHz.

Figure 7 shows the top only results for different scan areas. Model 1 was used and the scan areas exceeded the PCB in both x- and y direction with 10 mm up to 100 mm. Unfortunately the result show that using the equivalent sources on top only is not sufficient and in addition there is no clear relation between the deviation from the direct solution and the scan area.

C. Random phaise noise and no phase information

In Figure 8, different phase noises was added to the full Huygens' box of model 1. For each frequency and each field-component a random angle +- "max error" was added to the Huygens' box data. In addition no phase information (i.e. only amplitude) and completely random phase was tested. The results show that the prediction of maximal radiated emission is quite indifferent for random phase noise. Even +- 45° random noise introduced only a deviation about 1 dB. The maximal deviation increased to 5 dB for +- 90° random phase noise. Completely random noise was far away and if only the amplitude data is present the simulations overestimate the maximal radiated emission by several dBs although the deviation decreased with frequency.

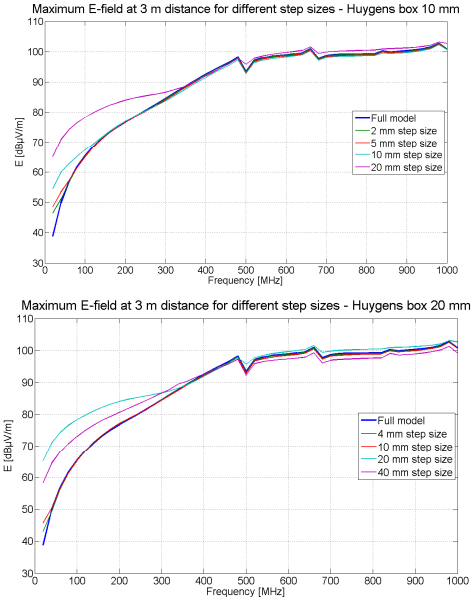

Figure 5: Evaluation of the needed step size vs. scan height, model 1.

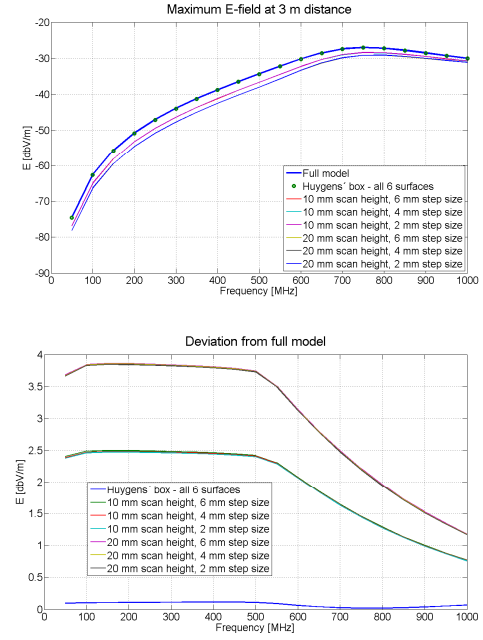

Figure 6: Evaluation of the need of a full Huygens' box with different scan heights and different step sizes, model 2.

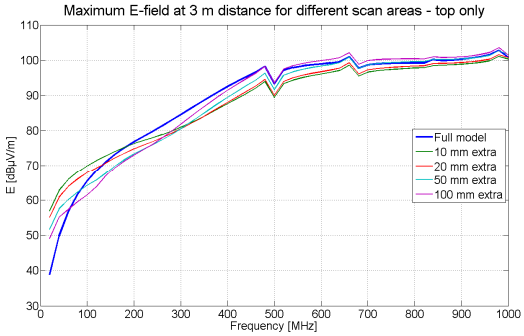

Figure 7: Evaluation of the need of a full Huygens box with different scan areas, model 1.

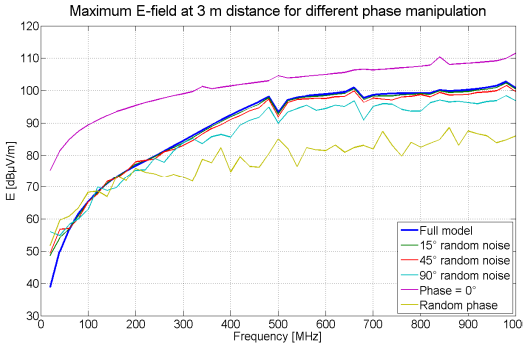

Figure 8: Evaluation of different phase manipulations, model 1.

Model 2 gave similar results. In Figure 9 +- 45° and +- 90° was added to the top only scan and the procedure was repeated three times. Figure 9.b shows the deviation caused by this random phase error. Again up to +- 45° the deviation was almost within 1 dB while +- 90° caused larger deviation. As for the other introduced errors the deviation decreased with increasing frequency.

D. Systematic phase shift between E- and H-field probe

In Figure 10, the phase of the H-field was unchanged while the phase of the electric field at all frequencies and all components was added a certain value. For model 1 the phase shift introduced a small deviation up to 3 dB while for model 2 the deviation was below 0.5 dB.

Beforehand, we had expected that this phase shift be equivalent to an insufficient probe calibration was very critical. At least mathematically, field produced by J and M are vector-summed at observation point, so it was expected that the phase relation between E- and H-field was critical. If the radiation is dominated by either J or M in model 2, the unexpected robustness can possible be explained by that.

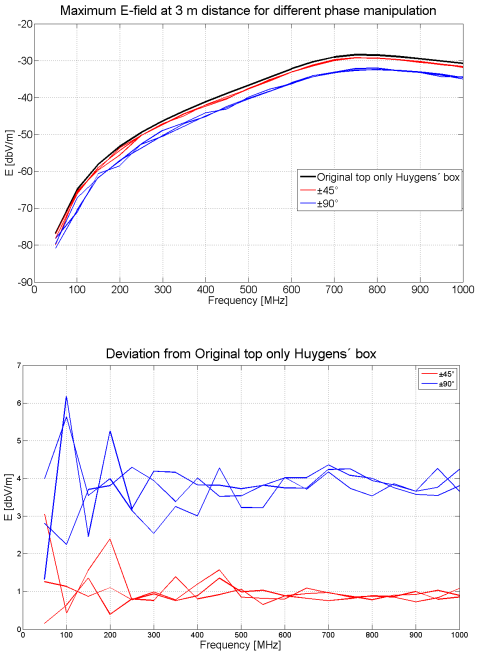

Figure 9: Evaluation of random phase error, model 2.

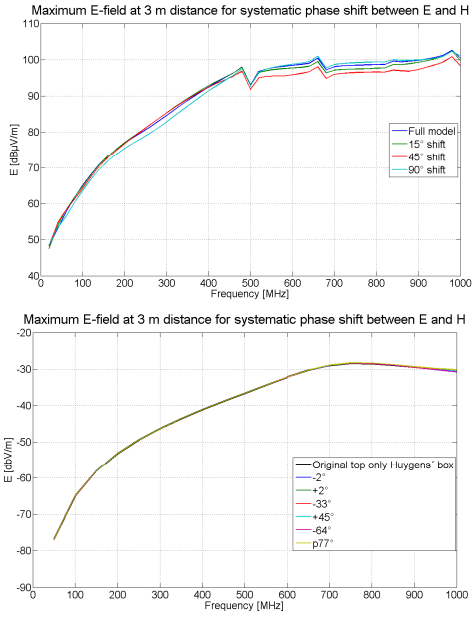

Figure 10: Systematic phase shift between E- and H-field probes, top model 1, bottom model 2

E. Systematic Phase shift across the PCB in one direction

In Figure 11, a phase gradient was added for all frequencies and components. From y_{min} to y_{max} a linearly decreasing phase error was added. The maximal far-field was quite robust to this systematic phase shift, even 30° phase error caused only a deviation up to 1 dB except for the low frequencies.

V. CONCLUSIONS

In this paper, we have studied the significance of different near-field scan issues by simulating to different structures with two different numerical methods. The conclusion is summed up in the table 1.

Predicting of the maximal radiated emission seems to be quite robust against different kind of phase errors. Perhaps counterintuitive it appears that the high frequency prediction of maximal far-field radiation is more robust to insufficient data set or manipulated data set than low frequency.

Unfortunately, the study also showed that the equivalent sources on all six surfaces are needed. Because of practical difficulties like cables, this issue can be one of the largest challenges.

The conclusions are based on a simple near-field to far-field transformation without nearby structures. The needed accuracy may be higher in this case.

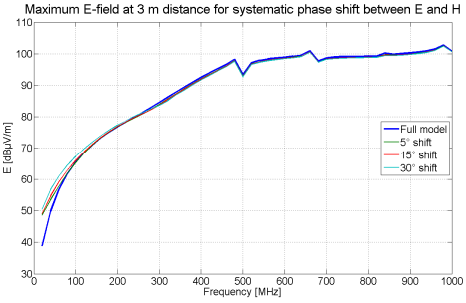

Figure 11: Systematic phase across the PCB, model 1.

TABLE I. CONCLUSION

Issue	Conclusion
Step size	Step size < scan height / 2
Full Huygens' box needed?	Yes. Otherwise risk of several dB´s underestimation of the maximal radiated – especially for frequencies below 300 MHz
Random phase noise	Very robust. +- 15° causes less than 1 dB error.
Phase shift between E- and H-field probes.	Can cause up to 5 dB error in the predicted maximal radiated emission.
Systematic phase shift across the PCB.	Very robust. 30° across the PCB causes less than 1 dB error.

REFERENCES

[1] J. Brown and E. V. Jull, "The prediction of aerial radiation patterns from near-field measurements," Proc. Inst. Elec. Eng., vol. 108, part B, no. 42, pp. 635-644, Nov. 1961

[2] J-R Regué, M. Ribó, J-M Garrell, A. Martín, "A Genetic Algorithm Based Method for Source Identification and Far-Field Radiated Emissions Prediction From Near-Field Measurements for PCB Characterization", IEEE Transactions on Electromagnetic Compatibility, Volume 43, No 4, Nov. 2001

[3] Shi, J.; Cracraft, M.A.; Zhang, J.; DuBroff, R.E.; Slattery, K.; "*Using near-field scanning to predict radiated fields,* "Proceedings of IEEE International Symposium on Electromagnetic Compatibility, Silicon Valley, 2004.

[4] H. Weng, D. G. Beetner, R.E DuBroff, "*Prediction of Radiated Emissions Using Near-Field Measurements*" IEEE Transactions on Electromagnetic Compatibility, Volume 53, No 4, Nov. 2011

[5] T. K. Sarkar and A. Taaghol, "Near-field to near/far-field transformation for arbitrary near-field geometry utilizing an equivalent electric current and MoM," IEEE Trans. Electromagn. Compat., vol. 47, no. 3, pp. 566–573, Mar. 1999.

[6] C. A. Balanis, *Advanced Engineering Electromagnetics*, New York: John Wiley & Sons, Inc., 1989, chapter 7

[7] Rengarajan, S.R.; Rahmat-Samii, Y., "The field equivalence principle: illustration of the establishment of the non-intuitive null fields", Antennas and Propagation Magazine, IEEE, Volume 42, Issue 4, Aug 2000

[8] CST Microwave Studio, Version 2011, www.cst.com

[9] EMCoS Ltd., EMCoS EMC Studio, Version 6.0, www.emcos.com

Paper F

How to Handle a Huygens' Box Inside an Enclosure

Morten Sørensen[1], Ivan Bonev Bonev[1], Ondrej Franek[1], Gert Frølund Pedersen[1], Hans Ebert[1]
[1]Antennas, Propagation and Radio Networking section, Aalborg University, Niels Jernes Vej 12, 9220 Aalborg, Denmark, {mos, ibb, of, gfp, heb}@es.aau.dk

The paper has been published in the
Electromagnetic Compatibility (EMC), 2013 IEEE International Symposium on,
Aug 2013, pp. 802–807.

The layout has been revised.

How to handle a Huygens' box inside an enclosure

Sørensen, Morten; Bonev, Ivan Bonev; Franek, Ondrej; Pedersen, Gert F.; Ebert, Hans

Published in:
2013 IEEE International Symposium on Electromagnetic Compatibility (EMC)

DOI (link to publication from Publisher):
10.1109/ISEMC.2013.6670520

Publication date:
2013

Document Version
Early version, also known as pre-print

How to Handle a Huygens' Box Inside an Enclosure

Morten Sørensen [#1], Ivan Bonev Bonev [#2], Ondrej Franek [#3], Gert Frølund Petersen[#4], Hans Ebert[#5]

[#]Antennas, Propagation and Radio Networking, Department of Electronic Systems, Faculty of Engineering and Science, Aalborg University,
Niels Jernes Vej 12, 9220 Aalborg, Denmark

[1] mos@es.aau.dk, [2] ibb@es.aau.dk, [3] of@es.aau.dk, [4] gfp@es.aau.dk, [5] heb@es.aau.dk

***Abstract*— It has been suggested that it is possible to replace printed circuit boards with a Huygens' box (HB) representation obtained from a near-field scan in simulation of far-fields from an apparatus. However, the surface equivalence theorem requires that the environment outside HB is the same in the near-field scan and in the apparatus. This is seldom the case in common type of apparatus. This paper discusses how to handle HB inside typical enclosures. It is demonstrated that if the most important features of the printed circuit board are included inside HB, the introduced error in radiated fields caused by violating the surface equivalence theorem can be lower than 2 dB. It is also demonstrated that if the printed circuit board is galvanically connected to the enclosure, the near-field scan must be performed under same conditions.**

I. Introduction

Near-field scan has been used as hot-spot finding tool within the EMC society for many years. In recent years the interest in near-field scanning as a radiated emission pre-compliance test has considerably grown and the first proof of concept based on mainly simulations but also measurements has been carried out [1]-[3].

The very ambitious goal is that one should be able to do near-field scan of a printed circuit board (PCB) used in an apparatus and then use the measured near-field as a source for simulation of the far-field from the apparatus with chassis, cables etc.

There are two different dominating approaches to the far-field prediction. One approach uses the near-field as a basis for source reconstruction by help of an equivalent set of electric and/or magnetic dipoles [4] while another approach uses tangential near fields on a surface entirely enclosing the module [3]. These fields distributed on the closed surface, the Huygens' box (HB), then act as sources generating the same fields as the original module outside of this surface.

Both methods have problems when other structures are close to the source and interact with the source. The limitation of the latter method follows directly from the theory, namely that a correct prediction of the field outside the box requires that the near-field is measured in the exact same environments as in the final apparatus. [5] E.g. if the near-field is measured on a HB surrounding a PCB in free space, this HB cannot be used as source for simulation inside an enclosure not present at the time of measurement. The result may be inaccurate.

In a real apparatus, PCBs will of course be close to other structures. Studies on how to overcome difficulties like that are scarce. In [6] and [7], brief investigations on how to handle attached cables were done, nearby cable was studied in [8], and finally a ground plane was studied in [9].

PCBs are often placed inside metal enclosures like racks and these enclosures can both attenuate the radiated emission and increase the maximum radiated emission because of resonances. In [10], a PCB was placed in a small box with just one opening and the differences in the near-fields between the full model and HB model were observed.

In this paper, we would like to further elaborate on how large the far-field error will be with respect to the full model, and whether it is possible to reduce the far-field error by including some of the features from the radiating structure. In addition, we will also look at the differences when the PCB is galvanically connected to the enclosure compared to the situation with the PCB floating.

So the purpose of this paper is not to investigate the shielding effectiveness of different enclosures. The purpose is to investigate the error in the predicted far-field when a Huygens' box from a "free space" near-field scan is used inside an enclosure, that was not present when the near-field scan was carried out and how to reduce these far-field prediction errors.

In Section II the Huygens' box method is introduced. The objective with the simulations and a description of the models are given in Section III. The results are presented and discussed in Section IV and finally Section V draws the conclusions.

II. Huygens' Box Method

In Fig. 1 a radiating structure is placed inside a boundary, S, marked with dotted lines. The surface equivalence theorem states that an arbitrary structure containing sources of electric and magnetic fields can be represented by electric and magnetic currents on a surface that encloses the structure, such that they produce the same field outside the surface while producing null field inside [5], [11]. The space around the HB must be the same in the original problem and in the equivalent problem. If the volume has a shape of a box, it is often called a Huygens' box.

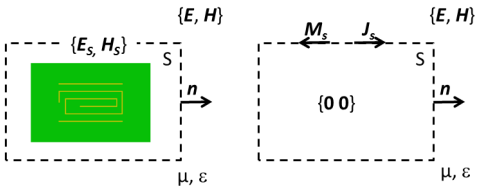

Fig. 1. The surface equivalence theorem.

The equivalent electric and magnetic currents are given by $\boldsymbol{J_s} = \boldsymbol{n} \times \boldsymbol{H_S}$ and $\boldsymbol{M_s} = -\boldsymbol{n} \times \boldsymbol{E_S}$, i.e. the tangential electric and magnetic fields on the surface of the closed box. In practice these tangential fields can be measured with near-field scans.

Many simulation tools can import HB and use the equivalent sources at the box surface as a source for simulations. We will call this "the Huygens' box method".

A. The Limitation of the Huygens' Box Method

The theory does not predict what happens if HB is placed inside a metallic enclosure or close to other structures and hence clearly violates the condition about having the same environment as the original and equivalent problem.

In the previous related work [6]-[10] it has been suggested to include the most important features of the structures such as ground plane and substrate. This is possible because the equivalent sources acting alone produce a null field inside the box. The idea is that the field reflected from nearby structures will be rescattered inside the Huygens' Box and hence acting like the original scenario.

B. Including full model inside the Huygens box restores the fields outside in the presence of obstacles

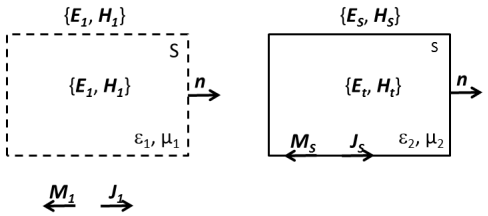

Fig. 2. The induction theorem.

Including the full model inside HB restores the original fields. It follows directly from an "inside-out" version of the induction theorem [5]. But let us start with the standard description of the induction theorem and assume a medium with constitutive parameters ε_1, μ_1, containing sources, and an obstacle with parameters ε_2, μ_2, see Fig. 2. The induction theorem states that the fields outside of the obstacle are given by a superposition of the original fields $\boldsymbol{E_1}$, $\boldsymbol{H_1}$ produced by the sources without the obstacle, and *scattered* fields $\boldsymbol{E_S}$, $\boldsymbol{H_S}$ which are generated by induced currents on the boundary of the obstacle, $\boldsymbol{J_s} = -\boldsymbol{n} \times \boldsymbol{H_1}$ and $\boldsymbol{M_s} = \boldsymbol{n} \times \boldsymbol{E_1}$,, and which radiate in the same environment, i.e. including the obstacle ($\boldsymbol{n}$ is the normal vector pointing outwards the obstacle). The fields inside the obstacle $\boldsymbol{E_t}$, $\boldsymbol{H_t}$ are the same, with the induced currents as well as with the total fields, which is a consequence of the boundary conditions as described in [5].

Our problem is arranged "inside-out", i.e. the whole region outside HB needs to be seen as the obstacle whereas the region inside corresponds to the background medium ε_1, μ_1. By reversing the direction of the normal vector $\boldsymbol{n}$ we arrive at the original formulas for currents on HB, which now produce the same fields outside (as in the obstacle above), and the scattered fields inside. Both regions must be present with their respective parameters, the region outside (the obstacle, ε_2, μ_2) and the region inside (ε_1, μ_1) with the full model of the PCB.

III. Test Setup

A. The objective of the experiment

The objective of this study is to investigate the HB method when the conditions for the surface equivalence theorem are not satisfied. By using only simulations we exclude the uncertainty of the measurements.

The workflow of the simulations is described in Figs. 1 and 3. A full model of the PCB was simulated in free space and the tangential components of the E- and H-fields on HB 10 mm around the structure was extracted (Fig. 1).

Next step was to place the PCB inside an enclosure and simulate the far-field (Fig. 3.a), which served as a reference. In order to quantify the error of the methods proposed in section II A, different simulation scenarios were carried out.

- The PCB was replaced by HB inside the enclosure (Fig. 3.b).
- The ground plane and the ground plane + substrate was placed inside HB (Fig 3.c)
- The full PCB model was placed inside HB (Fig 3.d).

After that we moved on to a setup where the PCB was connected to the enclosure in order to see, whether the connection to the enclosure requires changes in the method.

Again the HB was extracted from free space (Fig. 1), but in addition HB was extracted where the PCB was connected to an infinite ground plane (Fig. 4). In this scenario the HB enclosed the connections to the ground and the bottom side of the HB was 0 (no tangential field component in the infinite ground plane made of perfect conducting material).

The two different types of HB were then used in scenario b and c in Fig. 3.

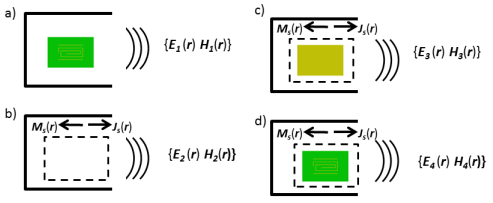

Fig. 3. Simulation scenarios.

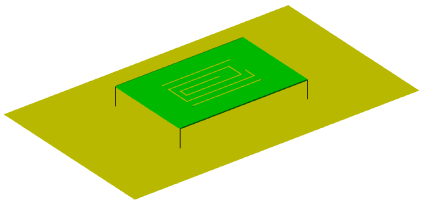

Fig. 4. A Huygens' box was extracted from a simulation with a PCB connected to an infinite ground plane.

In all scenarios the difference in the far-field between the Huygens' Box simulations and the reference was evaluated after the following metric:

$$\text{Peak increase} = 20 \cdot \log10\,(\max(E_{\text{Huygens'}})/\max(E_{\text{reference}}))$$

where $\max(E_{\text{Huygens'}})$ is the maximum in the far E-field of the Huygens' Box model and $\max(E_{\text{reference}})$ is the maximum of the far E-field of the reference case. The maximum is taken across both theta and phi components - equivalent to the difference in two far-field measurements according to CISPR 22.

B. *The models*

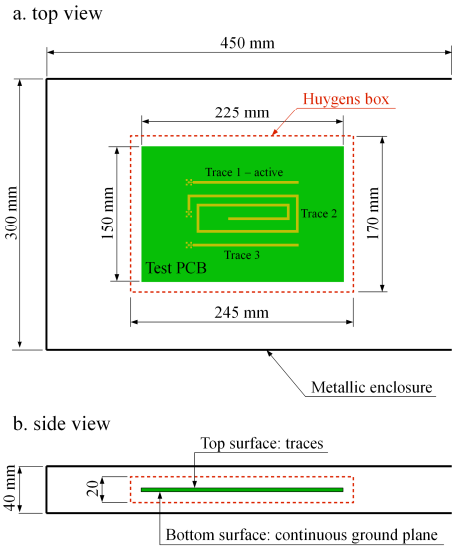

Fig. 5. The test PCB and enclosure 1.

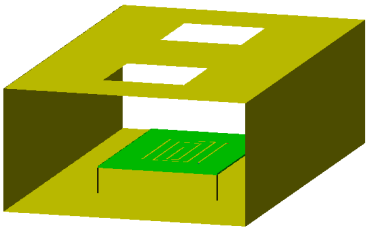

Fig. 6. Enclosure 2.

The simulated PCB is shown in Fig. 5a. A simple 150 x 225 mm PCB with three traces on the top layer and full unbroken ground plane were chosen. The substrate was a 2 mm thick lossy FR4 layer with relative permittivity 4.35 and conductivity 10^{-3} S/m. Only one trace was excited and terminated (trace 1). The trace was 2 mm wide and both source and load impedances were 50 Ω. The simulations were carried out with an in-house numerical code implementing the finite-difference time-domain (FDTD) method [12].

The number of mesh cell is proportional with $(1/\text{cell size})^3$ and in addition the time step is proportional with cell size. Hence going from 2 mm mesh cells to 1 mm mesh cells increases simulation time 16 times. We chose 2 mm mesh cells and perfectly matched layers as the absorbing boundary condition. The importance of the discretization will be discussed later.

In Method of Moments the effect (shielding, scattering) of Perfect Electric Conductor (PEC) depends much on the on the discretization. In FDTD it is different since the field is forced to be zero inside PEC.

The Huygens' box implementation, i.e. using near-field sources, is still experimental and the code does not yet allow wide band excitation of near-field sources. Hence the HB method is evaluated at frequencies from 20 MHz to 1 GHz, with 20 MHz step and in addition frequencies are added at which resonances occur.

The time step for the cell size of 2 mm was $\Delta t = 3.8483 \cdot 10^{-12}$ s. The majority of the simulations have number of time steps between 30 000 and 100 000, but some of the resonance frequencies required up to several million time steps before the energy criterion was met.

The simulations were carried out on a cluster computer with 24 computers. Each computer contains two Xeon X5650 six core 2.66 GHz CPUs, 145 GB RAM, a 53GB scratch partition, Gbit ethernet and Infiniband interconnect.

With the purpose to increase the credibility of the conclusions, two different boxes were tested in the simulation (Fig. 5 and 6).

Enclosure 1 had the dimension 450 x 300 x 40 mm and was open in one end. The PCB and HB were placed in the middle of the enclosure.

Enclosure 2 had dimensions 500 x 300 x 150 mm, open in both ends and in addition two openings in the top with the size

of 100 x 100 mm. The PCB was placed 1 cm above bottom and placed in the space between the holes in the cabinet.

In both cases the simulations were done with and without the galvanic connections to the enclosure (Fig. 6 shows the set-up with galvanic connections).

IV. Results and Discussion

Fig. 7 shows the radiated emission in 3 m distance from the PCB in free space, from the PCB floating inside the enclosure and from the PCB inside and galvanically connected to the enclosure in the corners of the PCB. The simulations were done with input power 1 mW for every 20 MHz and in addition for frequencies where the S-parameter for the full model simulation had resonances. It is clear that maximum radiated emission from the PCB inside the enclosure differs from the free space set-up and that connecting the PCB to the enclosure also has a large effect on the maximum radiated emission. It would be very useful, if it is possible to predict these attenuations and resonances based on the Huygens box method with an uncertainty well below the effect of the enclosure and the connections.

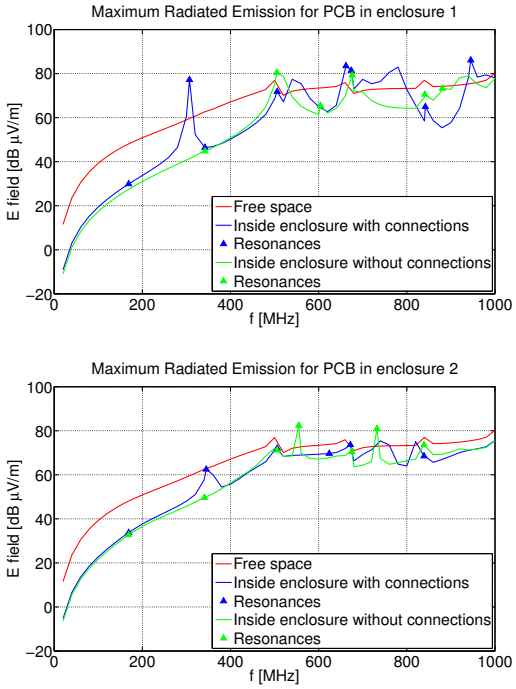

Fig. 7. Maximum radiated emission from the PCB in free space, floating in the box and galvanically connected to the box. Top: Enclosure 1. Bottom: Enclosure 2.

A. *Peak increase for Enclosure 1, PCB not galvanically connected*

Fig. 8 shows the peak increase for the PCB inside enclosure 1 (not galvanically connected to the enclosure). With the purpose of testing the implementation of the HB method in the FDTD code, the peak increase for a free space simulation is also included, i.e. a HB was extracted from a free space simulation and used for a predicting the free space far-field. As expected the peak increase is 0 (black curve coincides with the blue curve).

In Section II.B we stated that including the full model inside the Huygens box restores the fields outside in the presence of obstacles. This is also verified in the figure where the peak increase for HB full model is 0 as expected.

Simulations with HB empty and the ground plane inside HB are almost coinciding, which explains why the red curve is only visible by the markers. The figure shows that including ground plane and substrate makes the peak increase smaller compared to empty HB. The difference between the reference simulation and HB simulation is within ±2 dB when ground plane and substrate are included.

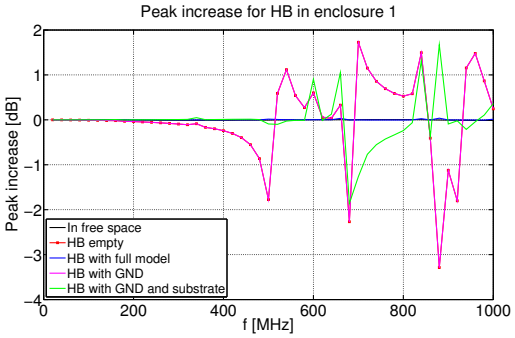

Fig. 8. Peak increase for HB in enclosure 1.

B. *Peak increase for Enclosure 2, PCB not galvanic connected*

Fig. 9 shows the peak increase for HB in enclosure 2. Enclosure 2 is larger and more open than enclosure 1. The difference between the HB and the reference are in general smaller in enclosure 2 compared to the smaller and more closed enclosure 1. The figure shows again that including ground plane and substrate reduces the peak increase compared to an empty HB and HB with just the ground plane. When we included both ground plane and substrate, the difference was below ±1 dB. The importance of including the lossy substrate is clear for the strong resonance frequency 555 MHz.

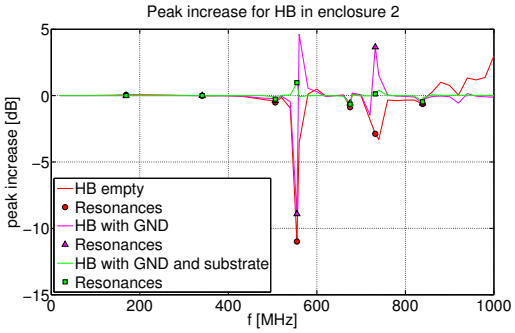

Fig. 9. Peak increase for HB in enclosure 2

C. *Peak increase for PCB galvanically connected in enclosure 2*

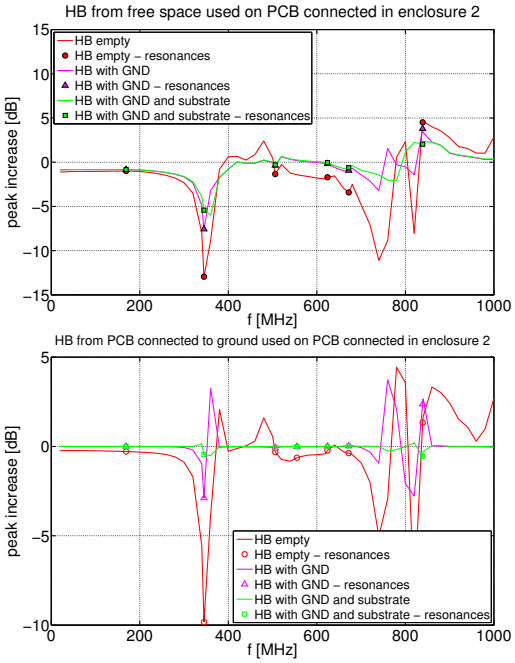

Fig. 10 Peak increase for two different HB's used on a PCB connected to enclosure 2. Top: The HB extracted from free space simulation. Bottom: The HB extracted from a simulation with a PCB connected to an infinite ground plane.

Often PCBs are connected to the chassis. In order to avoid resonances, designers will typical make the connection through a RC circuit. In this paper we made the choice to test the worst case: a 0 Ω galvanic connection to the ground. In Fig. 10 two different approaches for this set-up are compared.

First we used the same HB as in the other simulations, i.e. a HB extracted from a free space simulation. The errors increased compared to the set-up, where the PCB was not connected to the enclosure. Even when the ground plane and the substrate were included, the peak increase was between –6 dB and 2 dB and the large peak increases are present at many frequencies. Fig. 7 shows that the connection to the enclosure caused an increase of the radiation of approximately 10 dB from 340 – 360 MHz, but Fig. 10 shows that this resonance is underestimated by approximately 6 dB if the HB from free space is used.

Then we changed the simulation and used a HB that was extracted from a simulation, where the PCB was connected to an infinite ground plane (Fig. 4). Fig. 10 shows that there were still large errors, if we used the empty HB, but when we included the ground plane and the substrate inside the HB, the error almost disappears, the difference was below ±0.6 dB.

It follows from this experiment, that if a PCB is connected to a metal structure in the product, the PCB must also be connected to a metal structure in the near-field measurements.

D. *Peak increase for different PCB heights*

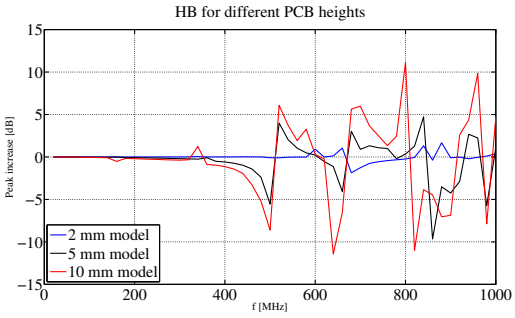

Fig. 11 Peak increase for different PCB heights in enclosure 1.

Until now the suggested method, i.e. to include the most important features in the HB, has been successful. However, the reader may ask: what are the most important features? The ground plane must be responsible for most of the rescattering inside the HB and hence it is expected that including ground plane and the lossy substrate will provide good results.

Another case occurs if the PCB is more complicated and other structures that can rescatter are present. We tried to change the dimensions of the PCB and tested the method on two other PCBs, where the thickness of the substrate and the trace width were changed to 5 mm and 10 mm respectively.

Fig. 11 shows the HB simulation with ground plane and substrate included for the three different heights of the PCB in enclosure 1. It emerges clearly that the higher the PCB the worse the peak increase becomes. The trace, termination,

source and ground plane form now a relatively large loop, which can interact with the surroundings. The rescattering from the loop is not taking into account when only the ground plane and substrate is included.

E. The influence of the discretization

In order to ensure that some of the observed differences are not simply the result of insufficient modelling detail, we tried a coarser mesh (10 mm) for the 10 mm high PCB in enclosure 1 (section *D.*) HB simulation with ground plane and substrate included for the two different cell sizes is shown in Fig. 12.

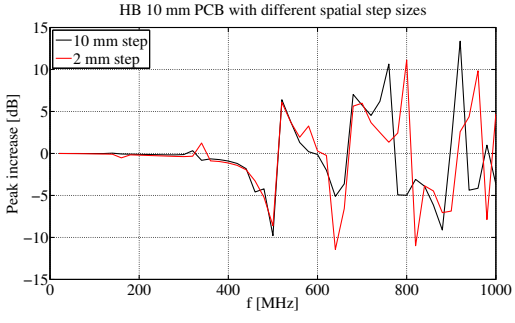

Fig. 12 Peak increase for different spatial step sizes for the 10 mm PCB in enclosure 1.

Going from a fine 2 mm mesh (5 cells across the trace) to a coarse mesh (only 1 cell across the trace and 15 cells across the ground plane) change the "bad" peak increase frequencies but not the overall amplitude.

We also tried a finer mesh (1 mm) for HB in enclosure 1 (section *A*) and in this case a finer mesh caused even worse peak increase for the resonance frequencies compared to 2 mm mesh cell.

V. Conclusion

In this paper, we have compared scenarios of a PCB model inside two different enclosures with similar scenarios where the PCB has been replaced by HB. The comparison was carried out for both the scenario where the PCB was floating inside the enclosure and the scenario where the PCB was galvanic connected to the enclosure.

We have seen that such replacement can cause a significant error in the far-field prediction. However these errors can be reduced by several dB, if main features of the PCB are included in the HB. Best results were obtained if we included both the ground plane and the substrate. Still, if other sources of rescattering, ground plane and substrate may not be sufficient.

If the model of the structure is converging to the full original model, excluding the sources, then the error can be made almost negligible and theoretical zero.

The study also shows that if the PCB is connected to the enclosure, the HB must also be extracted from a simulation/measurement with a ground plane.

It can therefore be concluded, that the HB method may be used as a field source in simulations of PCBs inside enclosures, but only if the main features of the PCB is included in the HB.

If the results can be generalized to other structures and other noise sources, i.e. other kinds of PCBs, the HB method could be a useful precompliance test based on near-field scan and simulations.

Acknowledgment

The present work has been supported by the Danish Agency for Science, Technology and Innovation. The authors also gratefully acknowledge the support from the Danish Center for Scientific Computing (DCSC) for the hybrid Linux cluster "Fyrkat" at Aalborg University, Denmark.

References

[1] Vives-Gilabert, C. Arcambal, A. Louis, F. de Daran, P. Eudeline, and B. Mazari, "Modeling magnetic radiations of electronic circuits using near-field scanning method," *IEEE Transaction on Electromagnetic Compatibility*, vol. 49, no. 2, pp. 391–400, May 2007.

[2] X. Tong, D. W. P. Thomas, A. Nothofer, P. Sewell, and C. Christopoulos, "Modeling electromagnetic emissions from printed circuit boards in closed environments using equivalent dipoles," *IEEE Transaction on Electromagnetic Compatibility*, vol. 52, no. 2, pp. 462–470, May 2010.

[3] H. Weng, D. G. Beetner, and R. E. DuBroff, "Prediction of radiated emissions using near-field measurements," *IEEE Transaction on Electromagnetic Compatibility*, vol. 53, no. 4, pp. 891–899, Nov. 2011.

[4] Vives-Gilabert, Y.; Arcambal, C.; Louis, A.; Eudeline, P.; Mazari, B.; "Modeling Magnetic Emissions Combining Image Processing and an Optimization Algorithm" *IEEE Transactions on Electromagnetic Compatibility*, Volume 51, No 4, Nov. 2009

[5] C. A. Balanis, *Advanced Engineering Electromagnetics*, New York: John Wiley & Sons, Inc., 1989, chapter 7

[6] Sørensen M., Franek O., Pedersen G.F., Baltsen K.A., Ebert H. "Perturbation of near-field scan from connected cables", *IEEE International Symposium on Electromagnetic Compatibility*, 2012

[7] Kam K., Radchenko A., Pommerenke D., "On different methods to combine cable information into near-field data for far-field estimation" *IEEE International Symposium on Electromagnetic Compatibility*, 2012

[8] Franek O., Sørensen M. Ebert H. Pedersen G.F. "Influence of Nearby Obstacles on the Feasibility of a Huygens Box as a Field Source, *IEEE International Symposium on Electromagnetic Compatibility*, 2012

[9] Franek, O., Sørensen M., Ebert H., Pedersen G. F., "Near-Field Characterization of a Printed Circuit Board in the Presence of a Finite-sized Metallic Ground Plane, *PIERS Kuala Lumpur Proceedings. The Electromagnetics Academy*, 2012. P. 1146-1149 (PIERS Proceedings).

[10] Franek, O., Sørensen M., Ebert H., Pedersen G. F., "On the Applicability of the Surface Equivalence Theorem Inside Enclosures." *International Conference on Electromagnetics in Advanced Applications Proceedings*. 2012. p. 946-948.

[11] Rengarajan, S.R.; Rahmat-Samii, Y., "The field equivalence principle: Illustration of the establishment of the non-intuitive null fields", *IEEE Antennas and Propagation Magazine,* Volume 42, Issue 4, Aug 2000

[12] A. Taflove and S. C. Hagness, *Computational Electrodynamics: The Finite-Difference Time-Domain Method*, 3rd ed. Boston: Artech House, 2005.

Paper G

Review of the Huygens' Box Method with Different Sources Near Obstacles

Morten Sørensen[1], Ivan Bonev Bonev[2], Ondrej Franek[2], Gert Frølund Pedersen[2]
[1]EMC Laboratory, Missouri University of Science and Technology, Rolla, MO 65401, USA, sorensenmo@mst.edu
[2]Antennas, Propagation, and Millimeter-Wave Systems Section, Department of Electronic Systems, Aalborg University, 9220 Aalborg, Denmark, {ibb, of, gfp}@es.aau.dk

The paper has been submitted to
IEEE Transactions on Electromagnetic Compatibility, September 30, 2018

Review of the Huygens' Box Method with Different Sources Near Obstacles

Morten Sørensen, *Member, IEEE,* Ivan Bonev Bonev, Ondřej Franek, *Member, IEEE,* and Gert Frølund Pedersen, *Member, IEEE*

***Abstract*—The Huygens' box (HB) method of replacing an arbitrary module mounted in an apparatus with a set of current sources on a closed surface is reviewed. A numerical study is performed, with different noise sources, represented by its HB, in combination with different obstacles. The study shows that if the ground plane and substrate is included in the HB, the accuracy of HB method generally is good. However, if the coupling between the module and the obstacle is strong, the method fails at a few resonances. In the search for the methods general limits it is shown, that the method cannot predict the maximum radiated emission of power plane resonances without including the vias in the HB.**

***Index Terms*—Surface Equivalence Principle, Huygen's Box Method, Near-field scan, Electromagnetic Simulations.**

I. Introduction

PRE-COMPLIANCE test at module level makes it possible to predict compliance early in a project. Several methods have been investigated over the years and a few standards for handling EMC at integrated circuit (IC) and module level have been written e.g., IEC 61967 [1].

As clock frequencies increase, ICs, microstrips, power-ground plane resonances increasingly radiate by themselves instead of being the source for common mode radiation by attached cables. With the right software installed on the printed circuit board (PCB), one can measure the PCB with power supply cable alone in a semi anechoic chamber (SAC) and get an estimate of the radiated emission from the final apparatus caused by this PCB. However, enclosures and obstacles near the PCB can change the radiated emission significantly and hence methods for predicting radiation from PCBs, when it is mounted in an apparatus, are needed.

A very ambitious idea is to measure the tangential component of the PCB's near-field (E and H) and use the measured near-field as a source for simulation of the far-field from the PCB mounted in the apparatus.

The scientific world has not yet agreed on a method and there are two different dominating approaches to the far-field prediction. One approach uses the near-field as a basis for sources by help of an equivalent set of electric and/or magnetic dipoles [2]–[5] while another approach uses tangential near fields on a surface entirely enclosing the module [6]–[10]. These fields that are distributed on the closed surface, named Huygens box (HB), act as sources generating the same fields as the original module outside of this surface. The latter method is the basis of this article.

Both methods are inaccurate when the PCB is measured in free space and afterwards placed inside an enclosure or near an obstacle which interact with the source, (i.e., scattering and re-scattering between source and enclosure/obstacle.) The limitation of the HB method follows directly from the theory, namely that a correct prediction of the field outside the box requires that the near-field is measured in the exact same environment as the environment used in the simulation of the far-field outside the box.

In real products, PCBs will be mounted on a chassis, be inside an enclosure, and/or near cables etc. In order to have the full benefits from the combination of near-field measurements and numerical methods, the simulations must take the scattering/re-scattering into account. Studies of how to include this interaction are scarce. For the equivalent dipole method, the method can be extended to a dipole-dielectric conducting plane model to account for the interactions between the PCB and the enclosure by including the basic physical features of the PCB [2], [11].

A similar method can be used for the Huygens' box method. In [12] a simple microstrip PCB was placed nearby a cable with different lengths and in another study [13] the same PCB was placed just above a large metallic plate with different sizes and distances between PCB and plate. In both cases the errors caused by violating Huygens' principle could be mitigated by including major features of the substituted object, without the need to use the full model.

A more thorough investigation of the effect of enclosures was conducted in [14], [15]. The studies compared scenarios of a simple microstrip PCB inside two different enclosures with similar scenarios where the PCB has been replaced by a HB. The comparison was carried out for both the scenario where the PCB was floating inside the enclosure, and the scenario where the PCB was galvanically connected to the enclosure.

The HB replacement could cause a significant error in the far-field prediction. However, these errors were below 2 dB, if ground plane and dielectric of the PCB were included in the HB – except for a few resonance frequencies with very high Q-factors. It was also shown that if the PCB is grounded in the apparatus, the near-field scan must also be carried out with grounding, otherwise the error could becomes significant.

In the above work, the method was validated with only one PCB and two enclosures. The method's relative success could be a coincidence. It was concluded that further studies were

Morten Sørensen is with the EMC Laboratory, Missouri University of Science and Technology, Rolla, MO, 65401 USA (e-mail:sorensenmo@mst.edu).

Ivan Bonev Bonev was, Ondrej Franek, Gert Frølund Pedersen are with the Antennas, Propagation, and Millimeter-Wave Systems Section, Department of Electronic Systems, Aalborg University, 9220 Aalborg, Denmark (e-mail: of@es.aau.dk; gfp@es.aau.dk).

needed in order to make a trustworthy conclusion.

It is very time-consuming to measure both E- and H-fields and, in addition, depending of the nature of the source, one of the field components (*E* or *H*) can be weak and difficult to measure. [10], [16] succeeded in filling up the HB with perfect magnetic conductor material and use only the H-field in order to predict the far-field radiation.

The study presented in this paper elaborates on the above mentioned enclosure studies [14], [15]. The method was tested with several combinations of PCBs and environments with the purpose to gain better understanding of the method and especially its limits. The models in previous work have predicted maximum far-field with less than 2 dB error, except for very narrow banded strong resonances; therefore, focus in this study was to search for the method's general limitations.

In Section II, the HB method is introduced and it is proved, that including full model inside the HB restores the fields outside in the presence of obstacles. The objectives of the simulations and different simulation scenarios are given in Section III. The results are presented and discussed in Section IV. Section V reviews the method based on the present study and previous studies, and draws the conclusions.

II. The Huygens' Box Method

The surface equivalence principle and its application related to near-field scanning and predicting radiated emission has been described in several papers, e.g. [7], [14], [17], [18]. The surface equivalence principle requires that the space outside the HB must be the same in the original problem and in the equivalent problem. If the space outside the HB changes from the original problem to the equivalent problem, the method is no longer valid.

A. Near Obstacles

It follows from an inside-out formulation of the traditionally formulated induction theorem [19] that if the full model is included inside the HB, the equivalent problem restores the original fields.

Let us assume a medium with constitutive parameters ϵ_1, μ_1, containing sources represented by electric and magnetic current densities $\vec{J}_1$ and $\vec{M}_1$ as shown in Fig 1(a). A (Huygens') box is shown, but the theory does not require a specific surface. These sources radiate the fields $\vec{E}_1$ and $\vec{H}_1$ everywhere. Now let us assume that an obstacle with the parameters ϵ_{ob}, μ_{ob} is placed outside the volume *V* as shown in Fig 1(b).

This obstacle perturbs the original field and the total field inside V_1 is now a superposition of the original field without obstacle and the scattered field from the obstacle:

$$\vec{E} = \vec{E}_1 + \vec{E}_s \qquad \vec{H} = \vec{H}_1 + \vec{H}_s, \tag{1}$$

where $\vec{E}$ and $\vec{H}$ are the total field with the obstacle present, $\vec{E}_1$ and $\vec{H}_1$ are the original field without the obstacle and $\vec{E}_s$ and $\vec{H}_s$ are the scattered fields due to the obstacle.

The transmitted field outside *V* is denoted $\vec{E}_t$ and $\vec{H}_t$ and is the field of interest for the Huygens' box investigation. It can be calculated by help of an equivalent problem defined in Fig 1(c) which allow us to determine $\vec{E}_s$ and $\vec{H}_s$ inside *V* and $\vec{E}_t$ and $\vec{H}_t$ outside *V*. In Fig 1(c) the fields inside *V* are $\vec{E}_s$ and $\vec{H}_s$ and outside the fields are $\vec{E}_t$ and $\vec{H}_t$. In order to radiate such fields and satisfy tangential boundary conditions, it is necessary to introduce equivalent current densities $\vec{J}_i$ and $\vec{M}_i$:

$$\begin{aligned} \vec{J}_i &= \hat{n} \times (\vec{H}_\mathrm{s} - \vec{H}_\mathrm{t}) \\ \vec{M}_i &= -\hat{n} \times (\vec{E}_\mathrm{s} - \vec{E}_\mathrm{t}) \end{aligned} \tag{2}$$

where $\hat{n}$ denotes normal vector oriented inside *V*.

The tangential components of the fields must be continuous across boundaries. Hence Fig 1(b) implies that

$$\begin{aligned} \vec{E}_1|_\mathrm{tan} + \vec{E}_\mathrm{s}|_\mathrm{tan} &= \vec{E}_\mathrm{t}|_\mathrm{tan} \\ \vec{H}_1|_\mathrm{tan} + \vec{H}_\mathrm{s}|_\mathrm{tan} &= \vec{H}_\mathrm{t}|_\mathrm{tan} \end{aligned} \tag{3}$$

If 3 is rewritten and substituted into 1 the equivalent currents in Fig 1(c) can be written as

$$\begin{aligned} \vec{J}_i &= -\hat{n} \times (\vec{H}_1) \\ \vec{M}_i &= \hat{n} \times (\vec{E}_1) \end{aligned} \tag{4}$$

With the new expression for the equivalent currents, the problem in Fig 1(c) can now be reduced to the equivalent in Fig 1(d). The field outside the HB is equivalent to the field radiated by the original fields $\vec{E}_1$ and $\vec{H}_1$ without an obstacle and with the original medium with constitutive parameters ϵ_1, μ_1 included in the HB. In practice, it means that it is possible to do a near-field scan in "free space" condition and then use the "free space" measured tangential field as a source for simulations of near obstacles as long as the scanned PCB is included in the HB. Of course it is of no use if it is necessary to include all details in the HB because then it would be easier to just do a full wave simulation of the PCB, but if it is possible to judge which elements of the PCB that are responsible for the scattering, one could approximate the field by including the most important parts of the PCB.

III. Simulations Setup

The purpose of this study was to investigate the HB method near obstacles in further details, and especially search for its general limitations. Hence a number of PCB structures were placed in different environments and tested by simulations.

A. Numerical Details

All simulations were carried out with an in-house numerical code implementing the finite-difference time-domain (FDTD) method [20]. The implementation has uniform spatial discretization and 2 mm mesh cells were chosen.

The HB implementation in to the code, i.e., using near-field sources, does not yet allow wide band excitation of near-field sources. Hence the HB method was evaluated at frequencies from 20 MHz to 1 GHz, with a 20 MHz step, and, in addition, some frequencies were added at which resonances occur. The simulation input power was 0 dBm. Further numerical details can be found in [14].

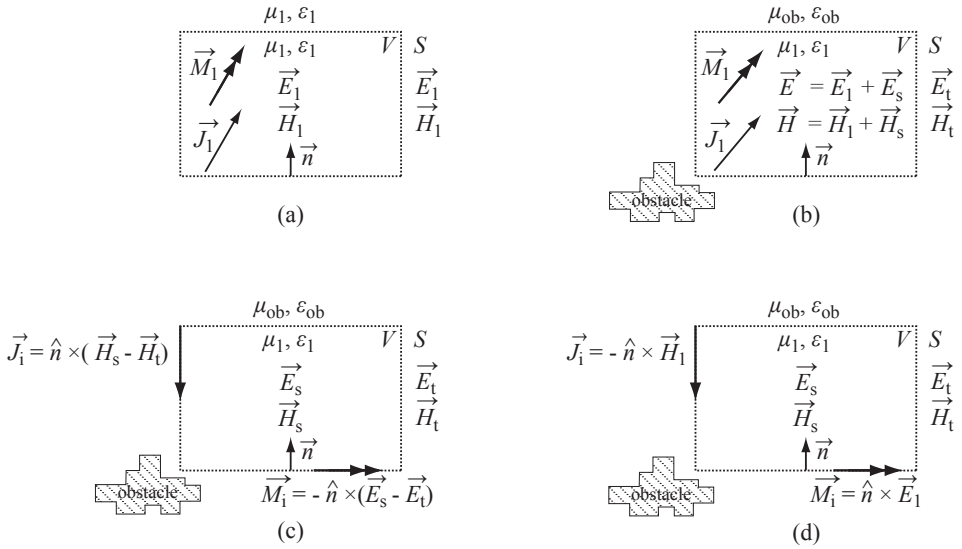

Fig. 1. Geometry for the inside out version of the induction theorem. (a) Sources in a homogeneous medium. (b) The homogeneous medium outside is replaced with an obstacle. (c) Equivalent problem. (d) Reduced equivalent problem.

B. Workflow

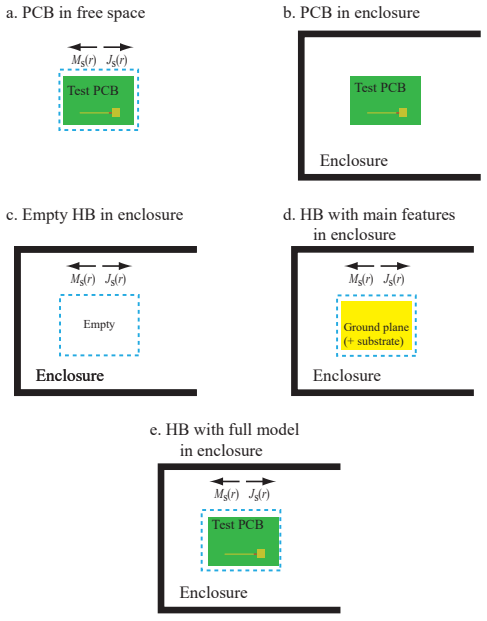

Fig. 2. The simulation workflow.

The workflow of the simulations is illustrated in Fig. 2.

1) A full model of the PCB was simulated in free space and the tangential components of the E- and H-fields on a HB 10 mm around the structure was extracted as shown in Fig. 2(a). 10 mm correspond to a typical scanning height.
2) The far-field from the radiating structure placed in a reflective environment was simulated as reference. This is illustrated in Fig. 2(b).
3) The radiating structure was replaced by the equivalent sources from 1) with an empty HB as shown in Fig. 2(c).
4) Parts of the radiating structure (e.g., ground plane and substrate) were included in the HB in order to take scattering into account as shown in Fig. 2(d).
5) With the purpose to validate the simulation, the full radiating structure was included in the Huygens' box as shown in Fig. 2(e). The full structure was passive, (i.e., the structure was not excited, but the 50 Ω source impedance was still present.)

C. Sources

Three categories of PCB sources were used in the simulations.

1) 50 Ω Microstrip - Source 1: A simple 150 mm × 225 mm two layer PCB with three traces on the top was modeled as shown in Fig. 3. The substrate was a 2 mm thick lossy FR4 layer with relative permittivity 4.35 and conductivity 10^{-3} S/m. Only the upper trace was excited and terminated. The lowe trace and spiral formed trace were floating in order to make possible resonances. The active trace was 120 mm long and 2 mm wide and both source and load impedances were 50 Ω. A version with a 50 mm long orthogonal slot in the ground plane below the trace was also used. The slot change the near-field significant and radiated emission is increased several dB

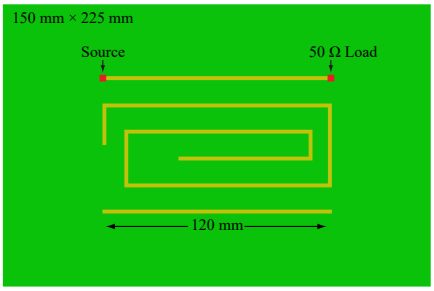

Fig. 3. A simple microstrip above a 150 × 225 mm ground plane.

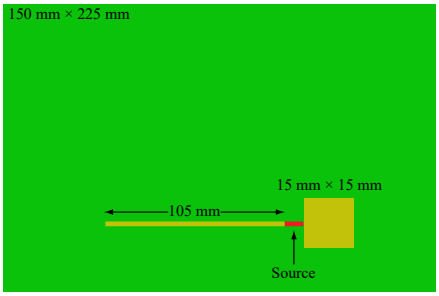

Fig. 4. A microstrip connected to an IC on a PCB.

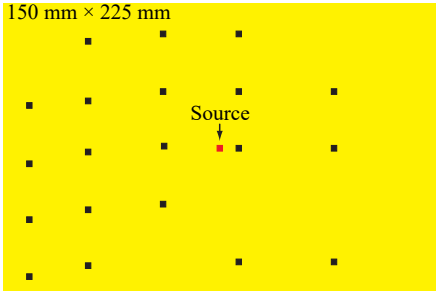

Fig. 5. Two ground planes with 19 randomly distributed vias excited with a port between them.

because of the slot.

2) IC / Heat Sink Radiation - Source 2: The three traces were replaced by a microstrip connected to a 15 × 15 mm metal ground mimicking a radiating IC with a heat sink on a PCB. The PCB is shown in Fig. 4.

3) Power-ground Plane Resonances - Source 3: Two 150 × 225 mm ground planes were excited with a port between the planes mimicking radiating plane resonances as shown in Fig. 5. 19 vias, connecting the planes, that were distributed over the board. In one version, the board was excited in the center and in another version, the board was excited in the corner.

A more complicated version of the above PCB was also used as a source. The full size top ground plane was replaced with

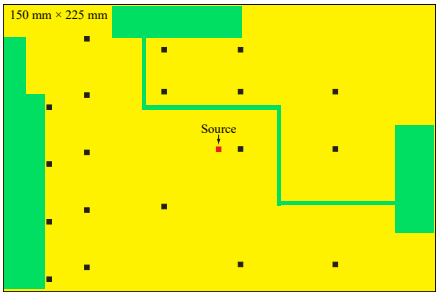

Fig. 6. A full ground plane with two separated ground fill and 19 vias.

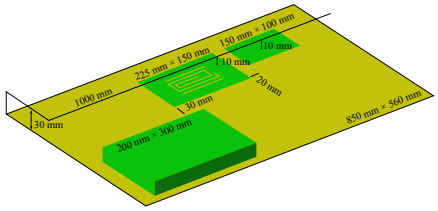

Fig. 7. The microstrip PCB in a TV set environment with several scatters near the radiating source.

a more typical ground fill consisting of two irregular ground fill separated from each other as shown in Fig. 6. The model was excited with a 50 Ω port between the large left ground fill and the bottom full ground plane.

D. Obstacles

Two different environments were used in the investigation. A large ground plane with a cable, a metal box and a ground plane near the source mimicking a TV set was used for further investigation of the method. A narrow enclosure serving as worst case was used in the search for the limits of the method.

1) Ground plane, cable and Metal Box - Environment 1: The method was tested in an environment mimicking a TV set. The source PCB was placed floating 2 cm above a 85 cm × 56 cm large ground plane. A 1 m long cable was placed 1 cm above the radiating PCB. Another 20 cm × 30 cm metal structure was placed 3 cm away from the radiating PCB, and a 10 × 15 cm metal plate was placed 2 cm away from the radiating PCB. Two different cabling routes were tested. The two routes were a cable in a L-shape in contact with the ground plane as shown in Fig. 7 and a long straight floating cable. The overall purpose with this structure was to test the HB method in an environment with several scatterers near the radiating source.

2) Narrow Enclosure - Enviroment 2: In the search for the general limit of the method, the radiating PCBs were placed in the center of a narrow enclosure with the dimension 450 mm × 300 mm × 40 mm and open in one end as shown in Fig. 8. With a height of only 40 mm, the enclosure was placed in the reactive near-field of the PCB and the HB. The radiated field will be scattered and rescattered multiple times.

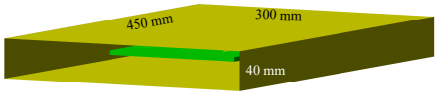

Fig. 8. The radiating PCBs were placed in a narrow enclosure open in one end.

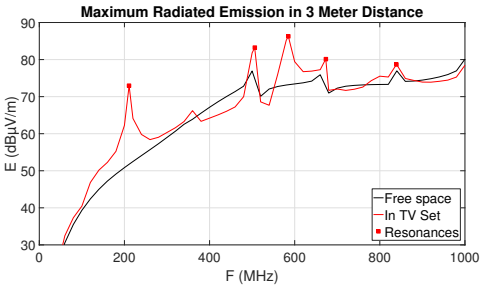

Fig. 9. Maximum radiated emission in 3 m distance from the microstrip PCB in free space vs. in the TV set environment. Resonances are denoted by squares.

IV. Results and Discussion

The maximum field is the focus in an EMC radiated emission measurement. Hence, in all scenarios, the errors introduced by the HB method were evaluated as the difference in the far-field between the HB simulations and the reference:

$$\text{Far-field error} = 20 \cdot \log_{10} \frac{\max(E_{\text{Huygens'}})}{\max(E_{\text{reference}})} \qquad (5)$$

where $\max(E_{\text{Huygens'}})$ is the maximum far E-field of the Huygens Box model and $\max(E_{\text{reference}})$ is the maximum far E-field of the reference case. The maximum is taken across both theta and phi components - equivalent to the difference in two far-field measurements according to CISPR 35. However, the field is evaluated on the whole sphere, and no conductive floor is included in the evaluation. It is somewhat subjective what is acceptable for far-field errors caused by the HB method. If the errors are below 2 dB, it is still significantly smaller than the common 6 dB measurement uncertainty in the EMC society.

With the purpose to obtain a reliable conclusion, the method was tested in different cases. However, due to the limited number of pages, only some representative or illustrative examples are presented in details and the rest of the results are only briefly summarized.

A. Microstrip PCB in TV set Environment

The PCB with three microstrips and an unbroken ground plane (source 1) was placed in the TV set (environment 1) as shown in Fig. 7. Fig. 9 shows the radiated emission in 3 m distance for the PCB in free space versus the PCB in the TV set environment with the L-shaped cable 20 mm above the PCB. As one would expect, the radiated emission increases up to 22 dB when the cable is placed above the PCB.

The setup mimics a situation where wrong EMC design with a cable above a PCB is unavoidable. The question is whether it is possible from near-field scan and simulation to predict radiated emission from a specific cabling and several scatterers nearby the source.

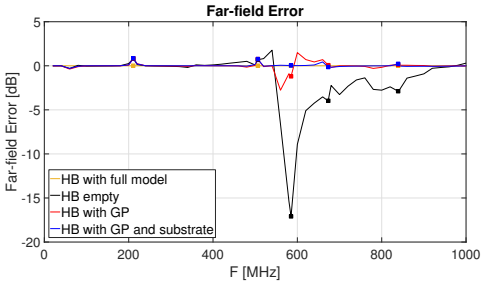

Fig. 10. Far-field errors for the microstrip PCB in TV set environment. Resonances are denoted by squares.

The far-field errors for the L-shaped grounded cable are shown in Fig. 10. In Section II-A, it was proved that including the full model inside the HB restores the fields outside the HB in the presence of obstacles. The far-field errors for HB full model were 0 dB as expected which served as a control of the HB method implementation in the FDTD code. When the HB was empty, the far-field errors became considerable, e.g., at 581 MHz where an empty HB underestimated the radiated emission by 17 dB. If the ground plane was included in the HB, the far-field errors were reduced to a maximum of 2.8 dB. If the lossy substrate was included also, the far-field errors were reduced to less than 1 dB – even at resonance frequencies.

The results for the floating cable were very similar. Maximum absolute far-field error with ground plane included was 2.3 dB, and when the substrate was also included, the absolute far-field errors were reduced to less than 0.5 dB – even at resonance frequencies.

B. Microstrip and IC / Heatsink PCB in Narrow Box

The microstrip PCB with a slot in the ground plane below the trace (source 1), as well as the IC / heat sink PCB (source 2) were placed in the narrow enclosure (enviroment 2). When the sources were placed in the narrow box, the maximum radiated emission decreased up to 20 dB at lower frequencies. From 400 MHz and up, the radiated emission both decreased and increased because of the box.

The far-field errors introduced by the HB method for the microstrip PCB with a slot in ground plane are shown in Fig. 11. A surprising fact is that the empty HB and the HB with only a ground plane caused almost the same far-field errors, (i.e., the black and red curve coincide in Fig. 11. One explanation could be that only TEx00 modes are excited in the enclosure, which have the E-fields orthogonal to the ground plane, and so adding the ground plane does not affect the fields. When the substrate is added the speed of propagation changes (in all directions), and the field distribution is changed, including the resonance frequency.

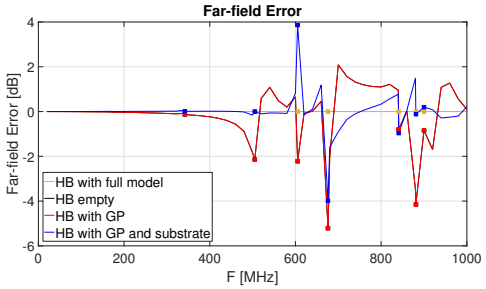

Fig. 11. Far-field errors for the microstrip PCB with slot in the ground plane inside the narrow box. Resonances are denoted with a square.

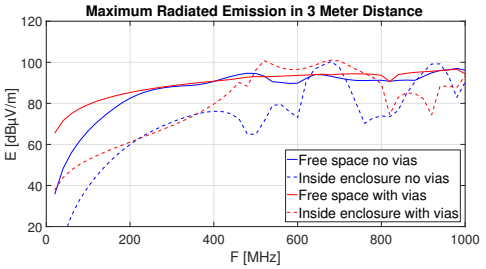

Fig. 12. Maximum radiated emission with and without vias and in free space and inside enclosure.

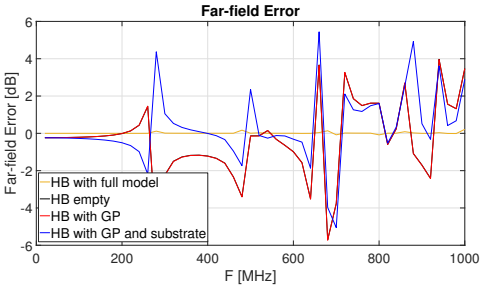

Fig. 13. Far-field error for the via PCB inside the narrow box.

The result is similar to the microstrip in a TV set environment. An empty HB introduces up to 6 dB error, however, if the ground plane and substrate are included in the HB, the errors are, in general, reduced to less than 1 dB. In contrast to the TV set, the far-field errors do not drop to an acceptable level at the resonance frequencies even with the ground plane and the substrate included in the HB. At 605 MHz and 676 MHz, the far-field errors are 4 dB and -4 dB respectively.

The far-field errors for the IC / heatsink PCB in the narrow box were very similar. In general, the far-field error introduced by the HB method was below 1 dB if ground plane and substrate were included in the HB. However, at the resonance frequency 603 MHz, the far-field error again was -4 dB.

The only features making the difference from the full model, with 0 dB far-field error, are the traces and the 50 Ω loads for the microstrip PCB, and the trace and IC / heatsink for the other PCB. At a glance, this is quite surprising. However, the observed strong resonances between the PCB and the box have a very high Q-factor and correspondingly narrow bandwidth. It is reasonable that the traces/loads/IC are a part of the resonances, and that these resonance are detuned without the features. For the TV set in contrast, the resonances are primarily caused by the cable which has a lower Q-factor compared to the narrow box.

C. Ground Plane Resonances in Narrow Box

Until now, the HB method has only failed for a few narrow banded resonances caused by strong interaction between source and environment. In the search for the general limit of the method, the question arose of what happens if the important features of the PCB included in the HB are a part of the source for radiation. Hence a PCB with two ground planes (source 3, Fig. 5) was simulated in free space and floating in the center of the narrow enclosure (environment 2, Fig. 8). The maximum radiated emission in 3 meter distance for the ground plane excited in the center, with and without 19 vias, is shown in Fig. 12. The results are shown in order to illustrate that the vias change both the amplitude and resonance frequencies of the radiated emission from the PCB. When the via PCB was placed inside the narrow enclosure, the maximum radiated emission changed up to 30 dB compared to a free space simulation of the via PCB. This illustrates the potential usability of the method, because, if a free space radiated emission measurement of a PCB is used as pre-compliance test, it will deviate much from the radiation of the apparatus which the PCB will be mounted.

Above 400 MHz, the radiation from the PCBs (with and without vias) does not variate much in free space. However, when the boards are placed inside the enclosure, there is up to 30 dB difference between the PCB with and without vias indicating a complex resonance system depending of the vias. If these differences are caused by the different near-fields (i.e., the different HBs) there is no problem for the HB method. On the other hand, if the differences are caused by strong coupling between the board and enclosure, this coupling will depend on the numbers and location of the vias. Hence, the vias will be a major feature that must be included in the HB simulation. This will require detailed knowledge about the PCB layout reducing the usability of the HB method.

The far-field errors for the via PCB with excitation in center are shown in Fig. 13. When the ground plane was included in the HB, it was without the vias. Again, the empty HB and the HB with only ground planes (no vias) caused almost the same far-field errors. Also the far-field errors changed when the substrate was included. The far-field errors were between ± 6 dB over the whole frequency span not limited to a few resonance frequencies. The far-field errors of the HB, with full model, is included in Fig. 13 in order to prove that the differences are positively caused by the different features included in the HB and not numerical errors.

If the board was excited in the corner instead of the center,

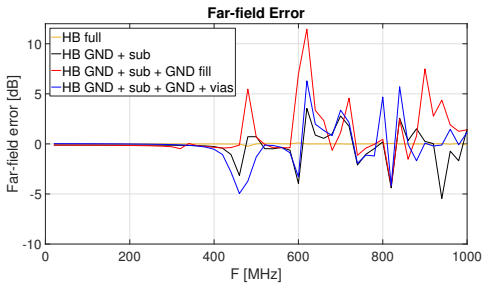

Fig. 14. Far-field error for the ground fill PCB inside the narrow box.

the far-field errors were very similar. The errors have similar amplitude ($\pm$6 dB) but is located at different frequencies.

D. Ground Fill Board in Narrow Box

The results in the previous section, indicated that vias can be a major feature for the HB method and hence required to be include in the HB for reliable results. Many two layers PCBs have a ground plane and a top layer partly covered with ground fill. The ground fill board shown in Fig. 6 was placed floating in the center of the narrow enclosure.

The far-field errors for the HB filled with different features are shown in Fig. 14. It has already been shown that the substrate is important for the method, so it was included in all cases. The substrate was combined with the ground plane (GND + sub), ground plane, and ground fill (but no vias) (GND + sub + GND fill), and finally two full size ground planes, (i.e., the top ground plane was full size and not the ground fill) with the vias (GND + sub + GND + vias). In all cases, the HB method introduces significant far-field errors from 400 MHz and up. Including everything except the vias is actually worst case, and shows that the vias are a major feature for the coupling between the narrow box and the PCB. If the vias are included with full ground plane instead of the ground fill, it also causes significant far-field errors, hence, the ground fill is also a major feature of the coupling.

V. Conclusion

When a PCB is placed in an apparatus, the maximum radiated emission typically change within $\pm$ 30dB compared to a free space measurement. Hence, a free space measurement of the PCB does not serve as a pre-compliance test. If the PCB's near-field on a closed surface is used as a source for simulation, it is, in many cases, possible to estimate the far-field of the PCB near obstacles with high accuracy by a combination of near-field measurements and simulations.

Several combinations of sources and environments have been investigated in this paper and [14], [15]. The different combinations and the far-field errors caused by the HB method are summarized in Table I.

The results indicate, that generally, the HB method itself only introduces small errors (less than 1 dB) if the environment does not have strong resonances. The results also indicate that the far-field error will increase with the Q-factor of the resonances. The method finds a limit when the far-field are predicted from PCBs, with plane resonances, places in a resonant environment. In that case, the unacceptable far-field errors are not restricted to a few resonance frequencies. The study has only investigated the numerical errors introduced by the HB method. On top of that, the method is off cause also sensitive to measurement uncertainty and errors.

TABLE I
Far-field Errors Introduced by the HB method

Source	Environment	Far-field errors caused by the HB methode
Microstrip PCB, unbroken ground plane.	TV set	Less than 1 dB error with ground plane and substrate included – even at resonance frequencies
Microstrip PCB, unbroken ground plane.	Half open box (50 cm $\times$ 30 cm $\times$ 15 cm)	Less than 1 dB error with ground plane and substrate included – even at resonance frequencies [14]
Microstrip PCB, unbroken ground plane.	Narrow box (environment 2)	In general less than 2 dB error with ground plane and substrate included. However, at a few resonance frequencies there were up to 10 dB far-field error [15]
Microstrip PCB with a slot under the trace (the slot is the noise source)	Narrow box (enviroment 2)	In general less than 1 dB error with ground plane and substrate included. However, at a few resonance frequencies there were 4 dB error.
IC / heatsink PCB	Narrow box (environment 2)	In general less than 1 dB error with ground plane and substrate included. However, at one resonance frequencies the error was 4 dB.
Power plane resonance between two planes connected with 19 vias	Narrow box (enviroment 2)	Unacceptable far-field errors up to 6 dB with ground planes and substrate included. The errors were not restricted to a few resonance frequencies.
Two layer PCB with ground fill and 19 vias	Narrow box (enviroment 2)	No matter which parts that were included in the HB, the method caused unacceptable far-field errors up to 10 dB. The errors were not restricted to a few resonance frequencies.

Acknowledgment

The present work has been supported by the Danish Agency for Science, Technology and Innovation. The authors also gratefully acknowledge the support from the Danish e-Infrastructure Cooperation (DeIC) for the hybrid Linux cluster Fyrkat at Aalborg University, Denmark.

References

[1] "IEC 61967: Integrated circuits measurement of electromagnetic emissions, 150 kHz to 1 GHz," 2003, first Edition.

[2] X. Tong, D. W. P. Thomas, A. Nothofer, P. Sewell, and C. Christopoulos, "Modeling electromagnetic emissions from printed circuit boards in closed environments using equivalent dipoles," *IEEE Trans. Electromagn. Compat.*, vol. 52, no. 2, pp. 462–470, May 2010.

[3] Y. Vives-Gilabert, C. Arcambal, A. Louis, F. de Daran, P. Eudeline, and B. Mazari, "Modeling magnetic radiations of electronic circuits using near-field scanning method," *IEEE Trans. Electromagn. Compat.*, vol. 49, no. 2, pp. 391–400, May 2007.

[4] M. Hernando, A. Fernandez, M. Arias, M. Rodriguez, Y. Alvarez, and F. Las-Heras, "EMI radiated noise measurement system using the source reconstruction technique," *Industrial Electronics, IEEE Transactions on*, vol. 55, no. 9, pp. 3258–3265, Sept 2008.

[5] Z. Yu, J. A. Mix, S. Sajuyigbe, K. P. Slattery, and J. Fan, "An improved dipole-moment model based on near-field scanning for characterizing near-field coupling and far-field radiation from an IC," *IEEE Transactions on Electromagnetic Compatibility*, vol. 55, no. 1, pp. 97–108, Feb 2013.

[6] J. Shi, M. Cracraft, J. Zhang, R. DuBroff, and K. Slattery, "Using near-field scanning to predict radiated fields," in *Electromagnetic Compatibility, 2004. EMC 2004. 2004 InternationalSymposium on*, vol. 1, Aug 2004, pp. 14–18 vol.1.

[7] H. Weng, D. G. Beetner, and R. E. DuBroff, "Prediction of radiated emissions using near-field measurements," *IEEE Trans. Electromagn. Compat.*, vol. 53, no. 4, pp. 891–899, Nov. 2011.

[8] X. Gao, J. Fan, Y. Zhang, H. Kajbaf, and D. Pommerenke, "Far-field prediction using only magnetic near-field scanning for EMI test," *Electromagnetic Compatibility, IEEE Transactions on*, vol. PP, no. 99, pp. 1–9, 2014.

[9] L. Foged, L. Scialacqua, F. Saccardi, F. Mioc, D. Tallini, E. Leroux, U. Becker, J. Araque Quijano, and G. Vecchi, "Bringing numerical simulation and antenna measurements together," in *Antennas and Propagation (EuCAP), 2014 8th European Conference on*, April 2014, pp. 3421–3425.

[10] M. Sørensen, O. Franek, and G. F. Pedersen, "Recent developments in using measured sources in computational emc," in *2015 9th European Conference on Antennas and Propagation (EuCAP)*, May 2015, pp. 1–5.

[11] X. Tong, D. W. P. Thomas, A. Nothofer, P. Sewell, and C. Christopoulos, "Reduction of sensitivity to measurement errors in the derivation of equivalent models of emission in numerical computation," in *IET 8th International Conference on Computation in Electromagnetics (CEM 2011)*, April 2011, pp. 1–2.

[12] O. Franek, M. Sorensen, H. Ebert, and G. Pedersen, "Influence of nearby obstacles on the feasibility of a Huygens' box as a field source," in *Electromagnetic Compatibility (EMC), 2012 IEEE International Symposium on*, Aug 2012, pp. 600–604.

[13] ——, "Near-field characterization of a printed circuit board in the presence of a finite-sized metallic ground plane," in *Progress In Electromagnetics Research Symposium (PIERS)*, March 2012, pp. 1146–1149.

[14] M. Sorensen, I. Bonev, O. Franek, G. Petersen, and H. Ebert, "How to handle a Huygens' box inside an enclosure," in *Electromagnetic Compatibility (EMC), 2013 IEEE International Symposium on*, Aug 2013, pp. 802–807.

[15] O. Franek, M. Sørensen, I. B. Bonev, H. Ebert, and G. F. Pedersen, "Influence of resonances on the Huygens' box method," in *2013 International Symposium on Electromagnetic Compatibility*, Sept 2013, pp. 381–384.

[16] X. Gao, J. Fan, Y. Zhang, H. Kajbaf, and D. Pommerenke, "Far-field prediction using only magnetic near-field scanning for emi test," *IEEE Transactions on Electromagnetic Compatibility*, vol. 56, no. 6, pp. 1335–1343, Dec 2014.

[17] M. Sorensen, O. Franek, G. Pedersen, K. Baltsen, and H. Ebert, "Perturbation of near-field scan from connected cables," in *Electromagnetic Compatibility (EMC), 2012 IEEE International Symposium on*, Aug 2012, pp. 594–599.

[18] K. Kam, A. Radchenko, and D. Pommerenke, "On different approaches to combine cable information into near-field data for radiated-field estimation," *Electromagnetic Compatibility, IEEE Transactions on*, vol. 56, no. 2, pp. 276–285, April 2014.

[19] C. A. Balanis, *Advanced Engineering Electromagnetics*. New York: Wiley, 1989.

[20] A. Taflove and S. C. Hagness, *Computational Electrodynamics: The Finite-Difference Time-Domain Method*, 3rd ed. Boston: Artech House, 2005.

Morten Sørensen (M'08) received the M.S. degree in physics from Aarhus University, Aarhus, Denmark, in 2005. From 2006 to 2017, he was an Antenna and Electromagnetic Compatibility (EMC) specialist with Bang & Olufsen, Struer, Denmark, including three years (2011-2014) as a Researcher and Technical Project Manager in the innovation consortium, EMC Design First Time Right. In 2017, he joined the EMC Laboratory, Missouri University of Science and Technology, Rolla, MO, USA, where he is a visiting Assistant Research Professor. Since 2018 he has been working part time with Amber Precision Instruments, San Jose, CA, USA. His current resarch interests include near-field scanning, emission source microscopy, electrostatic discharge, and system-level radiated emission.

Ivan Bonev Bonev received the B.Sc. and M.Sc. degrees (Hons.) in telecommunications from the Technical University of Varna, Varna, Bulgaria, in 2002 and 2004, respectively, where he also received the M.Sc. degree in electrical engineering in 2007. He received the Ph.D. degree in wireless communications from Aalborg University, Aalborg, Denmark in 2013. He was a visiting researcher at Ecole Politechnique de luniversite de Nantes, Nantes, France; Tampere University of Technology, Tampere, Finland; and Atlantic Cape Community College, Cape May Court House, NJ. His research interests include antennas, theoretical aspects of antenna systems, antenna interactions with a human body, hearing aid compatibility of mobile phones and specific absorption-rate problems. He is the recipient of the URSI young scientist award in group B Waves and Fields for 2011.

Ondrej Franek (S'02–M'05) received the Ing. (M.Sc.E.E. Hons.) and Ph.D. degrees in electronics and communication technology from Brno University of Technology, Brno, Czech Republic, in 2001 and 2006, respectively. He is currently an Associate Research Professor with the Department of Electronic Systems, Aalborg University, Aalborg, Denmark, where he is a member of the Antennas, Propagation and Millimeter-wave Systems Section. His research interests include electromagnetic theory and computational electromagnetics with a focus on fast and efficient numerical methods, especially the finite-difference time-domain method. He has developed the in-house fully scalable parallel FDTD code that has been used in research at Aalborg University to solve electrically large problems related to antennas, radiowave propagation and electromagnetic compatibility. Dr. Franek was a recipient of the Seventh Annual Siemens Award for outstanding scientific publication.

Gert Frølund Pedersen (M'14) received the B.Sc. and E.E. (Hons.) degrees in electrical engineering from the College of Technology in Dublin, Dublin Institute of Technology, Dublin, Ireland, in 1991, and the M.Sc.E.E. and Ph.D. degrees from Aalborg University, Aalborg, Denmark, in 1993 and 2003, respectively. Since 1993, he has been with Aalborg University where he is a Full Professor heading the Antennas, Propagation and Millimeter-wave Systems Lab with 25 researchers. He is also the Head of the Doctoral School on wireless communication with some 40 Ph.D. students enrolled. His research interests include radio communication for mobile terminals, especially small antennas, diversity systems, propagation, and biological effects. He has published more than 500 peer-reviewed papers, 6 books, 12 book chapters and holds over 50 patents.

Paper H

Recent Developments in Using Measured Sources in Computational EMC

Morten Sørensen[1], Ondrej Franek[1], Gert Frølund Pedersen[1]
[1]Antennas, Propagation and Radio Networking section, Aalborg University,
Niels Jernes Vej 12, 9220 Aalborg, Denmark, {mos, of, gfp}@es.aau.dk

The paper has been publish in
Antennas and Propagation (EuCAP), 2015 9th European Conference on, April 2015, pp. 1–5

Recent Developments in Using Measured Sources in Computational EMC

Morten Sørensen[1], Ondřej Franek[2], Gert Frølund Pedersen[3],
[1#] Antennas, Propagation and Radio Networking, Department of Electronic Systems,
Faculty of Engineering and Science, Aalborg University
Niels Jernes Vej 12, 9220 Aalborg Øst, Denmark
[1] mos@es.aau.dk, [2] of@es.aau.dk, [3] gfp@es.aau.dk

***Abstract*—This paper gives an overview of the recent developments in using near-field scanning for proactive EMC work. The aim is to use measured near fields as a source for simulations in order to predict radiated emission from printed circuit boards placed in a product. Far fields were predicted based on only H-fields on the top and bottom surface on a Huygens' box surrounding the board. Simulation of a simple board with microstrips and measurements of a complicated signal board were used to evaluate the proposed method.**

***Index Terms*—EMC, near-field scanning, Huygens' box.**

I. Introduction

All electronic devices shall pass a radiated emission test in order to be compliant with regulatory EMC requirements and before entering the market. As the clock frequencies increased in the past decade, direct radiation from microstrips, integrated circuits, FPGAs, printed circuit board (PCB) plane resonances etc. approaches or even exceeds the limits for radiated emission. Hence electronic manufacturers struggle with this legal authority requirement and developers look for new methods for doing pro-active EMC work and pre-compliance test.

A near-field (NF) electromagnetic (EM) scanner is an effective tool for locating the sources of radiation. A typical near-field plot of the magnetic field at a certain frequency (shown partly transparent over a picture of the PCB) is displayed in Fig. 1 where possible radiation sources become visible.

Several different NF EM scanners have been developed over the years. A typical near-field scanner is made by a XYZ-positioner [1], [2]. This positioner holds the scan probe as it is moved in a pre-defined pattern above the PCB. In order to measure the phase, three different approaches have been used:

1) Vector network analyzer [3], [4]
2) Phase coherent receivers [5]
3) High-speed oscilloscopes [2]

In [6] an automatic and sequential sampling algorithm for the NF scanning of PCBs and/or integrated circuits was presented. The sampling algorithm will find the positions where it is necessary to measure in order to have a representative picture of the field so that the rest can be skipped, reducing the numbers of measuring points.

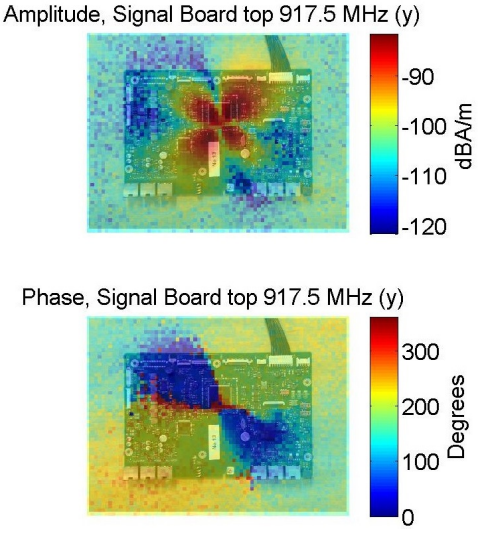

Fig. 1. A magnetic near-field scan, amplitude and phase, of a typical signal board.

High magnitude spot in the near field does not necessarily mean that this location is the source for radiation. E.g. a differential microstrip pair will in the NF region have a strong magnetic amplitude but this field is evanescent. In [7] emission source microscopy (ESM) technique was used to localize only active sources of radiation on a PCB. The ESM method uses the plane wave spectrum and back propagates the field to the source.

Inspired by the antenna society [8], using the NF scanning for predicting far-field has been an important research topic for several years.

Two different approaches are used in order to do the near-to-far-field transformation: source reconstruction technique [3], [9], [10] or surface equivalence principle (Huygens' box method) [11]–[13].

Despite significant progress, the method is not yet applicable for everyday use with advanced PCBs and the validation in the

above mentioned papers of the near-to-far-field transformation is primarily done by simulations and a few measurements of very simple structures. One of the limitations in the everyday use is that PCBs in real products are placed close to other structures and hence interact with the surroundings. This interaction can change the far field significantly from the free space condition in which the NF measurement is done.

For the Huygens' box method it has been shown that including the main features (e.g. ground plane and substrate) of the PCB in the Huygens' box will take re-scattering into account and give comparatively good results [14].

Advanced PCBs of today often have many cable connections running through the Huygens' box. These cables will make it very difficult to measure the sides of the Huygens box, where the cables go through. In some cases the result will be comparatively good if only the top side is measured, but in other cases measurements of all 6 sides of the Huygens' box are needed [15].

It is very time-consuming to measure both E- and H-fields and, in addition, it is difficult and very expensive to make a precise tangential E-field probe. Ref. [13] succeeded in filling up the Huygens' box with perfect magnetic conductor (PMC) material and use only H-field in order to predict the far-field radiation.

In this paper we combine the approximations and investigate whether it is possible to reduce the measurement to only H-field on the top and bottom surface of a PCB, which could reduce the effort and make the method useful in everyday research and development work. The investigation is based on simulation of a simple PCB and measurement of a real signal board.

In Section II a brief overview of the theoretical background of the method is presented. Section III describes the numerical experiment and the measurement setup. Results are shown and discussed in Section IV. Finally, conclusions are drawn in Section V.

II. Huygens' box Method

The Huygens' box (HB) method is well known and widely used in the electromagnetic area. It is derived from Love's equivalence principle [16] as illustrated in Fig. 2.

A radiating source generates electromagnetic fields in free space. The tangential components of the electric (E-) and magnetic (H-) fields on a surface S entirely enclosing the structure are extracted. According to Love's principle, electromagnetic fields outside of this closed surface can be recreated by the equivalent electric and magnetic currents on the surface. These currents are related to the original fields $\vec{E}$ and $\vec{H}$ on the surface by

$$\vec{J}_S = \hat{n} \times \vec{H}_2|_S, \qquad \vec{M}_S = -\hat{n} \times \vec{E}_2|_S, \tag{1}$$

where $\hat{n}$ denotes the normal vector oriented outwards from the surface.

Since the fields inside S are zero [17], it is possible to change the medium inside S without changing the field outside. Hence we are allowed to fill V_1 with PMC. Now the magnetic surface current $\vec{M}_1$ is short-circuited and considered to be zero. In this way we can reduce the equivalent problem and only consider the tangential magnetic fields.

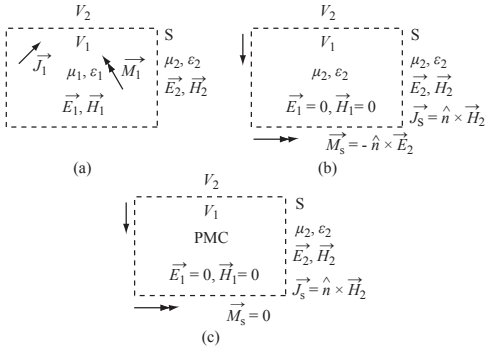

Fig. 2. Love's formulation of the surface equivalence problem: (a) original problem; (b) equivalent problem with surface currents - field inside is zero; (c) equivalent problem with PMC inside volume with the purpose to omit magnetic currents.

III. Test setup

A. Evaluation by simulations

The PCB shown in Fig. 3 was used as test case for the proposed method. A full model of the structure was simulated and the tangential components of the E- and H-field on a Huygens' box was extracted. The HB was positioned at a fixed distance of 10 mm from the PCB in all directions. In addition, the maximal electric far-field in 3 m distance was calculated for reference as representative for a radiated emission test like CISPR 22. The PCB was simulated in CST Microwave Studio with the transient solver (Finite Integration Technique) [18]. The field on the HB was written in the *.nfd-format, which is importable in CST. This format requires equidistant step sizes and some interpolation was made in MATLAB in order to have a step size of 2 mm.

Next step was to use the extracted HB as source for simulation of the far-field in 3 m distance. In order to quantify the errors of the methods proposed in section II, different simulation scenarios were carried out:

- The full HB with fixed 10 mm distance was used as source for a simulation, i.e. both E- and H-fields on all six faces.
- The tangential E-field was removed and in return the HB was filled with PMC. (CST does not provide PMC yet, therefore the PMC was approximated with a material with magnetic conductivity of 10^7 $\mathrm{S^{-1}m^{-1}}$.).
- The fields on X_{min} / X_{max} and Y_{min} / Y_{max} were removed corresponding to a near-field scan where only the top and bottom of the PCB is measured.
- The HB distance was increased to 20 mm and 40 mm.

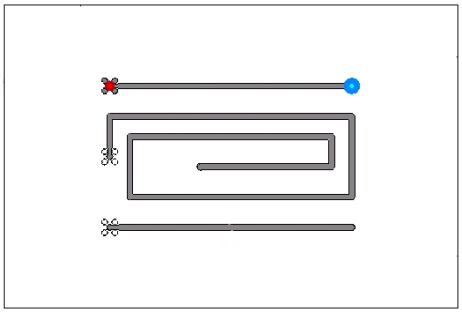

Fig. 3. The test PCB: A simple 150 x 225 mm PCB with three 50 Ω traces on the top layer with a full ground plane on the bottom layer. Only one trace was excited and terminated. Both source impedance and load impedance was 50 Ω.

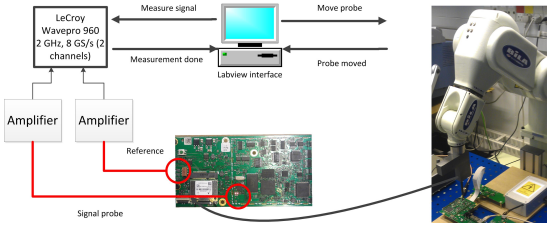

Fig. 4. Block diagram of the home made NF scanner.

In all scenarios the difference in the far-field between the HB simulations and the reference was evaluated using the following metric:

$$\text{Peak increase} = 20\log_{10}\frac{\max(E_{\text{Huygens}},)}{\max(E_{\text{reference}})} \quad (2)$$

where $\max(E_{\text{Huygens}})$ is the maximum in the far E-field of the HB model and $\max(E_{\text{reference}})$ is the maximum of the far E-field of the reference case.

B. Measurements

With the aim to validate the full near-field scanner setup (amplifier gain, cable losses, Fourier transformation etc.) a comparison between measurements and simulation of the simple PCB was carried out - see Fig. 3. The PCB was driven by a 20 MHz comb generator and the scanning hight was 10 mm, i.e. distance from PCB top to center of measuring probe.

The near-field measurements were carried out on a home-made near-field scanner. A block diagram is shown in Fig. 4. The gain of the amplifier and the cable losses were measured with a Rohde & Schwarz ZVB VNA. A Langer H-Field Probe RF-R 50 - 1 was used in the measurements and with the probe factors provided by Langer EMV-Technic [19]. The signal was measured with a LeCroy Wavepro 960 oscilloscope with 8 GS/s and afterwards Fourier transformed in MATLAB. The measurement length was 50 μs. The phase was measured relative to the reference probe, which was a homemade loop antenna. The reference probe was placed a short distance from the device under test. Close enough to measure the signal, but far enough away so it did not disturb the measurement.

As mentioned in Section I, validation of far-field prediction methods within the EMC society is typically based on ideal simulations or measurements of very simple structures. The long-term ambitious goal is to use the NF measurement for predicting far-fields in a broad frequency range from real PCBs and therefore we decided to evaluate the proposed method on a real signal board.

The test PCB was a signal board with a digital signal processor (DSP) on the top side and RAM on the bottom side, which ran with a test software which enabled the memory communication 100%. The magnetic near-field was measured on top and bottom of the PCB with the above mentioned near-field scanner. The scan area exceeded the PCB by 40 mm in all directions. Next the measured near field was imported to CST Microwave Studio in the nfd-format. The reduced HB (no measurements on the side) was filled with PMC and the far-field was simulated in CST.

For comparison, an azimuth scan of the signal board was made in a 3 m semi-anechoic chamber with absorbers on the floor.

IV. Results

For every comb frequency (i.e. every 20 MHz) the measured and simulated magnetic near fields were compared. Visual comparison of the amplitude for 640 MHz is shown in Fig. 5. Except for the x-component of the field just above the active microstrip, there was a very good agreement between measurements and simulations. Currents on the inactive microstrip (the snail, see Fig. 3) and asymmetries in the field were visible both in simulations and measurements. 640 MHz was representative for all the frequencies except for the frequencies below 100 MHz, where the measured near field was more blurred. At 500 and 1000 MHz the oscilloscope had an internal spurious frequency which disturbed the measurement.

In Fig. 6 the maximum simulated near field minus the maximum measured near field is shown. The deviation between measurement and simulation was -3/+2 dB. The ripple could be caused by impedance mismatch, probably at the oscilloscope port. This could possibly be corrected with an attenuator on the oscilloscope port.

The comparison shows that the NF scanner was able to measure the NF pattern with a small uncertainty on the amplitude.

The peak increase for the different scenarios described in section III-A is shown in Fig. 7.

- The full 10 mm HB: The result shows the numerical error, the interpolation of the field caused. Except for the lowest frequencies the introduced error was below 0.5 dB.
- The full 10 mm HB with only H-field (E-field deleted and HB filled with PMC): The result shows that CST MWS could handle (approximated) PMC with a reasonable small error introduced.

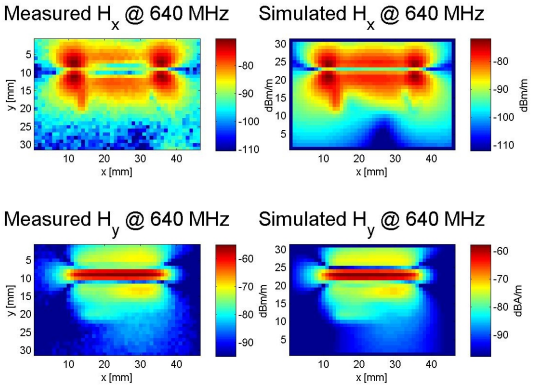

Fig. 5. Comparison of measured and simulated near fields 10 mm above the PCB.

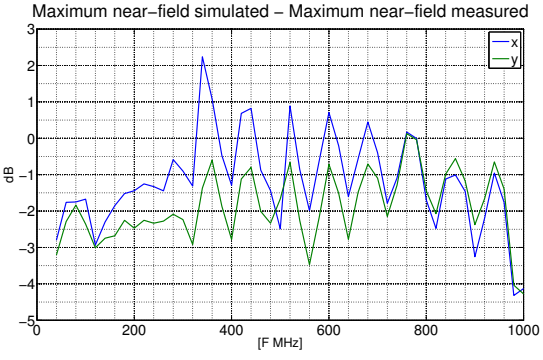

Fig. 6. Difference between maximum measured and simulated magnetic near field for every 20 MHz.

- Only H-field on top and bottom for different scan areas: The result shows that removing the side of the HB introduced up to 2 dB error in the predicted maximum far-field. The error seems to decrease as the scan area increases because of weaker fields on the omitted sides of the HB.

The comparison suggests that if the H-field can be measured with enough accuracy and dynamic range, it is possible to use only the H-field at the top and bottom of the Huygens' box. This conclusion was based on simulations of a microstrip and further studies are of course needed in order to investigate, whether the conclusion applies to other structures.

In Fig. 8 comparison between measured and simulated azimuth scans of the signal board is shown for two different frequencies. The y-component of the NF scan of the signal board at 917.50 MHz is shown in Fig. 1.

The agreement between measurements and simulations is fair and almost within 6 dB, which is the typical accepted uncertainty in the EMC society. However, the agreement at

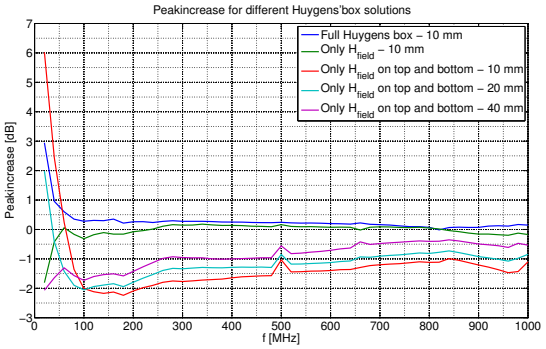

Fig. 7. Peak increase for every 20 MHz for the different scenarios described in section III-A

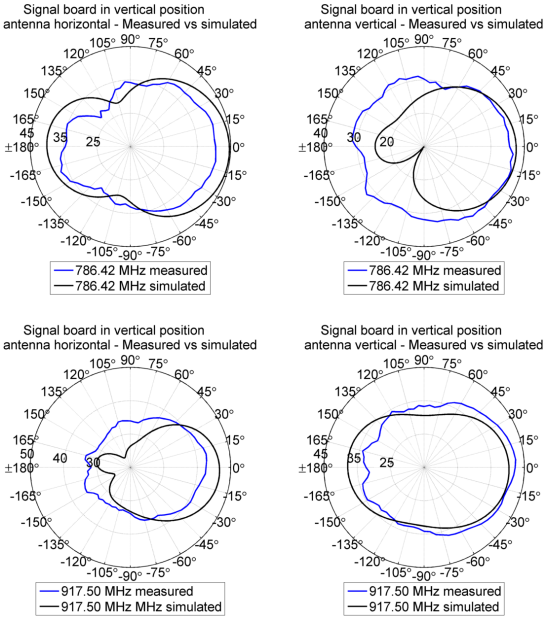

Fig. 8. Comparison between measurement- and simulation of azimuth scan of the signal board for 786.42 MHz and 917.50 MHz.

786.42 MHz with antenna vertical is poor and the simulations and the measurements differ more than 6 dB. The simulation has a null which is not detected in the measurement. Generally the radiation backward (the RAM side) is weaker in the simulations compared to the measurements. There are a number of possible explanations why the comparison is only fair and not good:

- The scan area was not large enough. The near field has not reached the noise floor at the edges of the scan area, which can be seen in Fig. 1. Hence significant radiating near field could be present outside the scanning area. (In

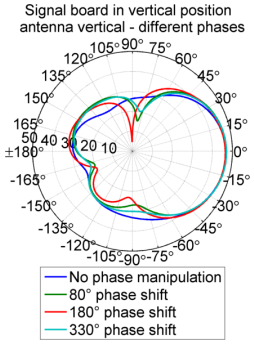

Fig. 9. Comparison of the azimuth scan with different phase manipulations.

our first try the scan area only exceeded the PCB by 20 mm and the agreement was even worse.)

- We measured only the H-field. At the RAM side, the field impedance could be high, i.e. the E-field is dominating, and hence the H-field is too weak to be measured correctly. The oscilloscope is only 8 bit limiting the dynamic range.
- In the measurement it is difficult to measure the phase at the top relative to phase at the bottom. After the top was measured the PCB was turned around and the bottom was measured. Hence we moved the reference probe and this could cause a phase shift between top and bottom. In Fig. 9 the simulation of different imposed phase shift between top and bottom is shown. It is clear, that if care is not taken and the phase between top and bottom is random, the far-field is changed. The field at top is dominant and if the phase at bottom is wrong, the field on top of the board in the simulation could cause false destructive interference backward.

V. Conclusion

In this paper, we have evaluated far-field prediction with only magnetic near-field scanning on top and bottom on a PCB. The evaluation based on a simulation of a simple PCB with a microstrip showed good results. Only 1-2 dB error was introduced, if the simulations was based on only the H-field at top and bottom of the PCB. The distance from PCB edge to scan area edge must be more than 40 mm, otherwise the fields on the side of the HB is still significant.

The evaluation based on a measurement and a simulations of a real signal board showed poor to fair results. The reason could be that the scan areas were insufficient, that E-field and not H-field was dominating or that the phase on the bottom of the PCB was measured incorrectly relative to the phase on top of the PCB.

The study has shown, that using measured sources in computational EMC has potential, but there is still lot of research to do before the method will be viable in commercial research and development.

References

[1] S. Kuehn, M. Wild, P. Sepan, E. Grobelaar, and N. Kuster, "Automated near-field emc/emi scanning system with active electro-optical field probes," in *Electrical Design of Advanced Packaging and Systems Symposium (EDAPS), 2012 IEEE*, Dec 2012, pp. 109–112.

[2] A. Mynster and M. Sorensen, "Validation of emc near-field scanning amplitude and phase measurement data," in *Electromagnetic Compatibility (EMC EUROPE), 2012 International Symposium on*, Sept 2012, pp. 1–6.

[3] Y. Vives-Gilabert, C. Arcambal, A. Louis, F. de Daran, P. Eudeline, and B. Mazari, "Modeling magnetic radiations of electronic circuits using near-field scanning method," *IEEE Trans. Electromagn. Compat.*, vol. 49, no. 2, pp. 391–400, May 2007.

[4] A. Tankielun, H. Garbe, and J. Werner, "Calibration of electric probes for post-processing of near-field scanning data," in *Electromagnetic Compatibility, 2006. EMC 2006. 2006 IEEE International Symposium on*, vol. 1, Aug 2006, pp. 119–124.

[5] T. Mager and C. Hangmann, "Advanced 3D nearfield scanner for automated measurement of phase and amplitude of abitrary shaped modules," Conference: EMC Design - First Time Right, January 29, 2013, Aarhus Denmark, http://emc-first-time-right.dk.

[6] B. Van der Streeck, F. Vanhee, B. Boesman, D. Pissoort, D. Deschrijver, I. Couckuyt, and T. Dhaene, "Practical implementation of a sequential sampling algorithm for emi near-field scanning," in *Electromagnetic Compatibility (EMC EUROPE), 2012 International Symposium on*, Sept 2012, pp. 1–5.

[7] P. Maheshwari, V. Khilkevich, D. Pommerenke, H. Kajbaf, and J. Min, "Application of emission source microscopy technique to emi source localization above 5 ghz," in *Electromagnetic Compatibility, 2014. EMC 2014. 2014 IEEE International Symposium on*, August 2014.

[8] A. Yaghjian, "An overview of near-field antenna measurements," *Antennas and Propagation, IEEE Transactions on*, vol. 34, no. 1, pp. 30–45, Jan 1986.

[9] X. Tong, D. W. P. Thomas, A. Nothofer, P. Sewell, and C. Christopoulos, "Modeling electromagnetic emissions from printed circuit boards in closed environments using equivalent dipoles," *IEEE Trans. Electromagn. Compat.*, vol. 52, no. 2, pp. 462–470, May 2010.

[10] M. Hernando, A. Fernandez, M. Arias, M. Rodriguez, Y. Alvarez, and F. Las-Heras, "Emi radiated noise measurement system using the source reconstruction technique," *Industrial Electronics, IEEE Transactions on*, vol. 55, no. 9, pp. 3258–3265, Sept 2008.

[11] J. Shi, M. Cracraft, J. Zhang, R. DuBroff, and K. Slattery, "Using near-field scanning to predict radiated fields," in *Electromagnetic Compatibility, 2004. EMC 2004. 2004 InternationalSymposium on*, vol. 1, Aug 2004, pp. 14–18 vol.1.

[12] H. Weng, D. G. Beetner, and R. E. DuBroff, "Prediction of radiated emissions using near-field measurements," *IEEE Trans. Electromagn. Compat.*, vol. 53, no. 4, pp. 891–899, Nov. 2011.

[13] X. Gao, J. Fan, Y. Zhang, H. Kajbaf, and D. Pommerenke, "Far-field prediction using only magnetic near-field scanning for emi test," *Electromagnetic Compatibility, IEEE Transactions on*, vol. PP, no. 99, pp. 1–9, 2014.

[14] M. Sorensen, I. Bonev, O. Franek, G. Petersen, and H. Ebert, "How to handle a huygens' box inside an enclosure," in *Electromagnetic Compatibility (EMC), 2013 IEEE International Symposium on*, Aug 2013, pp. 802–807.

[15] M. Sorensen, O. Franek, G. Pedersen, A. Radchenko, K. Kam, and D. Pommerenke, "Estimate on the uncertainty of predicting radiated emission from near-field scan caused by insufficient or inaccurate near-field data: Evaluation of the needed step size, phase accuracy and the need for all surfaces in the huygens' box," in *Electromagnetic Compatibility (EMC EUROPE), 2012 International Symposium on*, Sept 2012, pp. 1–6.

[16] C. A. Balanis, *Advanced Engineering Electromagnetics*. New York: Wiley, 1989.

[17] S. Rengarajan and Y. Rahmat-Samii, "The field equivalence principle: illustration of the establishment of the non-intuitive null fields," *Antennas and Propagation Magazine, IEEE*, vol. 42, no. 4, pp. 122–128, Aug 2000.

[18] "Cst microwave studio, http://www.cst.com."

[19] "Langer emv-technik, www.langer-emv.com."

Paper I

Design of TEM Transmission Line for Probe Calibration up to 40 GHz

Morten Sørensen[1], Shubhankar Marathe[1], David Pommerenke[1], Hamed Kajbaf[2], Jin Min[2]
[1]EMC Laboratory, Missouri University of Science and Technology, Rolla, MO 65401, USA, {sorensenmo, skmcr4, davidjp}@mst.edu
[2]Amber Precision Instruments, San Jose, California, USA, {hamed, jinmin}@amberpi.

The paper has been publish in the
Electromagnetic Compatibility (EMC), 2018 IEEE International Symposium on, Jul 2018

The layout has been revised.

Design of TEM Transmission Line for Probe Calibration up to 40 GHz

Morten Sørensen*, Shubhankar Marathe*, David Pommerenke*, Hamed Kajbaf†, Jin Min†
*EMC Laboratory
Missouri University of Science and Technology
Rolla, Missouri, USA
Email: sorensenmo, skmcr4, davidjp@mst.edu
†Amber Precision Instruments
San Jose, California, USA hamed, jinmin@amberpi.

***Abstract*—With the ongoing development of 5G wireless communication, frequencies as high as 40 GHz have become relevant for EMI near-field scanning. This paper describes the development process of two transmission lines with air dielectrics for probe calibration, namely a rod over ground plane and an air trace. Because of homogeneous dielectrics the transmission lines become almost pure TEM, which is preferable regarding probe calibration to a coplanar waveguide (quasi-TEM). The design process shows that at very high frequencies, transitions in the transmission line are critical and all small physical details must be included in the simulation model in order for it to be reliable.**

I. Introduction

Phase-resolved near-field scanning (NFS) has been widely used in electromagnetics and antenna research for many years. With the ongoing development of 5G wireless communication, mm wavebands above 20 GHz are being intensively studied [1], [2] and there is a great need for high frequency probes and calibration of them. In most EMC near-field scanning systems, a probe (or a set of probes) captures a large set of near-field data on a surface plane close to the device under test (DUT). For example, an E-field probe [3] or an H-field probe [4] can be used to visualize the E-field or the H-field near-field distribution over a DUT.

Various probe calibration methods suitable for different frequency ranges are published in the literature; the different calibration methods and their typical frequency ranges are mentioned in the IEEE Std 1309-2013 [5] and IEC 61000-4-20 Annex E covers E-field probe calibration in TEM waveguides [6].

Previous work [7] has shown that referring a measured voltage to the known fields of a 50 Ω transmission line (TL) is an effective method for calculating the probe factor. If the measurements are done with a Vector Network Analyzer (VNA) (see Fig. 1), the probe factor (PF) is given by:

$$PF = \frac{ref}{S_{21}} \tag{1}$$

where *ref* is the normalized near-field strength (*E* or *H*) from a simulation at a given input voltage and at a given height above the TL:

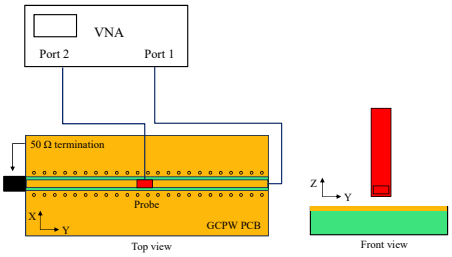

Fig. 1: A typical set-up for probe calibration by way of a coplanar waveguide and a VNA.

$$ref = \frac{Near\text{-}field_{\text{simulation}}}{V_{\text{simulation}}} \tag{2}$$

A pure TEM mode is convenient for calibration since pure TEM is frequency independent and the field components are well defined. But of course no physical case is pure TEM because it would require infinite conductivity and transitions, e.g., from connector to transmission line, will cause some non-TEM mode. In the imperfect physical world, the features of the transmission line for calibration could be prioritized as follows:

1) Well defined field component, i.e., the near-field must be orthogonal to the propagation and there should be no tangential component.
2) The near-field amplitude along a line across the TL must be as frequency independent as possible.
3) Impedance match in order to avoid reflections. If reflections arise, the calibration probe can measure the field along the line and relate the average to the average in the simulation.

A simple microstrip can be used up to a few GHz [8], [9] while a grounded coplanar waveguide (CPW) is better for higher frequencies [10]. Unfortunately, the inhomogeneous medium of a CPW causes non-TEM behavior [11] which is illustrated in Section III-C. Calibration becomes more difficult

with non-TEM modes (e.g., frequency dependent) and inaccurate because of the tangential field component. The purpose of this study was to design a structure that comes close to pure TEM.

This paper goes through the design process of two transmission lines in air, i.e., homogeneous dielectric. In Section II the design models are described. The first method was a rod above a ground plane (Section II-A), while the second method was an easier to manufacture air trace (Section II-B). Simulation and measurement results for the two design models are presented and discussed in Section III.

The calibration process depends entirely on the reliability of the simulations. Hence, Section III-A1 gives an example of the gap between simulations and measurements and how to bridge it. In Section IV, suggestions for further improvements are discussed. Finally conclusions are drawn in Section V.

II. Design Models

A. First Structure: Rod over Ground

A rod in air over a ground plane results in true TEM because of the non-dispersive dielectric. A 30 mm long rod was soldered with a 2.4 mm connector to a 0.203 mm thick by 1.27 cm long CPW from Southwest. An aluminum structure was machined as the ground plane. The distance between the rod and the ground plane was carefully tuned to 0.16 mm so that the impedance was 50 Ω, as shown in Fig. 2.

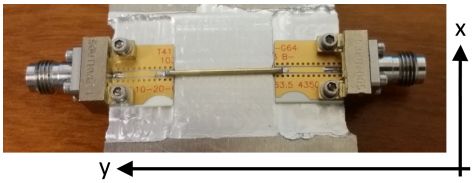

Fig. 2: The rod over ground plane.

B. Second Structure: Air Trace

A 2.4 mm Southwest connector was attached to 1 mm thick GPW with a 1 mm wide trace. The trace continues in an air trace which was made by a cutout slot in a PCB plated with copper. With carefully tuning of the distances, a 50 Ω transmission lines with low loss and almost pure TEM was obtained, as shown in Fig. 3. The advantage of this structure is it can be PCB manufactured and man-made craftsmanship is avoided. However, in PCB manufacturing the slot will be completely plated and the trace will be short circuited to ground. Hence, it is necessary manually to drill away the plating.

C. Simulations Models

The two transmission lines were simulated in CST Microwave Studio with the time domain (FIT) solver. Input power was normalized to 1 W. The number of mesh cells were 8 million for the rod over ground plane and 6 million for the air trace. The Southwest connector was included in the model as shown in Fig. 4. The model was excited with a waveguide port to the coaxial inner part of the connector with a diameter of 1.61 mm.

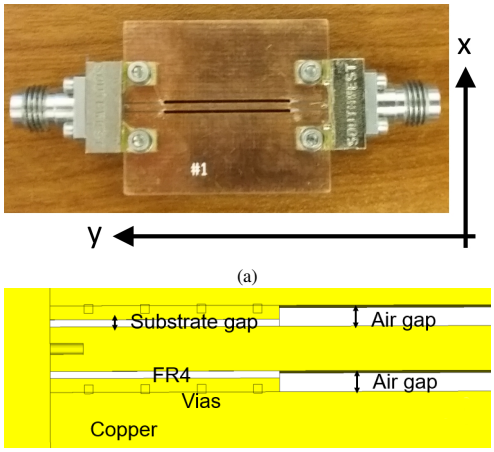

Fig. 3: The air trace. (a) Air trace with Southwest connector (b) The trace is separated from ground by milling the plating away at the end of slots and by making a cut in the trace at the backside.

III. Results and Discussion

Based on the desired features described in Section I, the calibration structure was evaluated with respect to the tangential field component (non-TEM mode), S-parameters, and amplitude across and along the trace. Time domain reflectometry (TDR) was used in measurements to analyze imperfections in the structure. The near-field was evaluated 1 mm above the TL, which is a typical scanning height for high frequency (up to 40 GHz) applications.

A. First Structure: Rod over Ground

The simulations results for the rod over ground are shown in Fig. 5 and Fig. 6. At a glance, the structure looks very promising. Fig. 5 shows that the orthogonal field across the rod is frequency independent up to 20-30 GHz while the curve shape starts to change and the amplitude starts to decrease approaching 40 GHz. The tangential field is very weak compared to the orthogonal field at all points across the rod so the non-TEM mode will not perpetuate the calibration. Fig. 6 shows that standing waves cause variation of the orthogonal field along the rod, which increases with frequency (up to 6 dB at 40 GHz) so it will be necessary to find the average field strength along the trace. The reflections are caused by both the transition from connector to CPW and the transition from CPW to rod. A simulation of the connector and CPW alone showed variations along the rod up to 3 dB at 40 GHz. Fig. 6

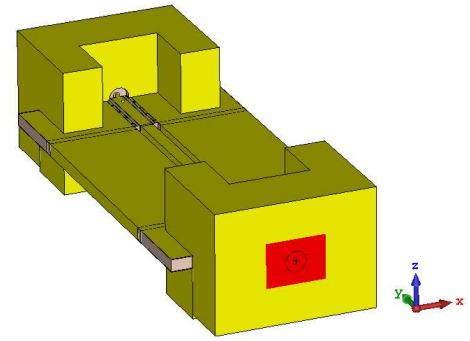

(a) CST model of the air trace.

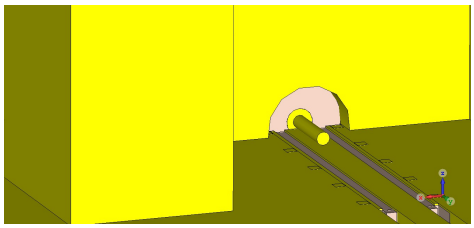

(b)

Fig. 4: Numerical model. (a) Air trace with Southwest connector (b) Transition from Southwest connector to air trace.

also shows S_{11} for the port of the transmission line and S_{21} between the two ports of the transmission line. S_{21} decreases as S_{11} increases. It seems that mismatch is the reason for the S_{21} decrease with frequency.

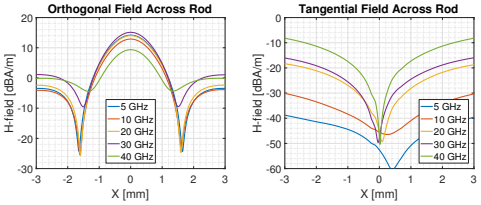

Fig. 5: Orthogonal and tangential field across the rod.

1) Bridging the gap Between Measurement and Simulations: H-field and S-parameters for the rod over ground were also measured. At first, there were large differences between the simulations and measurements. The variation along the trace was larger and the power transmitted from port 1 to port 2 (S_{21}) was much lower in the measurements compared to the simulations. As an example, the comparison of S_{21} is shown in Fig. 7. The physical and numerical models were compared in details and minor differences were observed. The three main

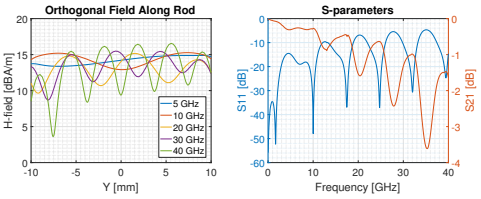

Fig. 6: Left: Orthogonal field along the rod. Right: S-parameters.

courses for the gap between simulations and measurements were in the following order, shown in Fig. 8:

1) Surface roughness on the machined ground plane causing large resistive loss.
2) Gap between CPW and machined ground plane causing further reflections and causing power to disappear as radiation.
3) Distance from end of CPW to first ground via causing further reflections and causing power to disappear as radiation.

The details were refined in the simulation and better agreement between simulations and measurement was obtained, as shown in Fig. 7.

Imperfections 2 and 3 in the physical model were corrected with silver paint, hence, the loss was lowered and standing waves on the rod were reduced. Surface roughness could easily be removed, but since the structure requires precise craftsmanship it was decided to choose a structure which could benefit from PCB manufacturing, namely the air trace.

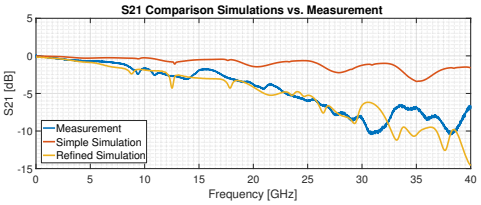

Fig. 7: Comparison between simulation and measurements of S_{21}.

B. Second Structure: Air Trace

In Fig. 9 and Fig. 10 the simulation results of the air trace are shown. Again, the structure seems promising up to 30 GHz. Orthogonal fields across the trace are frequency independent up to 25-30 GHz, but the curve shape and amplitude change as frequency approaches 40 GHz. The tangential field is negligible. Fig. 10 shows that standing waves become significant above 30 GHz (up to 7-8 dB at 40 GHz). Again, the reflections are caused by both the transition from connector to CPW and the transition from CPW to air trace. As frequency increases less power is transfered from port 1 to port 2 because of mismatch, dielectric loss and power radiated.

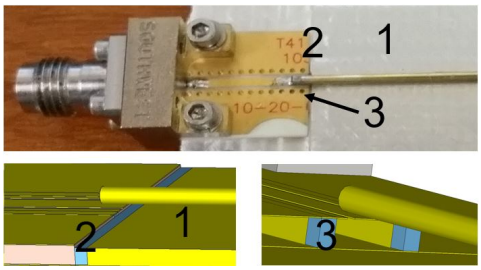

Fig. 8: The rod over ground plane. The 3 main courses for the gap between simulation and measurement are marked with numbers.

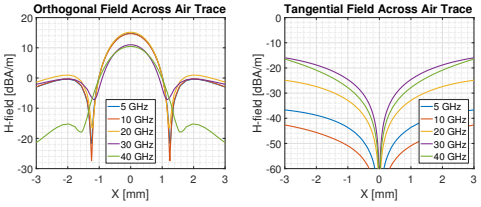

Fig. 9: Orthogonal and tangential field across the air trace.

1) Comparison Between Measurement and Simulations: Fig. 11 shows a comparison between simulations and measurements of S_{11} and S_{21}. Although there are differences in amplitude, there is good agreement regarding resonance frequencies and trends.

C. TEM vs. Non-TEM

As an illustration of the difference between the quasi-TEM behavior of a CPW and the more pure TEM of the air trace, the H-field across a 0.762 mm CPW is compared with the same field of the 1 mm thick air trace at 30 GHz. The H_y (tangential component) of the air trace is negligible compared the orthogonal field (H_x and H_z) at all points across the air trace. For the quasi-TEM CPW, the amplitude of the Hy component is comparable with the tangential components at x=-1 and x=1.

IV. Suggestions for Improvement

The measurement and simulations of the air trace revealed that the transition between CPW and air trace is very critical in order to avoid standing waves and loss. At 40 GHz the wavelength in free space is 7.5 mm. With a board thickness of 1 mm, the length of the detour the return current has to travel in the transition is more than 1/10 of the wavelength. Hence, this distance is comparable with the wavelength. One idea to overcome this problem is to make the board thinner. The air trace board was also designed with 0.8 mm and 0.6 mm thicknesses. Air and substrate gaps were adjusted to the thinner board in order to obtain 50 Ω.

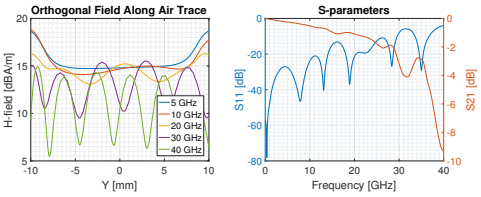

Fig. 10: Left: Orthogonal field along the air trace, Right: S-parameters.

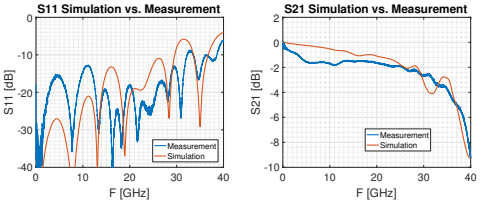

Fig. 11: Left: S_{11} simulation vs. measurement, Right: S_{21} simulation vs. measurement.

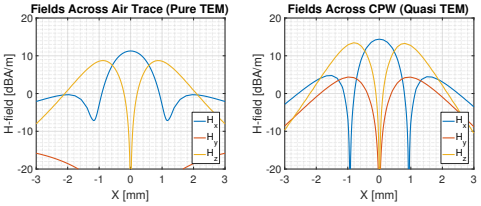

Fig. 12: Left: All three field components across the air trace, Right: All three field components across a CPW.

Fig. 13 shows both standing waves and loss are reduced with thinner boards. The variation along the trace at 30 GHz is reduced to approximately 3 dB for the 0.6 mm board corresponding to the reflections caused by the transition from Southwest connector to CPW.

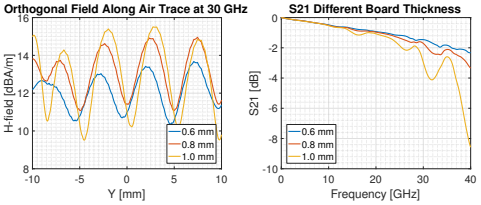

Fig. 13: Left: Standing waves are reduced with board thickness. Right: Loss is reduced with board thickness.

Another idea to overcome reflections could be to design attenuators along the line. But since there are two transitions in both ends i.e., connector to CPW and CPW to air trace, it

will require four attenuators causing a large reduction in the dynamic range.

V. Conclusion

Two different transmission lines in air (homogeneous dielectric) were designed for probe calibration up to 40 GHz: a rod over a ground plane and an air trace. Simulations and measurements show that it is possible to obtain almost pure TEM, but reflections and loss increase while the frequency approaches 40 GHz. This can be improved by decreasing the PCB thickness. However, it requires such small dimensions that PCB manufacturers are incapable of. The design study also made it clear that every physical detail must be included in the simulation in order to obtain good agreement. This is very important since the calibration method strongly depends on reliable simulations.

References

[1] T. S. Rappaport, G. R. MacCartney, M. K. Samimi, and S. Sun, "Wideband millimeter-wave propagation measurements and channel models for future wireless communication system design," *IEEE Transactions on Communications*, vol. 63, no. 9, pp. 3029–3056, Sept 2015.

[2] T. Wheeler, "Leading towards next generation "5G" mobile services," August 2015. [Online]. Available: https://www.fcc.gov/news-events/blog/2015/08/03/leading-towards-next-generation-5g-mobile-services

[3] G. Li, K. Itou, Y. Katou, N. Mukai, D. Pommerenke, and J. Fan, "A resonant e-field probe for rfi measurements," *IEEE Transactions on Electromagnetic Compatibility*, vol. 56, no. 6, pp. 1719–1722, Dec 2014.

[4] S. Shinde, S. Marathe, G. Li, R. Zoughi, and D. Pommerenke, "A frequency tunable high sensitivity h-field probe using varactor diodes and parasitic inductance," *IEEE Transactions on Electromagnetic Compatibility*, vol. 58, no. 1, pp. 331–334, Feb 2016.

[5] "IEEE standard for calibration of electromagnetic field sensors and probes (excluding antennas) from 9 khz to 40 ghz," *IEEE Std 1309-2013 (Revision of IEEE Std 1309-2005)*, pp. 1–111, Nov 2013.

[6] "Testing and measurement techniques – emission and immunity testing in transverse electromagnetic (tem) waveguides," *IEC 61000-4-20 Annex E*, 2010.

[7] J. Zhang, K. W. Kam, J. Min, V. V. Khilkevich, D. Pommerenke, and J. Fan, "An effective method of probe calibration in phase-resolved near-field scanning for emi application," *IEEE Transactions on Instrumentation and Measurement*, vol. 62, no. 3, pp. 648–658, March 2013.

[8] W. Liu, Z. Yan, and W. Zhao, "A study on calibration compensation and perturbation of electromagnetic probes," in *2017 7th IEEE International Symposium on Microwave, Antenna, Propagation, and EMC Technologies (MAPE)*, Oct 2017, pp. 195–199.

[9] M. A. Chahine, M. Khatib, A. Hami, R. Perdriau, and M. Ramdani, "Near field measurement system for the detection of electromagnetic field components radiated by microwave devices," in *2013 13th Mediterranean Microwave Symposium (MMS)*, Sept 2013, pp. 1–4.

[10] R. W. Jackson, "Coplanar waveguide vs. microstrip for millimeter wave integrated circuits," in *1986 IEEE MTT-S International Microwave Symposium Digest*, June 1986, pp. 699–702.

[11] S. Marathe, M. Soerensen, V. Khilkevich, D. Pommerenke, J. Min, and G. Muchaizde, "Effect of inhomogeneous medium on fields above gcpw pcb for near-field scanning probe calibration application," *IEEE Trans. Electromagn. Compat, Accepted for Publication*, 2018.

Paper J

Analysis of the Effect on Image Quality of Different Scanning Point Selection Methods in Sparse ESM

Morten Sørensen[1], Hamed Kajbaf[2], Victor V. Khilkevich, [1], Ling Zhang[1], David Pommerenke[1]
[1]EMC Laboratory, Missouri University of Science and Technology, Rolla, MO 65401, USA, {sorensenmo, khilkevichv, lzd76, davidjp}@mst.edu
[2]Amber Precision Instruments, 101 Bonaventura Drive, San Jose, CA 95134 USA, hamed@amberpi.

Accepted for publication in
IEEE Transactions on Electromagnetic Compatibility, August 2^{th} 2018.

Analysis of the Effect on Image Quality of Different Scanning Point Selection Methods in Sparse ESM

Morten Sørensen, *Member, IEEE,* Hamed Kajbaf *Senior Member, IEEE,* Victor V. Khilkevich *Member, IEEE,* Ling Zhang, *Student Member, IEEE,* David Pommerenke, *Fellow, IEEE,*

***Abstract*—Sparse emission source microscopy (ESM) is an efficient method to identity radiating sources. With the purpose to minimize the number of required measurement points, the presented work investigates how numerical properties of sparse ESM affects the quality of source reconstruction. A simulation model of a simple PCB was used instead of measurements to isolate the observed effect of the 2D discrete Fourier transformation (DFT) and the plane wave spectrum's numerical properties. The paper shows that sub-Nyquist is achievable and suggests uniform sampling is superior to nonuniform, in contrast to other reported uses of microwave imaging. Finally, the study shows that if the source reconstruction is based on uniform 2D DFT care should be taken with the previously suggested intelligent selection of sparse samples based on real-time observation of the measured field.**

***Index Terms*—Sparse Emission Source Microscopy (ESM), sampling rate, sub-Nyquist, source reconstruction, non-uniform sampling.**

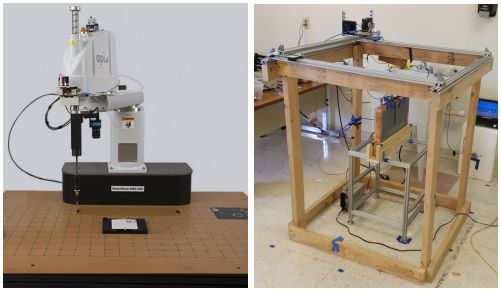

(a) (b)

Fig. 1. ESM can theoretically be done at all scanning heights. (a) A Precision near-field scanner. (b) Homemade hand held scanner with two position coders.

I. Introduction

As data rates and clock frequencies increase, EMI problems at several GHz have become significant. For example optical transceiver modules often cause EMI problems at several GHz [1] and the coming 5G wireless network operates at multiple GHz frequency bands [2], [3]. Legal authorities now set emissions requirements up to 40 GHz [4]. The wavelength at 10 GHz is 3 cm and radiated emission is caused by direct radiation from sub-elements of printed circuit boards (PCB), connectors, etc. rather than induced common mode currents on attached cables.

Emission Source Microscopy (ESM) is a measurement method that can identify the radiating sources of a complex system [5]. The phase resolved tangential electric field is measured on a plane above the device under test (DUT) and the plane wave spectrum is backpropagated to the source plane, where the radiating field sources are reconstructed with a resolution down to a half wave length. If the wave propagates in a medium with very high permittivity (e.g., water [6]), the resolution can be finer. Traditional near-field scanning measures the near-field very close to the DUT and hence the evanescent waves are often dominant, this may cause misinterpretation of the near-field scan. Contrary ESM directly reveals the sources for radiated emission. Previous work has shown that the method can distinguish between multiple radiating sources on a complex PCB above 5 GHz [7] and helps mitigate EMI problems above 10 GHz. [8].

In sparse ESM, the sources are reconstructed by measuring a relatively few number of points. In previous sparse ESM work [9] with non-uniform sampling and similar work with millimeter-wave imaging [10], [11], points are selected on a planar measurement grid with zeros where no measurement has been taken. The sources are reconstructed by backpropagating the plane wave spectrum of the measurement points including the zero grid.

Theoretically, ESM can be done at all distances as long as the aperture angle is large enough. For example, a traditional robotic near-field scanner with a measurement distance of a few cm and a 2D positioning rack with a measurement distance of 20-30 cm depending on DUT size is shown in Fig. 1.

Researchers often refer to the Nyquist spatial sampling rate as step size $< \frac{\lambda}{2}$, without further discussion. In microwave imaging, researchers have observed that it is possible in some cases to obtain acceptable image quality with step sizes larger than $\frac{\lambda}{2}$ [10]–[13]. Compressed sensing [14] and non-uniform Fourier transform [15] have also been used to obtain acceptable image quality with sampling below $< \frac{\lambda}{2}$. Non-uniform sampling is reportedly superior to uniform sampling when below Nyquist [11].

A manual scanner is an effective tool for fast scanning if the purpose is diagnostic, e.g., finding radiating sources. It has been suggested that the operator of the manual scanner can make intelligent decisions regarding the selection of measure-

M. Sørensen, V. Khilkevich, L. Zhang and D. Pommerenke are with the EMC Laboratory, Missouri University of Science and Technology, Rolla, MO 65401 USA (e-mail: sorensenmo@mst.edu; khilkevichv@mst.edu; lzd76@mst.edu; davidjp@mst.edu)

H. Kajbaf are with Amber Precision Instruments, 101 Bonaventura Drive, San Jose, CA 95134 USA (e-mail: hamed@amberpi.com).

Manuscript submitted February 7, 2018. Revised June 22, 2018; accepted August 2, 2018

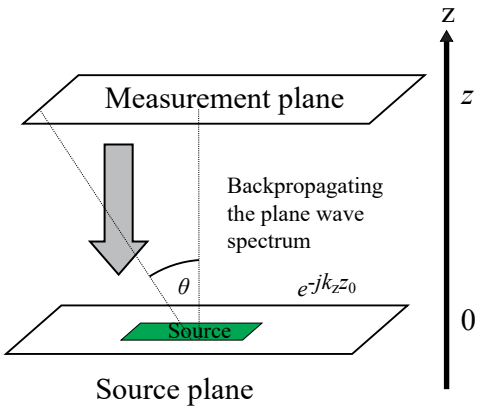

Fig. 2. 2D ESM algorithm.

ment points by viewing the real time reconstructed image [10] or by collecting denser measurements at the locations where the field intensity is strong [9].

Reducing the number of measurement points without degrading the quality of the reconstructed image is of large interest. In order to obtain the best picture quality with the fewest possible measurement points, a fundamental understanding of the effect of selecting measurement points is needed.

This study shows that an inherent property of ESM is the spatial sampling rate can be far below Nyquist without degrading the quality of the reconstructed image of the DUT itself. Furthermore, clustering measurement points degrade image quality of the DUT itself and, hence, intelligent manual selection of measurement points is difficult. Since random non-uniform selected measurement points to some degree also cause clustering, uniform sampling seems beneficial to non-uniform for ESM based on 2D DFT contrary other post-processing methods, e.g., compressed sensing.

Section II introduces the general 2D sparse ESM algorithm and discusses the 2D Fourier transformation vs. Nyquist spatial sampling rate and phase change. Based on this mathematical discussion, source reconstructions were performed for different selections of measurement points. The numerical model is described in Section III and the results are presented and discussed in Section IV. Some rules of thumb for the spatial sampling rate vs. measurement height are suggested in Section V and finally the conclusions are drawn in Section VI.

II. Sparse Emission Source Microscopy

A. 2D Sparse ESM Algorithm

The ESM algorithm is illustrated in Fig. 2. The tangential electric (or magnetic) fields are measured on a plane in discrete points and 2D Fourier transformed to the plane wave spectrum:

$$f(k_x,k_y)=\frac{1}{NM}\sum_{n=1}^{N}\sum_{m=1}^{M}E(x_n,y_m,z_0)e^{j(k_x x_n+k_y y_m)} \quad (1)$$

where k_x and k_y are the spectrum wavenumbers in the x- and y-directions [16]. The spectrum on the source plane can be found by backpropagating the plane wave spectrum to the source plane ($z=0$):

$$f(k_x,k_y,0)=f(k_x,k_y)\cdot e^{-jk_z z_0} \quad (2)$$

where

$$k_z=\sqrt{k^2-k_x^2-k_y^2} \quad (3)$$

Real k_z corresponds to radiating waves while k_z with a non-zero imaginary part correspond to evanescent waves. Before backpropagating, the non-real k_z is nullified and only the radiating part is reconstructed by inverse Fourier transformation:

$$E(x,y,0)=\mathcal{F}^{-1}(\mathcal{F}[E(x,y,z_0)]\cdot e^{-jk_z z_0}) \quad (4)$$

where z_0 is the scanning height and $\mathcal{F}^{-1}$ and $\mathcal{F}$ are the Fourier and inverse Fourier operators.

As known from the theory of optical lenses [17] the resolution of the backpropagated image can be no better than

$$R<\frac{\lambda}{2n\sin\theta} \quad (5)$$

where n is the refractive index and θ is one-half of the aperture angle as shown in Fig. 2. ESM is usually done in air with $n\approx 1$.

Sparse ESM can be measured with relatively few measurement points. If sparse ESM is done with non-uniform measurement points, a predefined grid of zero values is used to do the 2D Fourier transformation, which then is carried out on the matrix with the measured values and the zeros from the raw measurement grid. The zero grid is usually defined with a step size which is much smaller than the wavelength to minimize the phase errors in the measured field caused by the difference between the actual and discretized locations of the probe. A typical choice could be 1 mm step at 20 GHz, resulting in $\frac{1}{20}$ wavelength positioning error and corresponding small phase error. The zeros will cause noise in the image and the signal to noise ratio is approximately equal to the number of sparse samples independent of the density of the grid [9]. The fine measurement grid (with zeros and measurements) increases the number of pixels in the reconstructed image and visually helps to identify the radiating sources.

B. Nyquist Sampling Rate and Selection of Points

As mentioned in Section I, researchers often refer to the Nyquist sampling rate as step size $<\frac{\lambda}{2}$ without further analysis. A more precise formulation of the Nyquist sampling criterion requires samples be taken with a rate doubled relative to the fastest rate of change of the signal. A few wavelengths away from an electrically small source, spatial Nyquist criterion requires only that the phase shift from one sample to the next must be less than π at a given frequency [18].

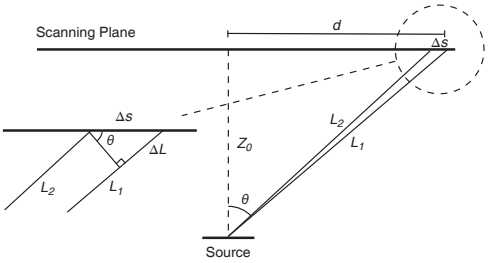

Fig. 3. The maximal phase shift occurs between two sampling points near the edge of the scanning plane.

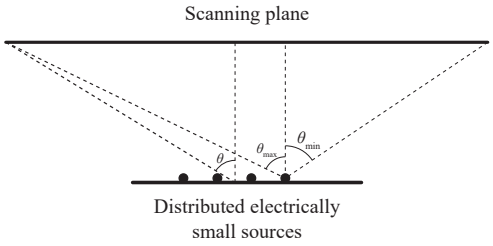

Fig. 4. Scanning of a DUT with distributed point sources requires a clarification of the angles. $\theta_{\max}$ determines the step size while $\theta_{\min}$ determines the resolution of the reconstructed image.

According to (5), a good resolution requires a large aperture angle and hence the source must be small compared to the measurement plane. In the microwave frequency range, typical sources (ICs, transmission line bends, connectors, etc.) are small, and, therefore they can be approximated as point sources. Let's consider radiation from an individual point source located at the center of the aperture as shown in Fig. 3. The maximal phase shift occurs between two sampling points near the edge of the scanning plane. In this ideal setup, the phase shift between two points on the measurement plane is given by:

$$k(L_1 - L2) = k\sqrt{d^2 + z_0^2} - \sqrt{(d - \Delta s)^2 + z_0^2} \approx k_0 \Delta s \cdot \sin\theta \tag{6}$$

where it is assumed that $z_0 \gg \Delta s$.

Nyquist sampling criteria requires the phase shift to be less than π and since $\lambda = 2\pi/k_0$ the maximum step size is given by

$$\Delta s < \frac{\lambda}{2\sin\theta} \tag{7}$$

For adequate scanning height (see Section II-C), the sampling criteria is given by a combination of wavelength and aperture angle. As the aperture angle approaches 90° the maximum step size comes close to $\frac{\lambda}{2}$. For further analysis, the phase shift distance in a point on the measurement plane is defined as the shortest distance to the next point 180° out of phase.

If the DUT is approximated as a point source the distance between a 180° phase shift on the scanning plane can be approximated with the same arguments as in (7):

$$d_{\text{phase shift}} \approx \frac{\lambda}{2\sin\theta} \tag{8}$$

where θ is the actual scanning angle. Equation (8) does of course only make sense for significant aperture angles, as the phase shift distance according to equation (8) approaches infinity as θ goes to 0.

C. Scanning Height and DUT Size

In the derivation of (7), it was assumed that the source on the DUT could be approximated with a point source. However, if the DUT is a combination of electrically small sources a clarification of the angles is needed.

Electromagnetic fields in linear media follow the superposition principle, hence, the total electric fields of several point sources are the sum of the individual fields:

$$E_{\text{total}}(x, y, z_0) = \sum_{n=1}^{N} E_n(x, y, z_0) \tag{9}$$

The 2D DFT is also a linear function and the plane wave spectrum of distributed sources is the sum of the individual plane wave spectrum:

$$\mathcal{F}(\sum_{n=1}^{N} E_n[x, y, z_0]) = \sum_{n=1}^{N} \mathcal{F}(E_{\text{n}}[x, y, z_0]) \tag{10}$$

Hence, for a DUT with distributed sources the minimum required steps size is still given by (7) where θ refers to the largest scanning angle as illustrated in Fig. 4. The resolution given by (5) is determined the minimum scanning angle. The angles can easily be determined geometrically as illustrated in Fig. 4.

The above statement is only true if each individual source is measured in the far-field. To do so, this places an additional condition on the scan height. For electrically large sources, this condition can be written as:

$$z_0 > \frac{2D^2}{\lambda} \tag{11}$$

where *D* is the largest dimension of the individual source approximated with a point source. For electrically small sources a few wavelengths is sufficient.

In general, it is not required to do ESM in far-field.

III. Test Model

With the purpose of demonstrating the effect of scanning height, sampling rate, and selection of measurement points on the image quality, a simple 1.4 mm two-layer PCB with a few sources was simulated. The PCB has a 100 mm × 100 mm

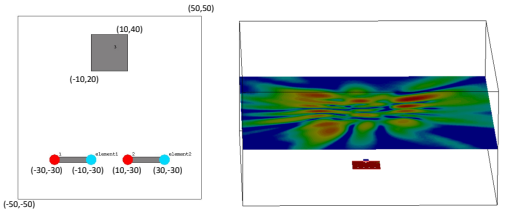

(a) (b)

Fig. 5. (a) The simulation model in CST. (b) The electric field above the PCB on a 900 mm × 900 mm plane was exported.

unbroken ground plane with two 20 mm long 50 Ω micro strips and a 20 mm × 20 mm metal box similar to a heat sink. The micro strip is excited with a 50 Ω S-parameter port in one end and terminated with 50 Ω in the other end. The micro strip is well impedance matched to 50 Ω so only the excitation and termination at the end will radiate. The microstrip itself is quasi-TEM and will not radiate. The heat sink is also excited with an S-parameter port in order to make it radiating. The board is shown in Fig. 5. The electric tangential phase resolved field at a 900 mm × 900 mm plane was extracted from the simulations at the heights 50, 100, 200, 300 and 400 mm. The 900 mm × 900 mm was chosen as representative for the size of a scanner as shown in Fig. 1 (b). The field was exported at 10, 15, and 20 GHz.

The simulations were done with the FIT solver in CST Studio Suites [19]. In order to avoid numerical dispersion, the mesh was very dense with more than 500 million mesh cells.

For this study, simulations have the advantage compared to measurement because the field monitors are perfect and do not have a beam width like horn antennas and open waveguides. Hence, the observed effects can be isolated to numerical properties of the sparse ESM method, i.e., aliasing, non-uniform sampling, and other properties of 2D DFT. Since non-uniform sampling is used in the study, a predefined grid of zero values is used and in addition the fine zero grid increases the number of pixels in the reconstructed image. These zeros affect the amplitude of the field in the reconstructed image and, hence, the amplitudes have been normalized according to the method mentioned in [9].

The ESM method was applied on the exported data in MATLAB and results observed.

IV. Results and Discussion

For reference, the reconstructed sources for 10 and 15 GHz with a measurement height of 300 mm are shown in Fig. 6. All 901 × 901 points on the measurement plane are used for reconstructing corresponding to a measurement with step size = 1 mm, far above the spatial Nyquist sampling rate.

The amplitude range in the image is 15 dB and only the reconstructed image of the PCB ± 50 mm is shown. The PCB is placed in the center of the measurement plane with corner position (400,400) and (500,500). At 10 GHz especially, the heat sink and the 50 Ω terminations radiate. At 15 GHz, both the excitation and termination points of the microstrip radiate

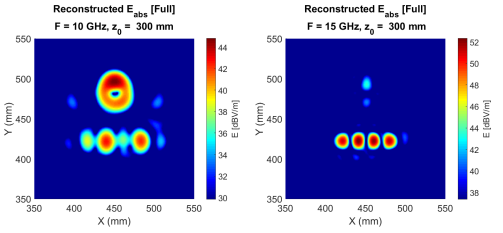

Fig. 6. Comparison of source reconstruction for 10 and 15 GHz both with z_0 = 300 mm.

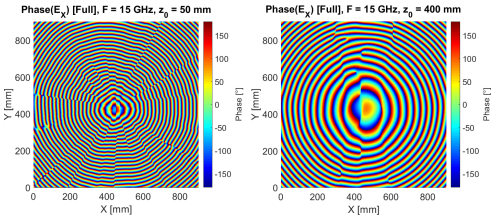

Fig. 7. Phase on the measurement plane with z_0 = 50 mm and z_0 = 400 mm.

while the radiation from the heatsink is weaker. The plots also illustrate the resolution of the image vs. wavelength according to (5) since the size of the radiating sources is larger at 10 GHz compared to 15 GHz.

In order to make arguments clear, only results for 15 GHz are shown in the following analyses, but the papers conclusions have also been verified for 10 and 20 GHz.

A. Sampling Rate and Aliasing

Fig. 7 shows the phase of the E_x field on the 900 mm× 900 mm measurement plane at the two extreme cases of the scanning height, z_0 = 50 mm and z_0 = 400 mm. The figure visualizes the discussion about phase shift in Section II-B. In the center of the measurement plane just above the DUT the phase is irregular and away from the center the gradient of the phase increases.

Fig. 8 shows the phase shift distance (8), i.e., the distance to the closest point 180° out of phase along the x-axis in the center of the measurement plane (y = 450). A short distance away from the center of the measurement plane, the simulated phase shift distance is in agreement with the analytical phase shift distance which support it is reasonable to approximate the sources as point sources. 50 mm above the PCB the phase shift distance approaches $\frac{\lambda}{2}$ very fast while even at the edge of the z_0 = 400 mm measurement plane, the phase shift distance is 0.7 λ. Hence, if the measurement is done at z_0 = 400 mm, the phase shift requirement for spatial sampling only 0.7 λ.

From (5) and (7) it is now possible to calculate the spatial sampling rate and scan area for a given required resolution. Assuming an aperture angle of 45° gives sufficient resolution, then a step size of $\frac{\lambda}{\sqrt{2}}$ is sufficient in order to avoid aliasing. An aperture angle of 45° gives a scanning square with a side length equal to double scanning height. Fig. 9 shows scanning

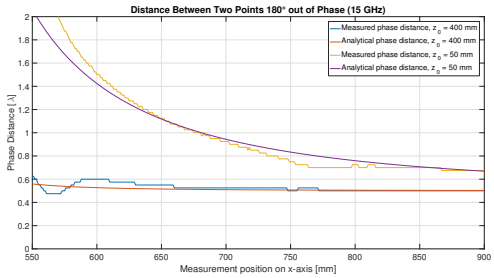

Fig. 8. Phase distance vs. position at the x-axis.

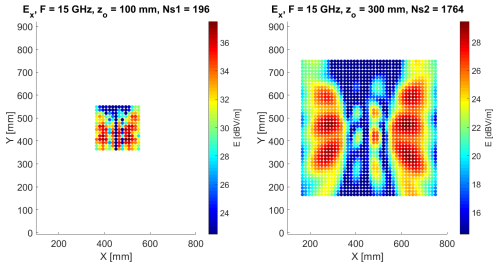

Fig. 9. The scanning points for z_0 = 100 mm (left) and z_0 = 300 mm (right) visualized.

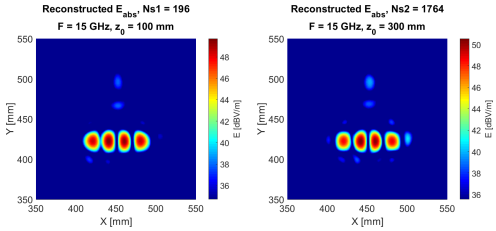

Fig. 10. The reconstructed image for z_0 = 100 mm (left) and z_0 = 300 mm (right) plane.

points corresponding to an aperture angle of 45° and a step size of $\frac{\lambda}{\sqrt{2}}$. If the scanning height is 100 mm, it requires 14^2 = 196 measurement points while a scanning height of 300 mm requires 3 × 3 times as many scanning points.

The reconstructed image is shown in Fig 10. The two images are very similar and despite step size larger than $\frac{\lambda}{2}$, there is no aliasing. From signal processing it is well known that with correct filtering, sampling above Nyquist does not provide more information. Even though the $z_0 = 300$ mm scanning image is based on 9 times more samples, the quality of the reconstructed image is not better because most of the points are just sampling points denser than the Nyquist phase requirement.

Since 9 times more scanning points on the z_0 = 300 mm does not improve the image quality, it is worth testing whether it is possible to obtain the same image quality from the z_0 = 300 mm plane with the same number of measurement points

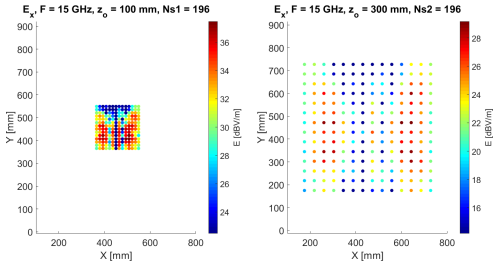

Fig. 11. 14^2 scanning points on the z_0 = 100 mm (left) and z_0 = 300 (right) plane.

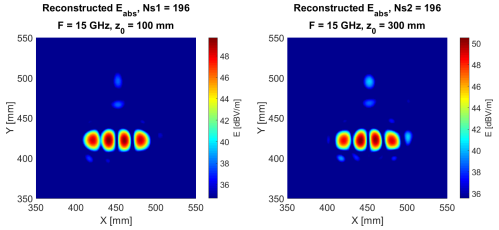

Fig. 12. Reconstructed image for 14^2 scanning points on the z_0 = 100 mm (left) and z_0 = 300 (right) plane.

as on the z_0 = 100 mm plane. The measurement points on the 100 mm plane were projected to the 300 mm plane as shown in Fig. 11 and the field information at the 300 mm plane was extracted. Hence, scanning the measurement plane further away provides same information about the radiated field as the scanning on the lower plane. On the 300 mm plane the step size is 3· $\frac{\lambda}{\sqrt{2}} = 2.1\lambda$. This is more than 4 times the restrictive $\frac{\lambda}{2}$ view on the Nyquist sampling.

The reconstructed image is compared with 196 points on z_0 = 100 mm in Fig. 12. Again, the two images are clear and very similar, but they are also based on the same information about the radiated field. Compared with Fig. 10 there is no significant difference.

At a glance, it seems surprising that a step size 4 times larger than $\lambda/2$ does not cause aliasing and that's not the truth either. Fig. 13 shows the reconstructed image on the whole plane and now the aliasing becomes clear. In 1D DFT higher frequencies than the sampling frequency are folded around the sampling frequency. Fig. 14 shows the normalized k-space for the two different number of samples. The aliasing in the k-space is clear and the higher frequency plane waves are leaking into the visible part of the k-space. However, as long as the spatial aliasing disturbance is far from the source, aliasing will not degrade image quality. The down-sampling will determine the number of aliasing images, which is limited by DUT size in order to avoid overlapping aliasing images with the DUT image.

B. Effect of Zero Grid

As mentioned in Section III a zero grid was used. The advantage of the zero grid is illustrated in Fig. 15. 14 × 14

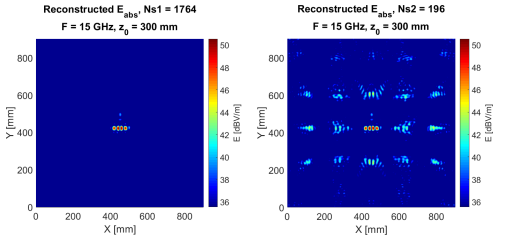

Fig. 13. Reconstructed image of 196 points on $z_0 = 300$. There is no aliasing in the interesting part of the reconstructed image (left) while the sub-Nyquist sampling causes aliasing outside the region of interest.

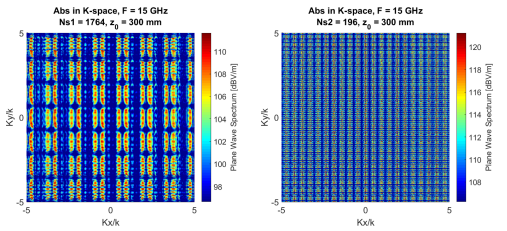

Fig. 14. The normalized k-space of 196 and 1764 points on $z_0 = 300$. When the sampling is sparse, the repetition pattern moves into the visible part (a circle with radius 1) of the k-space.

measurement points were taken at z_0 = 100 mm with and without using zero grid. The zero grid does not add more information, however, the increase in pixels makes it easier to identify the source.

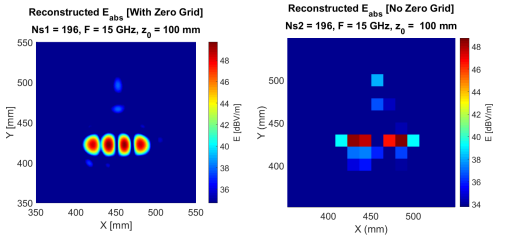

Fig. 15. The effect of zero grid illustrated for 14^2 measurement points with z_0 = 100 mm.

If samples are taken sub-Nyquist, the effect of the zero grid is even more clear. In Fig. 16 14 $\times$ 14 measurement points were taken at z_0 = 300 mm with and without using zero grid. It is clear that the sub-Nyquist only works with the zero grid. One reason obviously is that pixel size is equal to step size and with a step size of 2.1 λ it is not possible to distinguish sources with better resolution. The other reason is that the plane wave spectrum of the 14 $\times$ 14 measurement points without zero grid has no imaginary part and hence the aliasing occurs in the visible part of the plane wave spectrum.

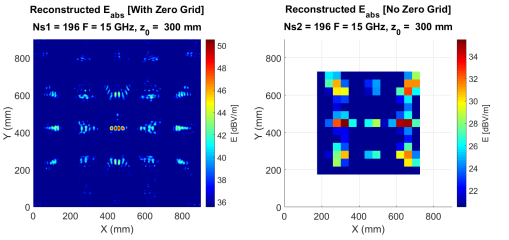

Fig. 16. The effect of zero grid illustrated for 14^2 measurement points with z_0 = 300 mm.

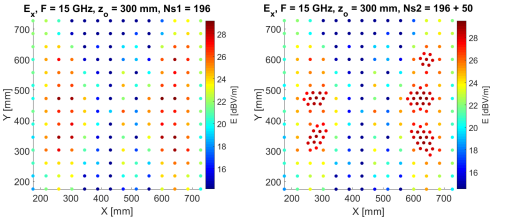

Fig. 17. 196 uniform points (left) and 196 uniform points + 50 extra points around high amplitude points (right).

C. Intelligent Sampling

As mentioned in Section I, it has been suggested that the operator of a manual scanner can select measurement points on the run in an intelligent way, e.g., by taking more measurements where there is a strong field. In order to mimic an intelligent operator, 196 measurement points on the $z_0 = 300$ mm were chosen uniformly as in Fig. 11. Next 50 points extra were added in regions with strong field amplitudes. Human behavior was mimicked by setting a minimum distance of 20 mm between 2 measurement points. The selected measurement points are shown in Fig. 17.

In Fig. 18, the reconstructed field with and without the 50 extra points is shown. The extra points actually degrade the image quality by adding non-uniform aliasing noise to the image. This phenomena is rather complex [20] and outside the scope of this paper but the effect is evident in Fig. 18. The aliasing does not occur because of sub-Nyquist. When 25% extra points were added to the 1764 points in Fig. 9 with a minimum distance of 6.7 mm, i.e., $\frac{1}{3}$ minimum distance compared to the 194 points example, the same degradation of the image quality was observed. If the minimum distance between extra points was reduced, the noise worsened. Adding extra points based on the gradient of the phase was also tried, but similarly to the amplitude-based extra points it caused noise. This result indicates that as long as uniform 2D DFT is used, uniform sampling gives the best picture quality in the area of interest. However, according to (1) weak E-fields do not contribute significantly to the Fourier transformation so areas with weak E-fields can be omitted from the scanning as long as the rest of the scanning is done uniformly.

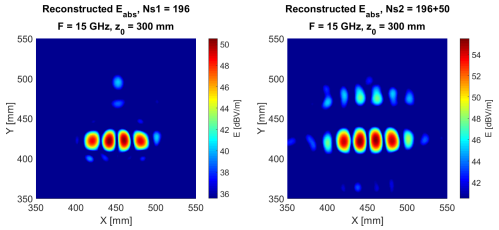

Fig. 18. Reconstructed image with and without 50 extra points.

D. Uniform vs. Random Sampling

As mentioned in Section I, other research areas use non-uniform sampling when below Nyquist. In compressed sensing it helps converging the reconstruction algorithm. In Fig. 19, uniformly vs. randomly selected scanning points are illustrated. Again, 196 scanning points were used corresponding to average step size of 2.1 λ.

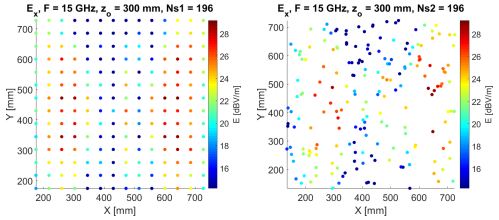

Fig. 19. 196 uniformly sampled points on the $z_0 = 300$ mm scanning plane (left) and 196 randomly selected points (right).

The reconstructed source image is shown in Fig. 20 including both a zoomed version showing the area of interest and the full scanning plane. The images show that the randomness causes background noise in the area of interest (compared with Fig. 12). This is probably caused by non-uniform aliasing similar to the extra point case described in Section IV-C. As observed in other research areas, the general aliasing on the whole plane is reduced (compared with Fig. 13). In ESM, only a small area in the center of the scanning plane is of interest, so in spite of less general aliasing, uniform sampling seems superior to nonuniform when reconstruction is based on 2D DFT of a uniform zero grid.

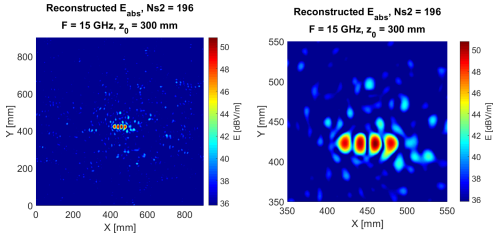

Fig. 20. Reconstructed image of the random sampled.

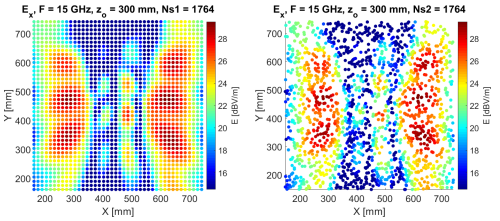

Fig. 21. 1764 uniformly sampled points on the $z_0 = 300$ mm scanning plane (left) and 1764 randomly selected points (right).

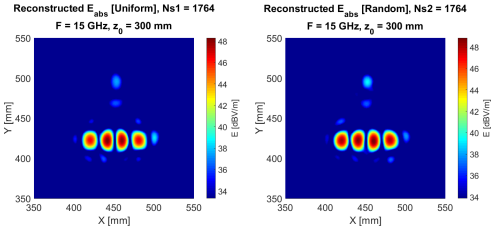

Fig. 22. Reconstructed image of the random sampled above Nyquist sampling.

It was also tested whether non-uniform scanning introduces background noise in the reconstructed image, if the spatial scanning rate is chosen above Nyquist. In Fig. 21 1796 non-uniform points were selected on the $z_0 = 300$ mm plane, i.e., average step size below the Nyquist criteria given in equation (7). The reconstructed source image is shown in Fig. 22. No background noise was introduced.

V. Selecting Sparse Measurement Points

Many decisions have to be made before a sparse ESM measurement is started. Based on the observations in Section IV some rules of thumb for selecting sparse measurement points and scanning height are suggested in this section.

First, select an aperture angle that covers the main beam of the radiation and gives the required resolution. The closer the DUT, the less number of measurement points is required in order to completely avoid aliasing. However, scanning height is not that important. If a larger scanning height is required for practical reasons, choose scanning points on a virtual lower scanning plane fulfilling the minimum scanning height mentioned in Section II-C. The scanning points, fulfilling Nyquist phase requirement, on this lower plane, can then be projected to the higher measurement plane without losing information about the radiating field, but at the expense of aliasing. As long as the aliasing does not overlap the DUT image it does no harm. If a handheld scanner is used with zero grid, try to obtain measurement points as uniformly as possible and avoid denser scanning in regions with strong amplitudes.

VI. Conclusion

A basic understanding of how the selection of measurement points affects image quality is required in order to make efficient sparse ESM with a low-noise reconstructed image. By

a simulated example and mathematical arguments, the effect of sampling rate vs. scanning height caused by 2D DFT is visualized. In a typical measurement set-up, it is possible to go far below the spatial Nyquist sampling rate because the spatial aliasing is folded outside the area of interest. It is a topic for further study to quantify and generalize aliasing overlapping or not with the DUT as a function of under-sampling and height. However, it is rather complex to generalize because the overlapping occurs in the spatial domain at the source plane and it is caused by aliasing in the plane wave spectrum on the scanning plane.

In the example where the individual sources can be approximated with point sources, measurement points on a lower plane could be projected to a higher plane given the same reconstructed image in the area of interest despite going sub-Nyquist.

Contrary to other source reconstruction methods, uniform selection of measurement point is superior to non-uniform selection when the source reconstruction is based on 2D DFT of an uniform zero grid with measurement points because aliasing away from the DUT does not affect diagnosing of the radiating sources. This applies only to the cases where the size of the DUT is small compared to the aperture, otherwise the aliases overlap with the DUT images.

Previously it has been suggested that an operator of a handheld scanner can make intelligent choices based on the real-time reconstructed image, but the results of the study indicates that this is difficult as long as uniform 2D DFT is used. Regardless of the criteria for extra point selection, it seems that clustering measurement points degrades the image quality. Using non-uniform FFT could be a solution for intelligent point selection.

Zero grid visually helps identify the sources by adding extra pixels. In addition, it is a prerequisite for going sub-Nyquist.

The study showed how image quality is affected by numerical properties of the sparse ESM method, basically the 2D DFT between spatial spectrum and plane wave spectrum. The image quality is, of course, also affected by the properties of the measurement equipment which must be considered while a sparse ESM scan is planned.

REFERENCES

[1] L. Zhang, X. Li, X. Jiao, J. Li, S. S. Toor, A. U. Bhobe, D. J. Pommerenke, and J. L. Drewniak, "EMI coupling paths and mitigation in optical transceiver modules," *IEEE Transactions on Electromagnetic Compatibility*, vol. 59, no. 6, pp. 1848–1855, Dec 2017.

[2] T. S. Rappaport, G. R. MacCartney, M. K. Samimi, and S. Sun, "Wideband millimeter-wave propagation measurements and channel models for future wireless communication system design," *IEEE Transactions on Communications*, vol. 63, no. 9, pp. 3029–3056, Sept 2015.

[3] T. Wheeler, "Leading towards next generation "5g" mobile services," August 2015. [Online]. Available: https://www.fcc.gov/news-events/blog/2015/08/03/leading-towards-next-generation-5g-mobile-services

[4] "Code of federal regulations, title 47, part 15 (cfr 47)," 2017.

[5] P. Maheshwari, H. Kajbaf, V. V. Khilkevich, and D. Pommerenke, "Emission source microscopy technique for emi source localization," *IEEE Transactions on Electromagnetic Compatibility*, vol. 58, no. 3, pp. 729–737, June 2016.

[6] V. Khilkevich, R. Ghorude, and D. Pommerenke, "Super resolution emission source microscopy using water immersion," in *2016 IEEE International Symposium on Electromagnetic Compatibility (EMC)*, July 2016, pp. 695–700.

[7] P. Maheshwari, V. Khilkevich, D. Pommerenke, H. Kajbaf, and J. Min, "Application of emission source microscopy technique to EMI source localization above 5 ghz," in *2014 IEEE International Symposium on Electromagnetic Compatibility (EMC)*, Aug 2014, pp. 7–11.

[8] X. Jiao, P. Maheshwari, V. Khikevich, P. Dixon, Y. Arien, A. Bhobe, J. Li, X. Li, D. Pommerenke, J. Drewniak, H. Kajbaf, and J. Min, "EMI mitigation with lossy material at 10 GHz," in *2014 IEEE International Symposium on Electromagnetic Compatibility (EMC)*, Aug 2014, pp. 150–154.

[9] L. Zhang, V. V. Khilkevich, X. Jiao, X. Li, S. Toor, A. U. Bhobe, K. Koo, D. Pommerenke, and J. L. Drewniak, "Sparse emission source microscopy for rapid emission source imaging," *IEEE Transactions on Electromagnetic Compatibility*, vol. 59, no. 2, pp. 729–738, April 2017.

[10] J. T. Case, M. T. Ghasr, and R. Zoughi, "Nonuniform manual scanning for rapid microwave nondestructive evaluation imaging," *IEEE Transactions on Instrumentation and Measurement*, vol. 62, no. 5, pp. 1250–1258, May 2013.

[11] ——, "Optimum 2-d nonuniform spatial sampling for microwave sar-based nde imaging systems," *IEEE Transactions on Instrumentation and Measurement*, vol. 61, no. 11, pp. 3072–3083, Nov 2012.

[12] D. M. Sheen, D. L. McMakin, and T. E. Hall, "Three-dimensional millimeter-wave imaging for concealed weapon detection," *IEEE Transactions on Microwave Theory and Techniques*, vol. 49, no. 9, pp. 1581–1592, Sep 2001.

[13] R. K. Amineh, A. Khalatpour, and N. K. Nikolova, "Three-dimensional microwave holographic imaging using co- and cross-polarized data," *IEEE Transactions on Antennas and Propagation*, vol. 60, no. 7, pp. 3526–3531, July 2012.

[14] H. Kajbaf, J. T. Case, Z. Yang, and Y. R. Zheng, "Compressed sensing for SAR-based wideband three-dimensional microwave imaging system using non-uniform fast fourier transform," *IET Radar, Sonar Navigation*, vol. 7, no. 6, pp. 658–670, July 2013.

[15] J. Song, Q. H. Liu, K. Kim, and W. R. Scott, "High-resolution 3-d radar imaging through nonuniform fast fourier transform (nufft)," *Commun. Comput. Phys*, vol. 1, no. 1, pp. 176–191, 2006.

[16] C. Balanis, *Antenna Theory: Analysis and Design*. Wiley, 2012. [Online]. Available: https://books.google.com/books?id=v1PSZ48DnuEC

[17] J. Goodman, *Introduction to Fourier Optics*, ser. McGraw-Hill physical and quantum electronics series. W. H. Freeman, 2005. [Online]. Available: https://books.google.com/books?id=ow5xs_Rtt9AC

[18] N. Nikolova, *Introduction to Microwave Imaging*, ser. EuMA High Frequency Technologies Series. Cambridge University Press, 2017. [Online]. Available: https://books.google.com/books?id=JN0qDwAAQBAJ

[19] "Cst microwave studio," 2017, http://cst.com.

[20] M. W. Maciejewski, H. Z. Qui, I. Rujan, M. Mobli, and J. C. Hoch, "Nonuniform sampling and spectral aliasing," *Journal of Magnetic Resonance*, vol. 199, no. 1, pp. 88 – 93, 2009. [Online]. Available: http://www.sciencedirect.com/science/article/pii/S1090780709001037

Morten Sørensen (M08) received the M.S. degree in physics from Aarhus University, Aarhus, Denmark, in 2005. From 2006 to 2017, he was an Antenna and Electromagnetic Compatibility (EMC) specialist with Bang & Olufsen, Struer, Denmark, including three years (2011-2014) as a Researcher and Technical Project Manager in the innovation consortium, EMC Design First Time Right. In 2017, he joined the EMC Laboratory, Missouri University of Science and Technology, Rolla, MO, USA, where he is a visiting Assistant Research Professor and since 2018, he has been working part time with Amber Precision Instruments, San Jose, CA, USA. His current resarch interests include near-field scanning, electrostatic discharge, ESM and system-level radiated emission.

Hamed Kajbaf (S08-M12-SM18) received the BS degree in electrical engineering from Shiraz University, Shiraz, Iran, in 2006 and he received the MS degree in biomedical engineering-bioelectric from Tarbiat Modares University, Tehran, Iran, in 2009. He received the PhD in electrical engineering from Missouri University of Science and Technology, Rolla, MO, in 2012. He has previously worked at SpaceX as EMC Design Engineer. He is currently a Principal EMC Engineer at Amber Precision Instruments, San Jose, CA. His research interests include EMC and RF instrumentation, EMC and microwave scanning systems, near-field electromagnetic and acoustic measurement, and array signal acquisition/processing.

Victor V. Khilkevich (M08) received the Ph.D. degree in electrical engineering from Moscow Power Engineering Institute, Technical University, Moscow, Russia, in 2001. He is currently an Assistant Professor with the Missouri University of Science and Technology, Rolla, MO, USA. His primary research interests include microwave imaging, automotive electromagnetic compatibility modeling, and high-frequency measurement techniques.

Ling Zang (S'16) received the B.S. degree in electrical engineering from Huazhong University of Science and Technology, Wuhan, China in June 2015, and MS degree from Missouri S& T in December 2017. He also worked in Cisco as a student intern from August 2016 to August 2017. He is now pursuing his PhD degree in EMC lab, Missouri S& T. His research interests include machine learning in EMC/SI applications, RFI analysis, Emission Source Microscopy technology and radiation analysis of optical transceiver modules.

David Pommerenke (F'15) received his Diploma and PhD from the Technical University Berlin, Germany in 1996. After working at Hewlett Packard for 5 years he joined the Electromagnetic Compatibility Laboratory at the Missouri University of S&T in 2001 where he is professor. His research interests are system level ESD, electronics, numerical simulations, EMC measurement methods and instrumentations. He has published more than 200 papers and is inventor on 13 patents. His main research interests are measurement/instrumentation ESD, and EMC. He is IEEE fellow and associated editor for the IEEE Transactions on EMC.

ISSN (online): 2446-1628
ISBN (online): 978-87-7210-338-9

AALBORG UNIVERSITY PRESS